DEVELOPING AN EARLY WARNING SYSTEM OF HIGHWAY SLOPE FAILURE BASED ON IN-SITU HYDRAULIC CONDUCTIVITY OF SOIL

by

ALINDA GUPTA

Presented to the Faculty of the Graduate School of

The University of Texas at Arlington in Partial Fulfillment

of the requirements

for the degree of

DOCTOR OF PHILOSOPHY IN CIVIL ENGINEERING

THE UNIVERSITY OF TEXAS AT ARLINGTON

August 2023

ACKNOWLEDGEMENTS

I wish to extend my heartfelt appreciation to Dr. MD Sahadat Hossain, my supervising professor, for his invaluable contributions that have led to the fulfillment of my academic journey. His unwavering guidance, consistent suggestions, and motivating influence have been indispensable in reaching this milestone. Beyond his role as an exceptional academic mentor, he has also served as a comprehensive source of direction for me.

I would also like to express my gratitude to my esteemed committee members: Dr. Xinbao Yu, Dr. Warda Ashraf, and Dr. Muhammad N. Huda, for their invaluable time, insightful suggestions, and constructive comments. Additionally, I extend my thanks to the Texas Department of Transportation (TxDOT) for their generous funding, which made this research possible.

I am deeply appreciative of the unwavering support from all the members of the SWIS community. A special acknowledgment goes to Dr. MD Aminul Islam, Dr. Muhasina Manjur Dola, Dr. Sachini Madanayake, and Dr. Md. Azijul Islam for their exceptional guidance, support, and assistance during the field installations, data collection, and performance monitoring phase.

In a heartfelt manner, I extend my gratitude to my parents for their boundless love, unwavering trust, continuous encouragement, and unwavering belief in me. Their sacrifices have paved the way for my journey. This research work and dissertation are dedicated to them as a token of my appreciation. I would also like to recognize the steadfast support of my wife, Jaita Saha, and my brother, Niloy Gupta, for their unwavering cooperation throughout this journey.

August 2, 2023

ABSTRACT

DEVELOPING AN EARLY WARNING SYSTEM OF HIGHWAY SLOPE FAILURE BASED ON IN-SITU HYDRAULIC CONDUCTIVITY OF SOIL

Alinda Gupta

The University of Texas at Arlington, 2023

Supervising Professor: MD Sahadat Hossain

Highway slope failure is globally a momentous issue. Highway slope failure poses a significant issue in transportation infrastructure. Several factors can contribute to slope failures, including geological conditions, weather events, and human activities. Weather events like heavy rainfall, cyclic shrinkage and swelling can trigger slope failures constructed on high plastic clays. It increases pore water pressure, causing soil saturation, and inducing failure. The consequences of highway slope failures are severe, ranging from traffic disruptions, road closures, and damage to vehicles and infrastructure, to potential injuries or loss of lives. Addressing and mitigating slope failure risks is crucial for ensuring the safety and functionality of transportation networks, as well as minimizing the economic and social impact of such events. The aim of the study is to develop an early warning system based on the hydraulic properties of regional soil. As a part of the study, two highway slope sections were selected: located over US 287 near Midlothian, Texas and beside I-20 highway near Parks Springs Blvd, Arlington, Texas. The test sites were instrumented with moisture and suction sensors to collect volumetric moisture content data and moisture suction data. These data were used to prepare field SWCC curve. In-situ hydraulic conductivity tests were performed using Mini-Disk Infiltrometer and Guelph Permeameter. In-situ hydraulic conductivity results showed 100 times higher values on surface than at two-feet depth due to surficial cracks

and porous soil at the surface. The results also showed significant seasonal variation. Soil Temperature and daily rainfall data were collected from NASA POWER website. Rainfall, soil temperature and volumetric moisture content data were correlated with the hydraulic conductivity results obtained from field tests. It was observed that the hydraulic conductivity increased with the increment in each parameter. A hydraulic conductivity prediction model was developed in this study incorporating the climatic data and 85% validity of the results were found from regression analysis. This prediction model can be used to evaluate the in-situ hydraulic conductivity based on the forecasted data. An analytical study was conducted incorporating the field test data to assess the threshold hydraulic conductivity of soil for different rainfall patterns. The study showed the limiting value of hydraulic conductivity that can saturate the soil for a maximum intensity of rain. It showed that hydraulic conductivity ranged from 10^{-4} cm/s to 10^{-6} can saturate the soil and hold the moisture inside the soil and make the slope vulnerable enough to fail. The numerical study was conducted by performing both seepage and slope stability analysis incorporating the field and laboratory test data. It was observed from the output that both intensity and duration played a significant role in slope failure mechanism. A high intensity rain or any prolonged rainfall event led to a drastic change in pore water pressure which eventually reduced the shear strength of the soil and be responsible for slope failure. The seasonal variation in hydraulic conductivity was incorporated and a limiting value was assessed for different climatic conditions. A rainfall intensity-duration equation was developed with different strength and hydraulic properties (such as, volumetric water content, hydraulic conductivity) by performing a parametric study. Using the parametric study results, the threshold hydraulic conductivity was determined to obtain a factor of safety greater than 1. Finally, an early warning system of shallow slope failure was developed using the threshold value of hydraulic conductivity from analytical and numerical study.

TABLE OF CONTENTS

LIST OF FIGURES

LIST OF TABLES

CHAPTER 1

INTRODUCTION

1.1 BACKGROUND

Slope failures and landslides stand as significant global disasters, inflicting substantial economic losses and casualties (Wright et al. 2005). These occurrences transpire in both natural and human-made slopes. The challenge is recurrent in regions where highway embankments are situated atop expansive clay. While high plastic clay possesses sufficient strength to support slopes under dry conditions, it exhibits vulnerability to cyclic swelling and contraction induced by weather-related factors like precipitation and evapotranspiration (Estabragh et al. 2015; Abbey et al. 2019). Over time, the soil tends to weaken, leading to diminished shear strength and reduced safety margins (McCormick and Short 2006; Wright et al. 2007). Additionally, the presence of shrinkage cracks on slopes creates paths for rainwater infiltration, potentially escalating the risk of water seepage. The combination of prolonged rainfall and cyclic soil behavior renders highway slopes more susceptible to failure. Employing an Early Warning System (EWS) emerges as an effective means to mitigate the impact of slope failures by enabling prompt detection and response.

Highway embankment slope failures can stem from multiple factors, including geological activities, hydrological influences, topographical features, weathering processes, vegetation, and climate-related loads (Zhang et al. 2011). The climate load encompasses elements such as rainfall, evapotranspiration, temperature, relative humidity, and wind speed specific to a particular location. Rainfall and temperature changes induce alterations in in-situ soil behavior that contribute to slope failure. Rainfall-triggered slope failures surpass those caused by other factors in frequency (Rahardjo et al. 2007; Rahimi et al. 2010; Lee et al. 2014), regardless of soil type. Different soil types react distinctively to rainfall: highly permeable soil saturates quickly, generating pore water

pressure, while less permeable soil saturates slowly, losing its negative pore water pressure. Consequently, sandy soil (highly permeable) slopes fail during intense short-term rainfall, whereas clay soil (low permeable) slopes fail during prolonged low-intensity rainfall (Hossain et al. 2013; Rahardjo et al. 2007).

Understanding the failure mechanism of slopes constructed with expansive soil due to rainfall necessitates grasping unsaturated soil mechanics. The soil's hydraulic properties in relation to matric suction follow a nonlinear relationship; rapid shifts in pore-water pressure significantly impact soil strength and slope stability. During dry periods, expansive soil develops cracks, compromising its integrity. The presence of these cracks significantly influences soil hydro-mechanical behavior, including clay volume changes, slaking, permeability, residual shear, and tensile strength (Kodikara 2018; Trabelsi et al. 2018). Furthermore, high plasticity clay soil loses its shear strength attributes, primarily cohesion intercept (c'), after undergoing cycles of wetting and drying (Rogers and Wright 1986; Hossain 2012). During rainfall, water infiltrates cracks more rapidly, saturating the soil and reducing shear strength by diminishing matric suction, consequently lowering effective stress. This results in decreased slope resistance, increased driving forces, and, ultimately, rainfall-induced slope failures (Brand 1981; Brenner et al. 1985; Chen, Lee, and Law 2004).

Various researchers have undertaken field monitoring (Uchimura et al. 2015; Rahardjo et al. 2019), laboratory flume tests (e.g., Tohari et al. 2007; Ahmadi-adli et al. 2017, Islam et al. 2022), and numerical simulations (Yubonchit et al. 2017; Lee et al. 2009) to explore slope failure mechanisms and establish criteria for impending failures. Traditional indicators encompass excessive strain development, ground shifting, rising water levels, advancing wetting fronts, and surface cracking or loosening. Abrupt changes in any of these factors signal imminent slope

failure, and the associated rainfall event is deemed critical. These parameters can be monitored through field instrumentation, although widespread implementation across highway slopes might be hindered by instrumentation and monitoring costs.

An alternative approach to determining failure criteria involves conducting numerical studies incorporating precipitation effects. Researchers have conducted uncoupled (e.g., Rahardjo et al. 2017) and coupled (Yubonchi et al. 2016; Griffiths and Lu 2005) seepage and slope stability analyses to ascertain the time required for slope failure under different conditions. A key conceptual distinction between saturated and unsaturated soil shear strength lies in the additional shear strength induced by soil matric suction. Finite element method (FEM)-based software such as SEEP/W, PLAXIS 2D PlaxFlow, SVFLUX, and Geo5 are commonly used for seepage analyses. Slope stability analyses can be performed using Limit Equilibrium (LE) methods (Bishop 1955; Morgenstern-Price 1965; Spencer 1967), Finite Element Method (FEM) (Duncan and Dunlop 1969; Griffiths and Lu 2005; Le et al. 2015), and probabilistic methods (Tang et al. 1976; Duncan 2000; Griffiths and Fenton 2004; Griffiths et al. 2006). Recent advancements in software, like SLOPE/W, include transient seepage and deformation analysis, allowing incorporation of variable soil parameters. Uncoupled analyses (seepage and slope, and deformation and slope) have gained popularity for transient analyses.

To mitigate the impact of rainfall-induced slope failures and associated damages, the development of a warning system that provides authorities with advance alerts for precautions is crucial. Researchers have devised empirical models (Caine 1980; Aleotti 2004; Guzzetti et al. 2007, 2020; Brand et al. 1984; Wilson et al. 1993; He et al. 2019; Bordoni et al. 2019) and physically based models (Fusco et al. 2019; Bordoni et al., 2019) to predict the likelihood of slope failure preceding rainfall events. Empirical methods rely on simple statistical correlations, such as

rainfall intensity-duration (ID) thresholds, between slope failures and rainfall events. While straightforward and user-friendly, these models have limitations in accounting for soil properties, spatial conditions, and slope geometry. Physically based models establish a link between slope failure and rainfall events by solving complex mathematical equations that represent the slope's physical processes. The factor of safety (FS) calculated from the model reflects the slope's stability, with values above unity indicating stability and values below unity indicating instability. Required timeframes for initiating slope failure can be determined through numerical analyses. Consequently, rainfall intensity-duration thresholds or criteria are formulated based on the results.

1.2 PROBLEM STATEMENT

Highway Slope, built on high plastic expansive soil, experience recurrent failure due to cyclic weather conditions. In Texas, most of the highway slopes are built on expansive soil containing Montmorillonite clay which is very vulnerable to cyclic weather loading. The Texas Department of Transportation (TxDOT) spends millions of dollars to repair the failed slopes and for annual maintenance along the state roads and highways. Moreover, it hampers regular mobility and causes time loss for the commuters. The maintenance and repairing cost can be minimized by taking early precautions against slope failure. To take precautions, it is necessary to develop an early warning system which can an effective measure to reduce the financial loss.

The occurrence of slope failure depends on various external factors such as rainfall, recurring vibrations from traffic, freezing and thawing etc. and on internal factors such as soil mechanical and hydraulic properties (Bhandari et al. 2022, Islam et al. 2021). In most cases, prolonged rainfall or excessive rainfall for a short period are the reasons for shallow slope failure. Rainwater infiltrates through the surface cracks formed during dry season and generates pore water pressure which decreases matric suction. From wet to dry season, it occurs in a circle and the soil

loses its shear strength and failure occurs (Islam et al. 2023). Antecedent rainfall (the rain falls in the days immediately preceding a slope failure) and rainfall patterns are essential factors in rainfall-induced slope instability (Rahimi et al., 2011; Rahardjo et al., 2008; Ng et al., 2001).

Generally, early warning system thresholds are developed based on empirical methods such as critical cumulative rainfall (Campbell 1975) or rainfall intensity (Caine 1980; Brand et al. 1984; Larsen and Simon 1993; Marchi et al. 2002; Aleotti 2004; Guzzetti et al. 2007). However, from previous literature it was observed that the impact of slope failure can be much stronger for a site with a comparatively less amount of rainfall. Most warning systems use empirical thresholds, which are developed based on statistical analyses of historical landslide and rainfall data without incorporating the geotechnical and hydrogeological components. Pradel and Raad (1993) showed that slopes made of clayey soils are more prone to failure. Therefore, it is necessary to consider the rainfall impact on topography (Chae et al. 2011) and hence, it is important to evaluate the physical properties of the soil and develop a physical threshold for the slope failure.

A method for slope-failure monitoring can be based on the observation of the Hydraulic properties of soil and its changes over time at shallow depth. Several studies show the numerical modeling and analysis of physical parameters to develop a threshold (Islam, 2021). However, a comprehensive field study is required to assess the hydraulic properties, the process of rainwater infiltration, the behaviors of soil cracks, and the mechanism of rainfall-induced slope failures. Therefore, in this study, an early warning criterion shall be developed based In-Situ hydraulic conductivity. And corresponding volumetric water content shall be incorporated with rainfall data. Numerical modeling shall be further done using the site-specific value to assess the reliability of the field study.

1.3 RESEARCH OBJECTIVES

The objective of the study is to develop an early warning system based on Hydraulic properties of the soil for rainfall-induced slope failure. The specific tasks, performed to achieve the objective of this research work is as follows:

1. Selection and preliminary investigation of the field study area.
2. Perform laboratory testing of Geo-physical properties.
3. Field instrumentation.
4. Monitor in-situ hydraulic conductivity of the study area using the Guelph Permeameter and Mini-Disk Infiltrometer.
5. Determine a prediction model based on In-situ hydraulic conductivity.
6. Perform an analytical study to determine the threshold hydraulic conductivity.
7. Numerical model of the slope failure using site-specific data and calibration with field monitoring result.
8. Develop an early warning system based on field monitoring data and numerical study.

1.4 DISSERTATION ORGANIZATION

Chapter 1 describes the background, problem statement, and objectives of the research. It's the total dissertation "in a nutshell". Chapter 1 is followed by an extensive literature review presented in Chapter 2. Chapter 3 includes the selection of the test sites and performing field investigation, field instrumentation and laboratory testing. The rest of the dissertation is divided into four papers. The first paper describes the process and monitoring of the in-situ hydraulic conductivity. It includes the seasonal variation of hydraulic conductivity on the surface and also at two feet depth. This chapter describes the relationship of rainfall pattern, volumetric water content, soil temperature with hydraulic conductivity. In the second paper, a prediction model was

developed and validated based on the monitoring data. The third paper covers the analytical solution of in situ hydraulic conductivity based on laboratory testing and field monitoring data. The final paper includes the numerical study based on the field hydraulic conductivity and the parametric study was followed to develop the early warning system in this chapter.

CHAPTER 2

LITERATURE REVIEW

2.1 INTRODUCTION

Slope failures occurring in unsaturated soils situated on expansive clay are commonly instigated by rainwater infiltration, particularly during wet periods. The infiltration of rainwater into a soil slope acts as a trigger for instability by altering the soil's moisture distribution and subsequently modifying the matric suction. Unsaturated expansive clay encounters elevated matric suction during dry intervals, contributing to an augmentation in the soil's shear strength. However, during prolonged wet spells, the soil's moisture content rises, leading to a reduction in matric suction. The extra shear strength bolstered by matric suction diminishes as moisture content increases, ultimately resulting in slope failure.

Furthermore, slopes established on high plasticity expansive clay face a risk of strength reduction due to cycles of wetting and drying, predominantly confined to the uppermost meters of the slope. Hence, it is imperative to pinpoint this moisture fluctuation zone, often referred to as the active zone. Alongside this, comprehending the field infiltration behavior and changes in shear strength is vital for accurately predicting the reaction and stability of earth slopes constructed on expansive clay when confronted with rainfall events.

Over the past two decades, significant strides have been taken to grasp the field infiltration behavior and shear strength characteristics of unsaturated soil. These endeavors will be extensively discussed in the forthcoming chapter.

2.2 SLOPE FAILURE

Slope failures are recurrent phenomena in soil mechanics. These failures are typically observed following prolonged episodes of rainfall, which induce a reduction in soil strength (Titi and Helwany, 2007). While slope failures can sometimes manifest warning signs beforehand, they can also occur abruptly without any prior indication. The stability of slopes is characterized by the equilibrium between the resisting forces provided by the shear strength of the soil and the gravitational forces attempting to displace the soil mass downhill. Hence, the stability of a slope is contingent upon the equilibrium between these driving and resisting forces. Disruptions in this equilibrium can lead to a loss of slope stability and eventual slope failure. Amplification of driving forces can stem from alterations in slope geometry, variations in seepage pressure, or the imposition of additional loads from traffic on highway embankments (Titi and Helwany, 2007). Conversely, the decline in resisting forces can transpire due to heightened pore water pressure, as water accumulates on impermeable underlying soil strata.

Slope failures manifest when the soil mass between the slope surface and the slip surface begins to migrate downward. As outlined by Titi and Helwany (2007), the extent of soil movement and the depth of the slip surface are contingent upon factors such as soil type, soil layering, slope geometry, and the presence of water. Abramson et al. (2002) categorized typical slide configurations in clay soils, encompassing translational, plane or wedge surfaces, circular slides, noncircular slides, and hybrids of these types. These various categories of slope failure types are visually depicted in Figure 2.1.

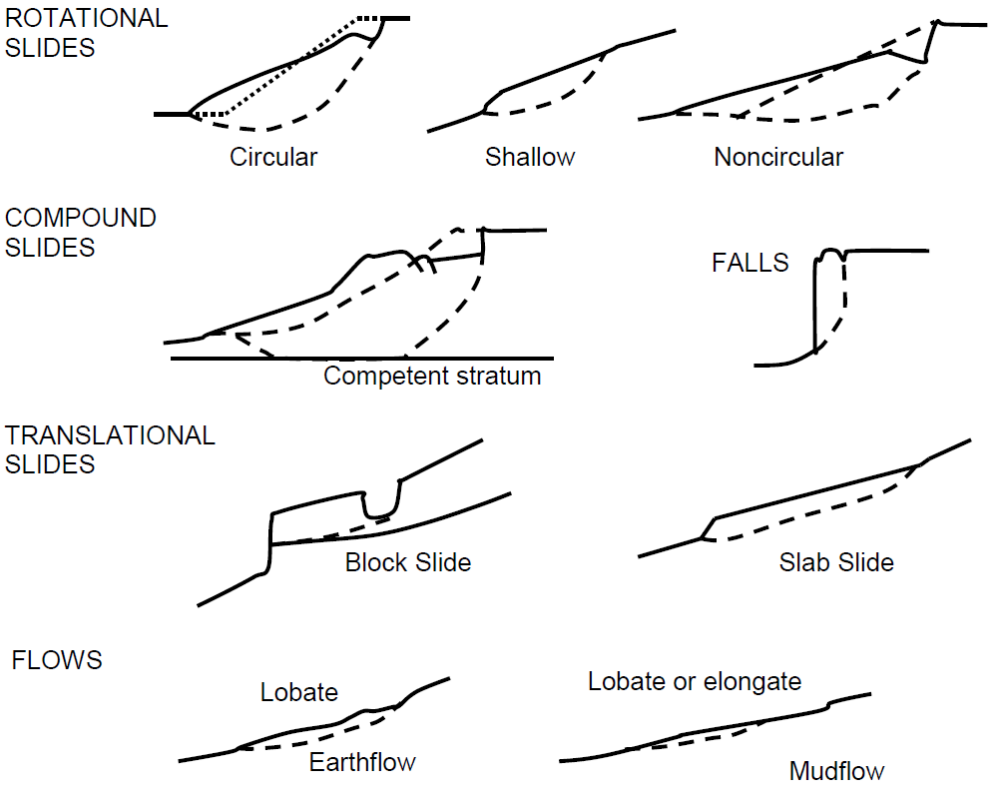

Figure 2.1 Types of Soil movement (after Abramson et al., 2002)

The factor of safety for a slope is determined by comparing the available shear strength along a potential sliding plane with the equilibrium shear stress necessary to uphold a slope that is just stable. This factor of safety is presumed to remain constant along the slip surface and can be defined in terms of stresses (both total and effective), forces, and moments. The choice of a suitable factor of safety for a standard slope design is influenced by several variables, including the quality and precision of soil data, the expertise of the design engineer and contractor, the extent of construction monitoring, and the potential consequences of slope failure (associated risk level) (Titi and Helwany, 2007). For most conventional slope designs, the recommended factor of safety typically falls within the range of 1.25 to 1.50 (Abramson et al., 2002).

2.3 SHALLOW SLOPE FAILURE

Across the United States, surficial slope failures are a frequent occurrence. Shallow slope failure specifically pertains to surface-level instabilities observed along highway cut and fill slopes as well as embankments. These instances of instability are particularly prevalent in fine-grained soils, especially in the aftermath of extended periods of rainfall. The term "surficial failure" implies that these failures remain shallow, with the failure plane typically situated at depths of 4 feet or less (Day, R. W., 1989). In many instances, the failure plane runs parallel to the slope face, as depicted in Figure 2.2.

While shallow slope failures usually do not pose a direct threat to human life or result in significant damages, they can pose risks to infrastructure. These risks encompass damage to guardrails, shoulders, road surfaces, drainage structures, utility poles, and slope landscaping (Titi and Helwany, 2007). Occasionally, debris resulting from shallow slope failures might obstruct highway pavements, impacting regular traffic flow. Furthermore, these failures can have economic implications for local and district-level highway agencies. Typically, repairs for shallow slope failures are undertaken at the local or district levels and often executed by maintenance crews as part of routine maintenance tasks (Islam 2022). It's worth noting that such repairs may offer a temporary resolution, as shallow slope failures often recur following a period of rainfall (Titi and Helwany, 2007).

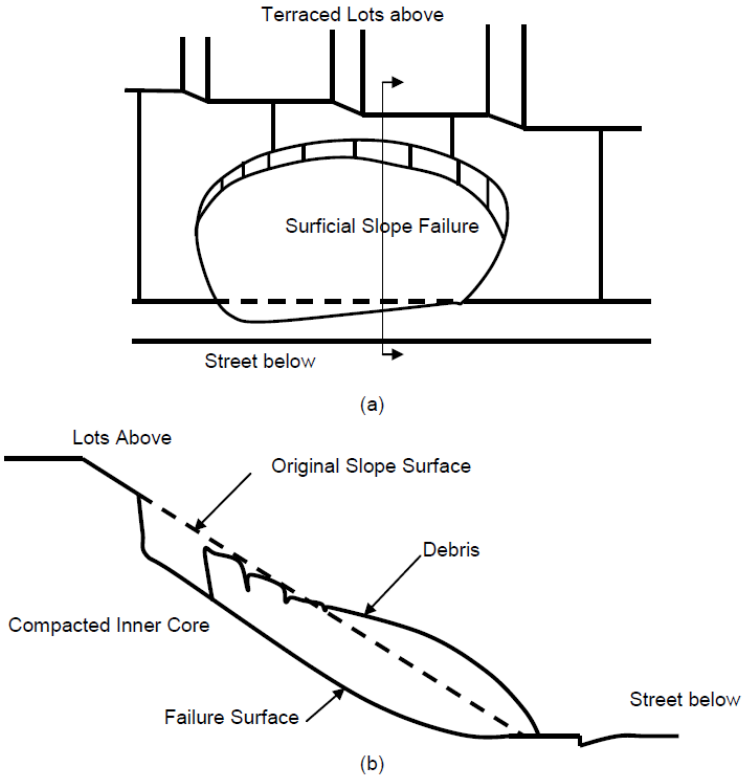

Figure 2.2 General shallow slope failures (redrawn after Day, R. W. 1989)

In general, the characteristics of shallow slope failures exhibit variability in terms of both depth and the extent of the affected area. These attributes are primarily contingent upon factors such as slope geometry, soil composition, soil saturation levels, seepage conditions, and prevailing climatic conditions (Titi and Helwany, 2007). According to Abramson et al. (2002), numerous instances of shallow slope failure arise when the intensity of rainfall surpasses the soil's infiltration rate, and this rainfall endures long enough to saturate the slope to a certain depth, thereby causing an accumulation of pore water pressure at that specific depth.

These slope failures often manifest parallel to the slope surface and are typically characterized as infinite slope failures. Different depths have been reported in literature based on case studies, although all these investigations indicate the shallow nature of surficial failures.

Evans (1972), cited in Titi and Helwany (2007), established the depth of failure surfaces for shallow slopes to be equal to or less than 4 feet. According to Loehr et al. (2000), shallow slope failures are defined as depths less than 10 feet, although they typically range between 3 to 6 feet. Titi and Helwany (2007) suggest that the recommended range for shallow failure depth is approximately 2 to 4 feet.

Changes in climate patterns can have adverse effects on slopes. During the summer, the upper layer of soil tends to dry out, and over prolonged periods with minimal rainfall, the depth of the dry soil zone gradually expands. This period might be characterized by the emergence of significant surficial cracks, which serve as preferential pathways for rainwater flow. The variation in water content typically remains confined to the surface soil layers, with relatively consistent conditions below the zone affected by annual fluctuations. This phenomenon is illustrated schematically in Figure 2.3, where an "active zone" is depicted, indicating a region of relatively uniform water content. The area following the active zone could be considered as an impermeable layer, and the soil is anticipated to lose its cohesion within the zone of moisture variation. The cyclical alterations in rainfall and temperature over seasons can contribute to the gradual loss of strength in expansive clay soils over time (Islam et al. 2021, Islam et al. 2022). Rainfall serves as the primary means of increasing moisture within the slope, thereby creating a saturation zone. Rainwater seeps through the voids and cracks and it is necessary to determine the rate of seepage in different seasons and sense the permeability or hydraulic conductivity of the soil and therefore predict the chances of slope failure.

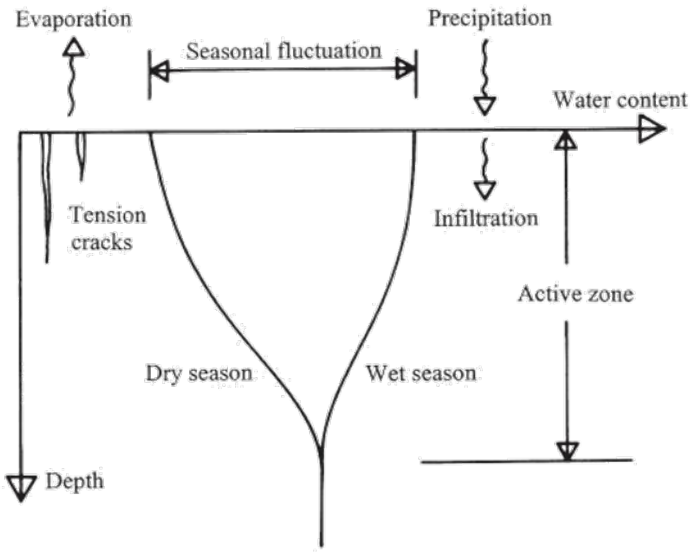

Figure 2.3 Seasonal water content variation with depth in unsaturated expansive soil (Lu and Likos, 2004)

2.4 FULLY SOFTENED CONDITION OF HIGH PLASTIC CLAY SOIL

Slopes with a moderate to steep incline, constructed on high plasticity clay, are particularly vulnerable to the softening effect occurring in the uppermost soil layer due to the alternating wet-dry cycles. This phenomenon leads to the gradual development of fully softened shear strength in the high plastic clay soil over time, a concept explored by Wright (S. G., 2005). The notion of fully softened strength was initially introduced by Skempton (1977) for both natural and excavated slopes within the context of the London Clays. Skempton's work revealed that the strength of slopes in the highly plastic London Clay diminishes over time, eventually reaching a state he termed "fully-softened" strength. This strength level falls between the peak and residual shear strength values, as depicted in Figure 2.3. Skempton (1977) emphasized that the fully-softened strength is comparable to the shear strength exhibited by the soil when in a normally consolidated state.

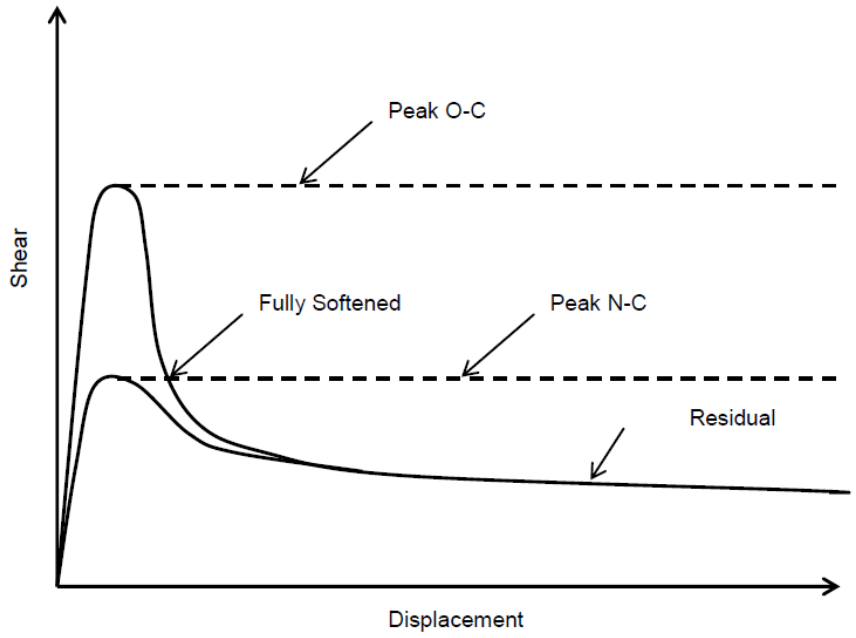

Figure 2.4 Comparisons of peak, residual and fully softened shear strength (redrawn after Skempton, 1970)

In a research endeavor by Rogers and Wright (1986), an investigation was conducted to delve into the failure mechanisms of slopes constructed atop highly plastic clay soil in the Texas region. The study noted that the pronounced high plasticity of the clays involved unique shrink-swell characteristics, rendering them susceptible to the effects of repeated wetting and drying in the field. This cyclic behavior potentially contributed to the soil's softening. To comprehensively examine this phenomenon, Rogers and Wright (1986) carried out direct shear tests on specimens extracted from the Scott Street and I. H. 610 site in Houston, Texas. This particular soil was identified as red clay.

In their experimentation, the researchers conducted four distinct series of drained direct shear tests on soil specimens that had undergone varying numbers of wetting and drying cycles,

specifically 1, 3, 9, and 30 cycles. The results of these tests yielded shear strength parameters, which are concisely summarized in Table 2.1.

Table 2.1 Summary of Shear Strength Parameters from drained direct shear tests on specimens subjected to wetting and drying cycles (Rogers and Wright, 1986)

Number of wet-dry cycles	**Cohesion, c (psf)**	**Friction angle, Φ**
1	29	23º
3	77	26º
9	33	25º
30	0	27º

Rogers and Wright (1986) observed that cyclic wetting and drying of soil resulted in a considerable reduction in shear strength, particularly in terms of the effective cohesion intercept, denoted as c'. Their direct shear tests further indicated that this decline in cohesion occurred within a relatively limited number of wetting and drying cycles. Strikingly, a significant portion of the strength loss transpired during the initial cycles. Despite this, the researchers pointed out that the wetting and drying conditions imposed on the specimens in the laboratory were more severe compared to those typically encountered during field cycles. Nevertheless, they emphasized that the effects of wetting and drying in both laboratory and field settings were believed to be analogous.

In a subsequent study, Kayyal and Wright (1991) introduced an innovative approach for testing triaxial specimens subjected to repeated cycles of wetting and drying. This novel procedure

facilitated greater moisture exposure and drying for the specimens, while also accommodating substantial lateral expansion and volume change during the drying process. The study focused on two distinct soil types: the Red clay (Beaumont clay) from Houston, Texas, and highly plastic clay soil from Paris, Texas.

Kayyal and Wright (1991) conducted a series of consolidated undrained compression tests with pore pressure measurements. These tests were performed on specimens subjected to repeated wetting and drying cycles, as well as on freshly compacted samples. The results yielded shear strength envelopes for both the Beaumont clay and Paris clay specimens, in their as-compacted conditions and after wetting and drying cycles. The graphical presentation of these envelopes is depicted in Figure 2.4. Notably, both envelopes exhibited distinct nonlinearity. Furthermore, the strength envelope for specimens subjected to wetting and drying cycles consistently lay below the envelope for specimens tested in their as-compacted state, particularly at lower levels of normal stress. Additionally, the intercept of the strength envelope for specimens exposed to wetting and drying was relatively small and could be considered negligible.

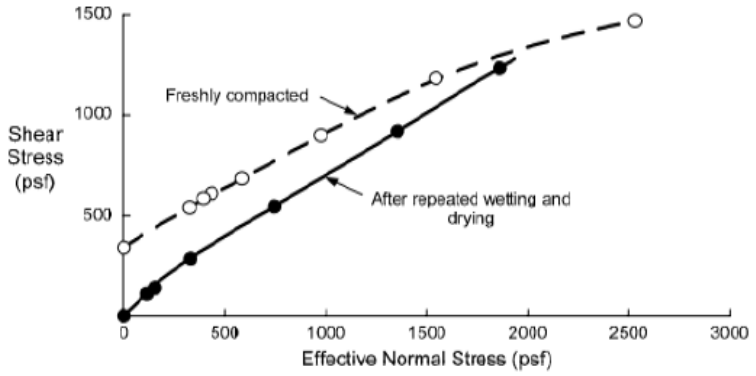

(a)

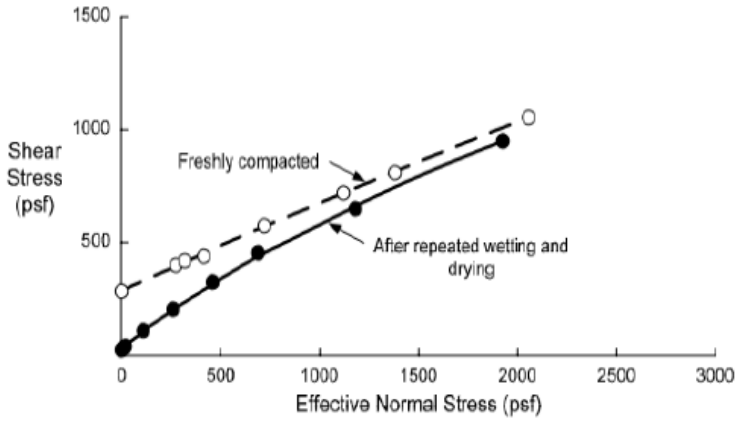

(b)

Figure 2.5 Shear strength envelopes in terms of effective stress a. Beaumont clay, b. Paris clay (Kayyal and Wright, 1991)

2.5 UNSATURATED SOIL MECHANICS

2.5.1 Unsaturated Soil Properties

Unsaturated soil mechanics is a branch of soil mechanics that deals with the behavior of soils that are not fully saturated with water. It focuses on the mechanical properties and behavior of soils in a partially saturated state, where both air and water occupy the pore spaces within the soil.

The main difference between unsaturated soil mechanics and saturated soil mechanics lies in the presence of air and water in the soil pores. In saturated soil mechanics, the soil is completely filled with water, and the behavior of the soil is primarily governed by the properties and interactions of water molecules. The flow of water through the soil, known as seepage, is a key factor in saturated soil mechanics. In saturated soil mechanics, the stress state variable is called the effective stress and is expressed as:

$$\sigma' = \sigma - u_w$$

where, σ' = effective normal stress, σ = total normal stress and u_w = pore water pressure

The promoter pressure is positive in saturated conditions. However, unlike saturated condition, Unsaturated condition is commonly viewed as three phase system such as solid, water and air as shown in Figure 2.6.

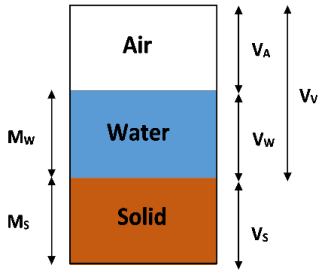

Figure 2.6 The phase diagram in unsaturated condition

In the realm of unsaturated soil mechanics, the presence of both air and water introduces a host of new complexities. The interplay between the air-water interface and the interactions involving soil particles, air, and water plays a pivotal role in shaping the behavior of unsaturated soils. Notably, the concept of air-water interfaces or contractile skins has been put forth as a potential fourth phase, as highlighted by Fredlund and Morgenstern (1977). In the context of unsaturated soil, this contractile skin experiences an air pressure denoted as u_a, which surpasses the corresponding water pressure, u_w. This pressure disparity gives rise to the development of a stress component known as matric suction (u_a-u_w). This contractile skin, which experiences a higher air pressure (u_a) than water pressure (u_w), within an unsaturated soil is depicted in Figure 2.7.

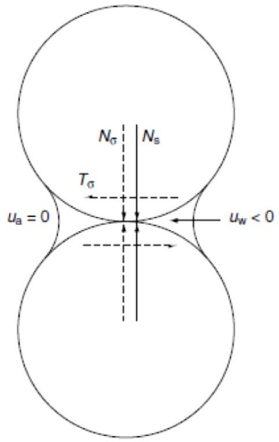

Figure 2.7 Influence of external stress and suction on inter-particleforces (Ng and Menzies, 2007)

Burdland and Ridley (1982) pointed out that changes in external stress, σ, do not necessarily translate into changes in suction, and the two stress systems have quite distinct mechanical effects. As a result, there are fundamental differences in how they are transmitted through the soil. And the point of particle contact, external stress applied to the boundary of the soil element produces both normal and tangential forces. In contrast the capillary effect resulting from suction increases only the normal forces at particle contacts and adds an additional bonding force.

Key concepts in unsaturated soil mechanics include soil-water characteristic curve, which describes the relationship between the degree of saturation and the soil's water content, and soil suction, which quantifies the attractive forces between soil particles and water. These concepts help in understanding and predicting the behavior of unsaturated soils under different conditions, such as changes in moisture content, drying and wetting cycles, and changes in stress levels.

Unsaturated soil mechanics finds applications in various engineering fields, such as geotechnical engineering, agricultural engineering, and environmental engineering. It is particularly important in the analysis and design of slopes, foundations, embankments, and other structures that interact with partially saturated soils.

Terzaghi (1943) presented the Mohr-Coulomb shear strength theory in terms of effective stresses, (σ-u_w) for a saturated soil.

$$\tau = c' + (\sigma - u_w) \tan\Phi'$$

Where, τ = shear strength of soil (kPa), c' = effective cohesion (kPa), (σ-u_w) = effectives stress (kPa) and ϕ' = effective friction angle (^{o})

In 1977, Fredlund and Morgenstern introduced constitutive equations designed for unsaturated soils. These equations were developed as an expansion of the constitutive equations originally intended for saturated soils. The purpose of these equations is to define how shear strength or volume change in soils is influenced by two distinct stress state variables. Interestingly, these constitutive equations exhibit a seamless shift towards the constitutive equations applicable to saturated soils, as the degree of saturation approaches 100% or the matric suction diminishes.

$$\tau = c' + (u_a - u_w) \tan\Phi^b + (\sigma - u_a) \tan\Phi'$$

$$c = c' + (u_a - u_w) \tan\Phi^b$$

Where, ($\sigma - u_w$) = net normal stress(kPa), ($u_a - u_w$) = matric suction (kPa), c = total cohesion and ϕ^b = angle indicating the rate of increase in shear strength with respect to a change in matric suction (^{o}).

In 2010, Goh and colleagues introduced an equation designed to predict the shear strength of unsaturated soil during both drying and wetting conditions. They made an assumption that the soil's shear strength is directly proportional to the matric suction in a linear manner, and this proportionality holds true when the matric suction is lower than the air-entry value. In cases where the matric suction surpasses the air-entry value, the connection between shear strength and matric suction becomes nonlinear. This nonlinearity is characterized by an escalating logarithmic discrepancy between the matric suction and the soil's air-entry value as the matric suction continues to rise.

$$\tau = c' + (\sigma - u_a)\tan\phi' + (u_a - u_w)\tan\phi^b \quad if\ (u_a - u_w) \le AEV$$

Where:

$\phi^b = \phi'$

$$\tau = c' + \left[(\sigma - u_a) + AEV\right]\tan\phi' + \left[(u_a - u_w) - AEV\right] b\Theta^{\kappa}\tan\phi'$$

$$if\ (u_a - u_w) > AEV$$

Where:

$$\kappa = \left[\log(u_a - u_w) - \log AEV\right]^y$$

$$y_d = 0.502\ln(PI + 2.7) - 0.387$$

$$b_d = -0.245\left\{\ln\left[n_d(PI + 4.4)\right]\right\}^2 + 2.114\left\{\ln\left[n_d(PI + 4.4)\right]\right\} - 3.522$$

2.5.2 Unsaturated Hydraulic Conductivity

Hydraulic conductivity, also known as permeability, is a fundamental property of porous media that measures its ability to transmit fluids. It is a critical parameter in hydrogeology and is commonly used to characterize the flow of groundwater through aquifers or the movement of fluids through soil.

The parameter commonly denoted as "K," hydraulic conductivity, signifies the constant of proportionality linking the fluid flow velocity in a permeable material to the hydraulic gradient. This gradient represents the alteration in hydraulic head (pressure) for each unit of distance along the pathway of flow.

The characteristics of saturated hydraulic behavior outline the maximum attainable water flow rate across a soil under a specific energy state. In scenarios of intense rainfall, the covering system might encounter either excessive water accumulation beyond its capacity or a state of complete saturation. The movement of water under saturated conditions adheres to the fundamental principle established by Darcy. In accordance with Darcy's law, the rate of water flow "Q" through a soil follows the expression:

$$Q = K_s \times \Delta H / L \times A$$

Where, Ks = saturated hydraulic conductivity, ΔH = difference in hydraulic potential, L = length of flow path through the cover and A = cross sectional area of the cover through which flow occurs. Figure 2.8 shows the concept of water flow through the saturated condition.

Figure 2.8 Water flow through the saturated condition (after TerraGIS)

Saturated flow arises when the pores within soil become completely filled with water. In soil structures where there exist extensive and uninterrupted pores, the speed of saturated flow can be substantial, particularly when prompted by notable disparities in both gravitational forces and pressure.

Conditions of saturated flow manifest in aquifers, which are strata of sediment and rock capable of holding water, as well as in waterlogged soil and in the lower layers of soil with restricted drainage capabilities. Even in well-drained soil, the upper layers located above stratified clay and topsoil horizons can become saturated shortly following heavy episodes of rain or irrigation. During this process, as gravitational water partially evacuates from sizeable water-saturated pores, these spaces become occupied by sizable air pockets, thereby leading to a significant reduction in the rate of water flow.

It's worth noting that substantial water transfer does not notably occur from minor water-filled pores to larger air-filled pores. The movement of water from a layer with fine texture (such as Clay Loam) to one with coarser texture (like Sand) transpires at a sluggish pace, particularly except when water potentials approach saturation, resulting in relatively unimpeded water flow. Indicative values of saturated hydraulic conductivity (K_{sat}) for various soil texture classes are shown in the table below.

Table 2.2 saturated hydraulic conductivity (K_{sat}) for various soil texture classes.

Soil Texture Class	**K_{sat} (mm/hr)**	**K_{sat} class**
Coarse Sand	360	Very Rapid
Sand	208	Rapid
Loamy Sand	61	Rapid

Loam Fine Sandy	36	Moderately Rapid
Sandy Loam	26	Moderately Rapid
Fine Sandy Loam	19	Moderately Rapid
Loam	13	Moderate
Silt Loam	7	Moderate
Silt	7	Moderate
Sandy Clay Loam	4	Moderately Slow
Clay Loam	2	Moderately Slow
Silty Clay Loam	1.5	Moderately Slow
Sandy Clay	1.2	Slow
Silty Clay	0.9	Slow
Clay	0.6	Very Slow

The Kozeny-Carman Prediction Model for K_{sat} efforts to predict the hydraulic turn soil structure attributes such as porosity, particle size etc. The idea was to evaluate the obvious connection between water flow and the distribution of solids and pore spaces in the soil medium. In 1927, was any introduced a model relating hydraulic conductivity to porosity.

$$K_s = k\,(\frac{\rho g}{\eta})$$

Where, k = permeability, ρ = liquid density, η = viscosity co-efficient of the liquid, g = acceleration of gravity.

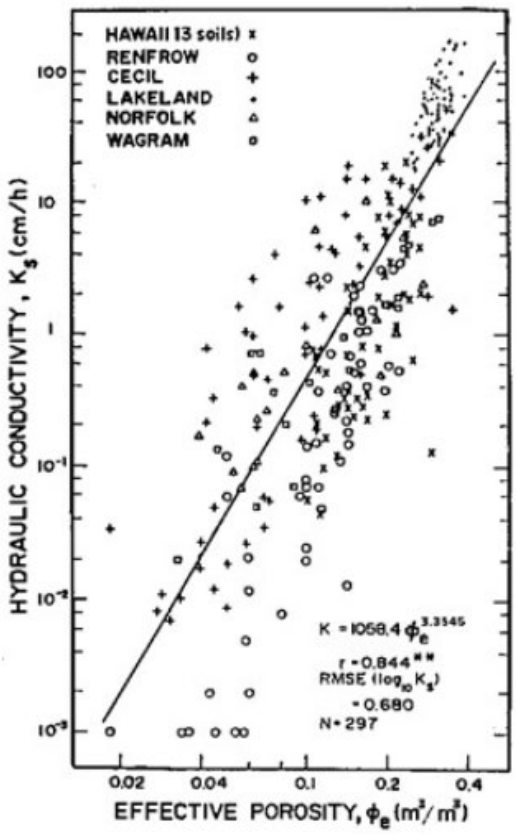

Figure 2.9 Relation between soil hydraulic conductivity and porosity

However, the Kozeny-Carman approach provides unsatisfactory estimates of hydraulic conductivity due to its assumption of uniform pore radius. It works well for sands and other materials with uniform pore sizes.

Flow of water in such rich soil is commonly described using Darcy's law, which can also be applied to unsaturated soil (Richards 1931; Fredlund and Rahardjo 1993).

$$-\frac{\partial \theta_w}{\partial t} = \frac{\partial}{\partial x}\left(K\frac{\partial h}{\partial x}\right) + \frac{\partial}{\partial y}\left(K\frac{\partial h}{\partial y}\right) + \frac{\partial}{\partial z}\left(K\frac{\partial h}{\partial y}\right)$$

In the context of the three-dimensional Cartesian coordinates (x, y, z), where θw represents volumetric water content, K denotes unsaturated hydraulic conductivity, and h stands for total

height, significant disparities exist between the flow of water in saturated and unsaturated soils. These discrepancies arise due to two fundamental factors.

Firstly, the capacity of unsaturated soils to retain water is subject to variation based on the soil suction, as characterized by the soil water characteristic curve (SWCC). Secondly, unlike in saturated soils, the primary coefficient in unsaturated soils isn't a constant value; rather, it fluctuates according to the metric section opening, as outlined by the work of Fredlund and Rahardjo in 1993.

In the scenario of water moving through pore spaces filled with water, the situation shifts when the soil transitions to an unsaturated state. In this case, air starts replacing some of the water within larger pores, prompting water to navigate through smaller pores. This alteration results in a heightened tortuosity of the flow path, as elucidated by Ng and Menzies in 2007. As soil matric suction increases, the volume of pores containing water diminishes further. Consequently, the coefficient of permeability pertaining to the water phase experiences a rapid decrease as the available area for water flow becomes limited. This concept is visually demonstrated in Figure 2.9.

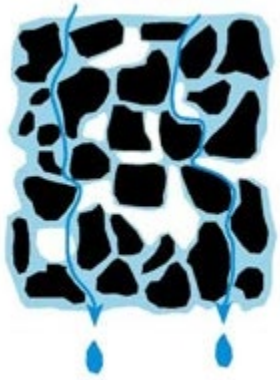

Figure 2.10 The flow of water in unsaturated condition (TerraGIS)

In the unsaturated soil, moisture in the soil pores is in tension, and the pressure is referred to as the negative pore water pressure or soil suction (ψ).

The concept of soil suction is important in unsaturated hydraulic conductivity. Figure 2.11 shows a conceptual illustration of suction, with the water pressure in a capillary tube below and above the free water surface. The water pressure below the free water surface is positive and increases with depth. In the capillary tube, water is held by capillary forces which is the negative pressure, or suction. ψ is a function of radius (r) of the capillary tube. Mathematically ψ is expressed in the form of the following equation.

$$\psi = 2\sigma\cos\beta/r$$

Like the illustration, in the water balance cover, water is retained in the soil due to the action of capillary forces which develop suction in the soil. Adsorptive forces between the water molecules and the surface of the solid particles also contribute to retaining water in the unsaturated soil of the water balance cover.

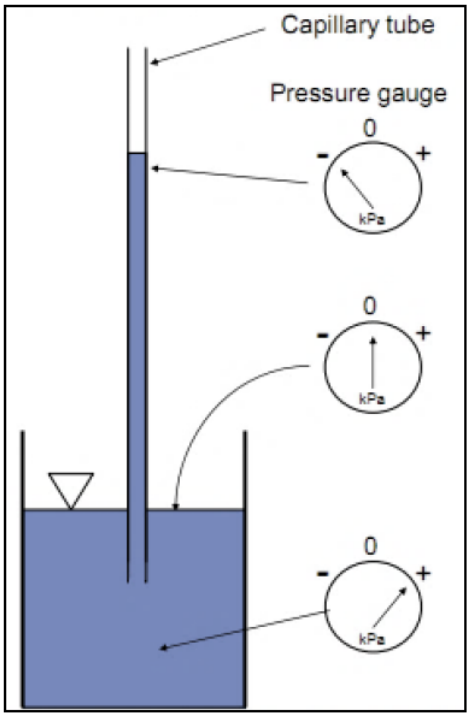

Figure 2.11 Soil Suction Concept (Albright et al., 2004)

Soil suction is inversely proportional to the volumetric moisture content (θ). θ is defined as the volume of water per total volume of soil. It decreases when the applied forces are large enough to overcome the capillary forces; therefore, the moisture content decreases as the suction on the pore water increases. Conversely, when the suction is reduced, the moisture content increases, and water fills larger pores.

2.5.3 Soil-Water Characteristics Curve (SWCC)

A soil water characteristic (SWC) curve delineates the quantity of water retained within a soil under equilibrium conditions at a given matric potential. This retention is expressed either as mass or volume water content (θm or θv). The SWC curve holds a pivotal hydraulic characteristic, as it offers insights into the extent and connectivity of pore spaces within the soil. Consequently, it is substantially influenced by factors such as soil texture, structural composition, and additional

constituents like organic matter. The comprehension of the SWC is of paramount importance when modeling water distribution and movement in partially-saturated soils. This understanding plays a critical role in effective water management and in predicting the transport of solutes and contaminants within the environment.

Typically, the SWC exhibits a highly nonlinear behavior and is comparatively challenging to accurately determine. Given that the range of water contents encountered in practical scenarios spans several orders of magnitude in matric potential, it is common to depict the matric potential on a logarithmic scale. Figure 1 visually portrays representative SWC curves for soils with different textures. The graph illustrates the impacts of porosity (or saturated water content) as well as the varying slopes of the relationships, resulting from diverse pore size distributions. These relationships are illuminated by the research of Tuller and Dani in 2003.

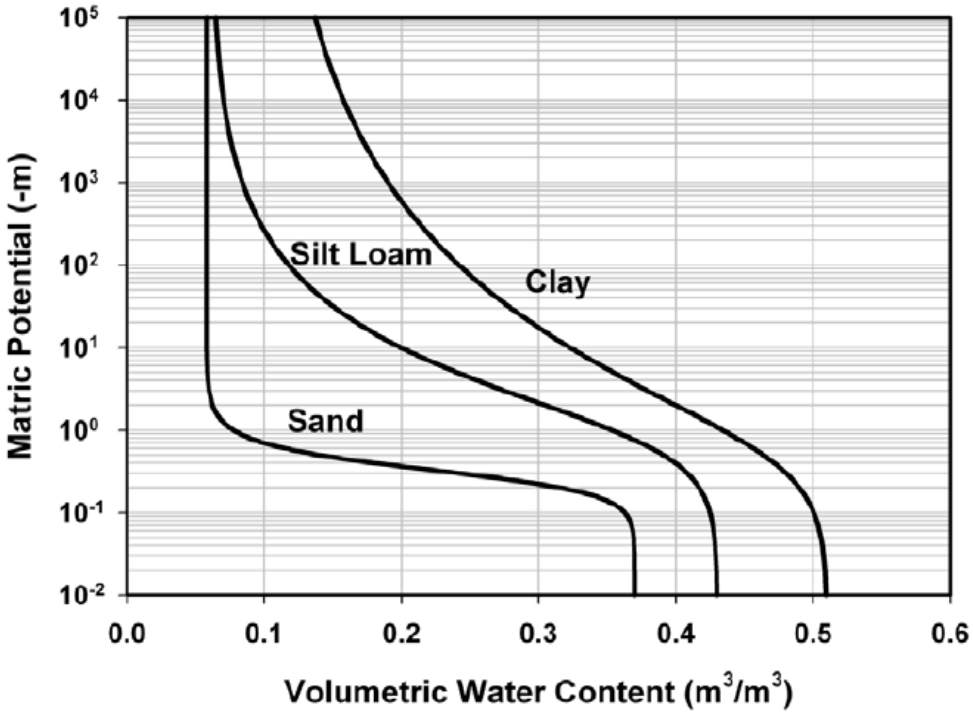

Figure 2.12 Typical soil water characteristic curves for soils of different texture.

Several terms exist in the literature to describe the Soil Water Characteristic Curve (SWCC), including Water Retention Curve (WRC), Soil Suction Curve, and Soil Moisture Release Curve, as highlighted by Kovacs (1981) and Aubertin et al. (2003). In this paper, the term SWCC is utilized when examining the relationship between soil suction and water content, derived from the same soil specimen. Conversely, if this connection is established using the soil suction of multiple remolded samples possessing varying water content, it is termed the Suction-Water Content Relationship (SWR), as noted by Malaya and Sreedeep (2010).

A SWCC acquired through the desaturation (desorption) or saturation (adsorption) of a soil sample, respectively, during drying or wetting processes is termed a desaturation or saturation curve. Fig. 1 displays typical drying and wetting SWCCs, illustrating a continuous S-shaped relationship characterized by hysteresis. Due to this hysteresis phenomenon, the suction value for a specific water content is greater in a drying curve compared to a wetting curve, as noted by Birle et al. (2008).

Key points pertinent to the SWCC are as follows:

1. The volumetric water content at saturation, θs, represents the water content when the soil is entirely saturated. This denotes the starting point of the drying path.

2. The Air-Entry Value (AEV), ψa, signifies the suction at which air first enters the largest pore within the soil sample during a drying process, following the formulation by Brooks and Corey (1964).

3. The Residual Water Content, θr, denotes the minimum water content below which no significant alteration in θ occurs concerning ψ. The corresponding suction to θr is termed the Residual Soil Suction, ψr, according to Yang et al. (2004).

4. The Water-Entry Value, ψw, on the wetting SWCC is defined as the suction point at which water content experiences a substantial increase during the wetting process, in accordance with the findings of Birle et al. (2008).).

A fully saturated soil specimen having a volumetric water content of θ_s desaturates in three stages, as depicted in Figure 2.13.

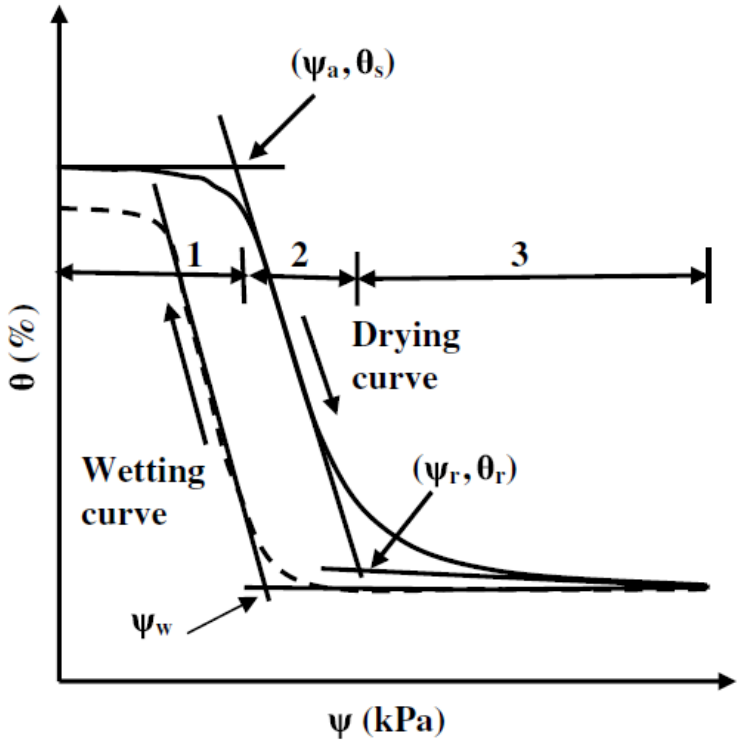

Figure 2.13 Idealized Soil Water Characteristics Curve (after Malaya and Sandeep 2012)

2.5.3.1 Influence of Suction Measurement Methodologies and Procedures on the SWCC

As detailed in the preceding section, the methodologies and procedures employed for measuring suction can significantly impact the Soil Water Characteristic Curve (SWCC). A study conducted by Nam et al. (2009) explored this by comparing SWCCs of four natural soils through six different methods: filter paper, dew point potentiometer, vapor equilibrium, pressure plate, Tempe cell, and osmotic techniques. Notably, this study utilized relative humidity and the axis translation method, which operate on distinct principles. Agus and Schanz (2005) also examined measurement methods—noncontact filter paper, psychrometer, relative humidity sensor, and chilled mirror hygrometer—all rooted in the concept of relative humidity. The chilled-mirror hygrometer method emerged as the most accurate and consistent among them.

In the comparison of methodologies, the filter paper method yielded results akin to the chilled-mirror hygrometer method when using soil samples of the same age. The psychrometer method exhibited slower response and measured lower total suction compared to the chilled-mirror hygrometer technique. Sreedeep and Singh (2011) demonstrated the impact of measurement methods on SWCCs of two fine-grained soils. Some instruments gauge soil suction under zero stress conditions (e.g., tensiometer and relative humidity method), while others operate under nonzero stress conditions (e.g., air pressure induced in a pressure plate setup). It remains unclear whether the applied stress condition, influenced by measurement methodology, ambiguously affects the SWCC.

Vanapalli et al. (1999) noted differences in the SWR (Suction-Water Content Relationship) obtained for clay till via continuous drying suction measurement and via remolded soil samples packed at varying compaction states, mainly dependent on initial molding water content. Graham

et al. (2001) found the SWR to exhibit significantly lower suction values than the SWCC. Malaya and Sreedeep (2010) confirmed this observation for higher water content, with less disparity between SWR and SWCC at lower water content. Blatz et al. (2002) observed non-similarity between SWCCs and SWRs of sand-bentonite material. However, alignment between SWCC and SWR occurred for soil samples with the same dry density and within a lower range of suction. Lourenco et al. (2009) emphasized the impact of response time, loss of contact, and soil type on high suction tensiometric measurements using continuous and discrete measurement methods. Fredlund (2002) highlighted variations in SWCCs obtained from compacted and slurried soil samples. Nevertheless, the influence of measurement methodology (imposed air pressure) on such findings remains unclear. Khoury and Miller (2008) revealed negligible effects of sample height on the SWCC of silty soil. Reduced sample height led to shorter SWCC establishment times. The SWCC obtained for swelling clay under no-volume-change condition differed from that of a compacted sample with volume-change condition (Delage et al. 1998).

Further research is necessary to quantify the variations in SWCC attributed to volume change in diverse types of swelling soils. Additionally, assessing the impact of measurement methodology and procedures on unsaturated behavior modeling could provide insights into the significance of these influences for different soil types..

2.5.3.2 Influence of Stress History on SWCC

According to Fredlund (1964) and Vanapalli et al. (1999), discernible discrepancies in the Soil Water Characteristic Curve (SWCC) are attributed to stress history, especially at low levels of suction. Remarkably, the Air-Entry Value (AEV) has been found to remain consistent irrespective of the preconsolidation pressure. Nevertheless, it's worth noting that the suction

capacity diminishes as the overconsolidation ratio (OCR) increases. Delage and Lefebvre (1984) employed mercury intrusion porosimetry to demonstrate that AEV increases with the preconsolidation pressure. Kawai et al. (2000) and Lee et al. (2005) observed a reduction in both AEV and the slope of the SWCC as the consolidation pressure on the soil sample grows.

Thu et al. (2007) discovered that both AEV and yield suction of the soil specimen escalate as the net confining stress rises. Yield suction refers to the matric suction point on the SWCC where the volume or degree of saturation of the soil specimen experiences a rapid decline, as outlined by Alonso et al. (1990). Notably, the slope of the drying SWCC beyond the yield stress and the wetting SWCC show no dependency on the net confining stress. The impact of varying confining stress on the SWCC is most significant within the low range of matric suction, where the soil's macropore and capillary forces predominantly operate (Gens and Alonso 1992).

Rassam and Williams (1999) have proposed a shear-strength model that factors in the influence of confining stress on the Air-Entry Value (AEV), adding to the understanding of how stress conditions impact the SWCC.Influence of Range of Measured Suction Data on the SWCC

Zapata et al. (2000) illustrated the impact of varying the number of suction data points and the extent of suction measurements on the determination of the Soil Water Characteristic Curve (SWCC). Their study revealed that even as few as three data points suffice to provide a solid representation of the complete SWCC for sandy soils. Furthermore, they observed that the variability in the SWCC stemming from different measured suction ranges amplifies with higher proportions of fine particles in the soil. This means that coarse soils exhibit a narrower range of suction variation, whereas fine-grained soils demonstrate greater variation, necessitating a greater number of measured points for accurately defining the SWCC.

Shah et al. (2006) explored the fitting equations for SWCCs of fine-grained soils based on data from pressure membrane extractor (ranging from 0 to 1,500 kPa) and dew point potentiometer (ranging from 0 to 80,000 kPa). They found that the SWCC fitting equations derived from pressure membrane extractor data showcased discrepancies beyond 1,500 kPa suction, whereas the fitted equations from dew point potentiometer data exhibited minimal deviations up to 105 kPa suction. This study underlines the influence of the range of measured suction data on the accuracy of the SWCC.

Nam et al. (2009) reported that the fitting equations by Fredlund and Xing (1994) and van Genuchten (1980) yield nearly identical SWCCs, except for high suction values. Conversely, the fitting equation proposed by Houston et al. (2006) exhibited significant deviations from experimental data beyond 1,500 kPa suction. Zapata et al. (2000) conducted a comparative analysis by fitting seven different SWCC equations to experimental data from three distinct soil types. Among the four-parameter SWCC equations, the van Genuchten (1980) equation demonstrated the most robust performance, while the Fredlund and Xing (1994) equation with a correction factor of "1" performed the best among the three-parameter equations. They also observed substantial discrepancies near the Air-Entry Value (AEV) for all soils when employing the Brooks and Corey (1964) equation.

2.5.3.3 Apparent Factors Influencing SWCC

The suction associated with a specific volumetric water content tends to increase as the soil type becomes progressively finer. This phenomenon can be attributed to the heightened presence of adsorptive and capillary forces within fine soil particles, resulting from their elevated surface area and smaller intraparticle pore spaces, as emphasized by Fredlund (2000) and Aubertin et al.

(2003). Gallage and Uchimura (2010) observed that the Air-Entry Value (AEV), residual suction, and hysteresis decrease as the effective size (D10) of the soil increases. Jotisankasa (2005) suggests that at low-suction ranges (0–100 kPa), the SWCC is primarily influenced by soil structure, while at higher suction levels, the composition and specific surface area of the soil play a more prominent role. This observation indicates that the SWCC becomes less dependent on soil fabric and more distinct at higher suction ranges (Jotisankasa et al. 2010). For highly structured soils, a multimodal SWCC is considered more suitable, as indicated by Camapum de Carvalho et al. (2002). Burger and Shackelford (2001) specifically noted the occurrence of a bimodal SWCC for naturally aggregated soils containing both microporosity and macroporosity. Cousin et al. (2003) highlighted the influence of rock fragments on the SWCC, revealing that disregarding rock fragments in calcareous soil can overestimate available water content (AWC) by up to 39%. The AWC for porous chalk surpasses 90%, whereas it's zero for basalt fragments (Poesen and Lavee 1994). A critical assessment by Baetens et al. (2009) underscores the significant influence of rock fragments, especially on the near-saturation portion of the SWCC.

As anticipated, soil suction increases with the plasticity of the soil (Marinho and Chandler 1993; Zapata et al. 2000). The study by Marinho and Chandler (1993) establishes a positive correlation between the liquid limit and suction capacity (C) for compacted and normally consolidated soils, where C represents the slope of the SWCC. Soils with a liquid limit exceeding 25% can be approximated by a straight-line SWCC for suctions ranging from 100 to 1,000 kPa. This suggests the potential use of a linearized SWCC for a specific range of suction variations, thus simplifying unsaturated soil modeling. The void ratio of the soil significantly impacts the AEV, where it generally decreases with an increase in void ratio (Vanapalli 1994; Peron et al. 2007). Specifically, for a given void ratio, the AEV is approximately ten times smaller in sand than

in loams (Nuth and Laloui 2008). While the overall shape of the SWCC remains unaffected by void ratio, the curve shifts toward higher suction values with decreasing void ratio. To account for this effect, SWCC models have been proposed to incorporate the influence of void ratio on water retention behavior (Gallipoli et al. 2003; Tarantino 2009). Romero et al. (2001) observed a decrease in total suction with increasing temperature at a particular water content. The temperature influence is more pronounced at low suction levels, attributed to temperature-dependent surface tension, alterations in clay fabric due to thermal disturbances, and changes in intra-aggregate fluid chemistry.

Regarding hysteresis, the drying SWCC exhibits higher suction for the same water content compared to the wetting SWCC, a result of the hysteresis phenomenon (Fredlund and Rahardjo 1993). Literature offers several interpretations and explanations for the observed hysteresis behavior in unsaturated soil, as elucidated by Fredlund (2000). These points include:

- Inequality in pore size distribution during wetting and drying cycles.
- Presence of trapped air bubbles during wetting, leading to reduced water content.
- Differences in contact angle of meniscus during wetting and drying.
- Swelling, aging, and soil shrinking phenomenon causing differential changes in soil structure.

Under field conditions, the impact of hysteresis is often overshadowed by soil heterogeneity and spatial variability (Canone et al. 2008). However, many researchers advocate for the consideration of appropriate drying or wetting SWCCs, depending on the specific problems, such as simulations of water transfer, solute transport, multiphase flow, and microbial activities

(Kool and Parker 1987; Russo et al. 1989; Heinen and Raats 1997; Mitchel and Mayer 1998; Si and Kachanoski 2000). Canone et al. (2008) suggest that employing a simplified hysteresis model can reduce errors stemming from uncertainties in soil hydraulic parameter values. However, the extent of these uncertainties hinges on the magnitude of hysteresis specific to each soil. Notably, coarse-grained soils exhibit smaller hysteresis than nonuniform, fine-grained soils (Yang et al. 2004). Experimental quantification of hysteresis for various soil types and its influence on unsaturated behavior modeling is a relatively understudied area. Normally consolidated clays or unconsolidated slurries exhibit more hysteresis, with soil samples progressively stiffening and becoming overconsolidated as the number of wet/dry cycles increases, eventually leading to a stable SWCC (Wilding and Tessier 1988; Pessaran 2002; Kodikara et al. 1999). According to Jotisankasa (2005), hysteresis renders the SWCC one of the most uncertain properties of collapsible soil, where the pore size distribution can be significantly influenced by the collapse phenomenon.

2.5.3.4 Empirical SWCC Models

Key requirements for all parametric SWC expressions are parsimony (as few parameters as possible) to simplify parameter estimation, and accurate description of SWC behavior at the limits (wet and dry ends) while closely fitting the nonlinear shape of θ-ψ_m measurements. An effective and commonly used parametric model for relating water content or effective saturation (Θ) to the matric potential was proposed by van Genuchten (1980) and is denoted as VG:

$$\Theta = \frac{\theta - \theta_r}{\theta_s - \theta_r} = [\frac{1}{1 + (\alpha\, \psi_m)^n}]^m$$

Where, θ_r and θ_s are the residual and saturated water contents, respectively, ψ_m is matric potential, and α, n, and m are parameters directly dependent on the shape of the θ(ψ) curve. A common simplification is to assume that m=1-1/n. Thus the parameters required for estimation of the model are θ_r, θ_s, α, and n. θ_s is sometimes known and is easy to measure, leaving only the three unknown parameters θ_r , α and n to be estimated from the experimental data in many cases. Note that θ_s is sometimes taken as θ at -1.5 MPa, θ air dry, or a similar meaningful value, though it is often advantageous to use it as a fitting parameter. Earlier versions of "van Genuchten type" power function models were proposed by Brutsaert (1966) and Ahuja and Swartzendruber (1972). Vogel and Císlerová (1988) and Kosugi (1994) modified aforementioned equation to include the matric potential at the air entry point.

Another well-established parametric model was proposed by Brooks and Corey (1964) and is denoted as BC:

$$\Theta = \frac{\theta - \theta_r}{\theta_s - \theta_r} = \left[\frac{\psi_b}{\psi_m}\right]^{\lambda} \qquad \text{when, } \psi_m > \psi_b$$

$$\text{Or, } \Theta = 1 \qquad \text{when } \psi_m \leq \psi_b$$

where ψ_b is a parameter related to the soil matric potential at air entry (b represents "bubbling pressure"), and λ is related to the soil pore size distribution. Matric potentials are expressed as positive quantities (i.e., in absolute values) in both VG and BC parametric expressions. Campbell (1974) uses the same power law function as BC to express degree of saturation ($S=\theta/\theta_s$) as a function of the air entry potential ψ_b and a factor b that can be related to soil texture:

$$\frac{\theta}{\theta_s} = [\frac{\psi_b}{\psi_m}]^{\frac{1}{b}}$$

ψ_b and b are derived as functions of the geometric mean diameter and geometric standard deviation of the particle size distribution (Campbell, 1985; Shirazi and Boersma, 1984). Campbell's (1974) expression is often used in relation with the fractal idealization of the soil porous system as discussed below.

Estimation of VG or BC parameters from experimental data requires sufficient data points to characterize the shape of the SWC, and a program to perform non-linear regression. Many computer spreadsheet software packages provide relatively simple and effective mechanisms to perform nonlinear regression. Details of the computational steps required for fitting a SWC to experimental data using commercially available spreadsheet software are given in Wraith and Or (1998). In addition, computer programs for estimation of specific parametric models are also available, e.g., the RETC code (van Genuchten et al., 1991). Figure 2.14 depicts fitted parametric van Genuchten (VG) and Brooks and Corey (BC) models to silt loam $\theta(\psi)$ data measured by Or et al. (1991). The resulting best-fit parameters for the VG model are: α =0.417 m-1; n=1.75; θ_s =0.513 m^3/m^3; and θ_r =0.05 m^3/m^3 (with r2=0.99). For the BC model the best-fit parameters are: λ =0.54; ψ_b=1.48 m; θ_s =0.513 m3/m3; and θ_r =0.03 m^3/m^3 (with r^2=0.98). Note that the most striking difference between the VG and the BC models is in the discontinuity at $\psi = \psi_b$ for BC.

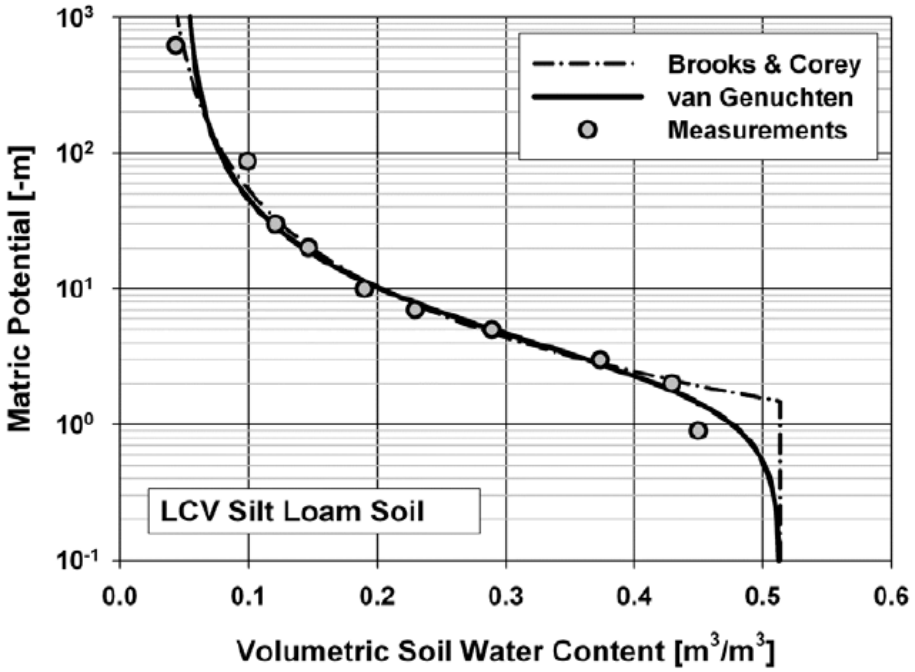

Figure 2.14 Van Genuchten (VG) and Brooks and Corey (BC) parametric models fitted t0 measured data for silt loam soil

A comprehensive collection of soil water retention and unsaturated hydraulic conductivity data, fitting the van Genuchten (VG) model, is accessible through the UNSODA (Leij et al., 1996) computer database compiled by the U.S. Salinity Laboratory. This extensive database incorporates information from diverse soil textures across the globe. While the authors have incorporated certain measures indicating the data's quality or reliability, users are advised to apply their own experience and judgment when adapting such data to their specific applications.

Extensive regression studies conducted by McCuen et al. (1981) and Rawls and Brakensiek (1989) offer a valuable resource concerning parameter values for the Brooks-Corey model across various soils. These studies include the estimation of hydraulic parameters based on other soil properties that are often more readily available. Such estimates might prove sufficiently accurate for specific applications, providing a preliminary approximation. Table 1 presents compiled values

for van Genuchten model parameters α and n, along with residual and saturated water contents, for different soil textural classes. It's important to acknowledge that significant variations in soil water retention relationships can be expected within given soil textural classes.

Table 2.3 Typical van Genuchten model parameters (α, n) including residual (θ_r) and saturated (θ_s) water contents compiled from the UNSODA database (Leij et al., 1996). N indicates the number of soils or samples of a given textural class from which the mean values are compiled.

Textural Class	N	θ_r [cm^3/cm^3]	θ_s [cm^3/cm^3]	α [1/cm]	n
Sand	126	0.058	0.37	0.035	3.19
Loamy Sand	51	0.074	0.39	0.035	2.39
Sandy Loam	78	0.067	0.37	0.021	1.61
Loam	61	0.083	0.46	0.025	1.31
Silt	3	0.123	0.48	0.006	1.53
Silt Loam	101	0.061	0.43	0.012	1.39
Sandy Clay Loam	37	0.086	0.40	0.033	1.49
Clay Loam	23	0.129	0.47	0.030	1.37
Silty Clay Loam	20	0.098	0.55	0.027	1.41
Silty Clay	12	0.163	0.47	0.023	1.39
Clay	25	0.102	0.51	0.021	1.20

The models discussed thus far fall into the category of empirical curve-fitting functions, characterized by freely adjustable model parameters linked to the specific mathematical shape of the function used, rather than directly reflecting physical characteristics of the porous medium. Notably, Brutsaert (1966) and, more recently, Kosugi (1994, 1996) proposed connections between the Soil Water Characteristic (SWC) and the pore-size distribution, formulated as a statistical log-normal distribution function. These scholars envisioned the soil's porous system as a collection of cylindrical capillaries (referred to as Bundle of Cylindrical Capillaries, or BCC) with radii

distributed according to a log-normal pattern. They leveraged the capillary rise equation to establish a link between matric potential and the effective medium saturation.

However, the applicability of these latter models is constrained to coarse-textured soils and scenarios where capillary forces dominate the matric potential. They tend to encounter limitations in finer textured soils boasting high specific surface areas, such as clay soils. In these cases, adsorptive surface forces come to the fore, particularly under drier conditions, leading to shortcomings in these models' predictions (Tuller and Or 2003)..

2.5.3.5 SWCC using filter paper method

Matric suction was assessed using the filter paper technique (FP), following the procedure advocated by Ridley et al. (2003). According to these authors, this well-established method has demonstrated consistent and reproducible results over numerous years. The procedure encompassed several steps: an initial dry Whatman N. 42 filter paper was placed on both sides of the soil sample, ensuring optimal contact between the paper and the sample. The setup was then enclosed using Plexiglas discs, and the entire assembly was sealed with cling film and tape to maintain airtight conditions. This sealed setup was placed within a closed glass jar and stored in a temperature-controlled environment for a duration of 7 days, allowing for equilibrium to be achieved. Following this period, the filter papers were carefully removed using tweezers and transferred to a sealed container with a lid, a deviation from the original plastic bag approach proposed by Ridley et al. (2003).

To determine water content, the filter papers were weighed using a highly sensitive balance accurate up to 0.0001 g. Subsequently, the filter papers were dried in an oven at a temperature of 110 °C for at least 10 hours, with the oven lid partially open, as per Bulut et al. (2001). The soil

samples were air-dried for a brief period until they reached the desired water content state for the subsequent measurement. This process was repeated iteratively to capture different water content levels. Throughout the entire process of matric suction measurement, the filter paper was consistently handled using tweezers, and efforts were made to promptly place the filter paper within the container. The complete setup of the filter paper technique is visually illustrated in Figure 2.15.

Figure 2.15 Filter paper testing method

The procedure described above for measuring suction was repeated every week until the sample reached an air-dry condition. This occurred when the water content of the filter paper reached equilibrium with the surrounding atmosphere at suction of approximately 30 MPa.

Several relationships between filter paper, water content and suction have been developed for different filter paper brands by different researchers. In the present work, the calibration curve for Whatman N. 42 recommended by ASTM D5298-03 was used. This calibration curve is presented as follows:

$$\text{Log } (\psi) = 5.327 - 0.0779w, \text{ for } w < 45.3\%$$

$$\text{Log } (\psi) = 2.412 - 0.0135w, \text{ for } w \geq 45.3\%$$

Where, ψ = matric suction and w = filter paper water content (%)

2.5.4 Field Variation in SWCC

The hydraulic characteristics of soil can undergo modifications when transitioning from laboratory analysis to real-world field conditions (Albright et al., 2009). The hydraulic properties of soil established through laboratory tests at a particular compaction might diverge in the field environment due to factors such as hysteresis, variations in soil structure due to phenomena like freeze-thaw cycles, wet-dry cycles, and biological intrusion (root growth and decay, burrowing organisms), as well as other soil-forming processes. These processes typically lead to a reduction in soil density and the formation of larger pores. Such alterations in soil structure subsequent to construction are more frequently observed in clayey soils compared to coarse-grained soils, ultimately resulting in decreased water storage capacity.

Albright and Benson (2009) conducted laboratory measurements of the Soil Water Characteristic Curve (SWCC) for various soil samples obtained from ACAP (Advanced Characterization of Alternative Cover Materials) sites. Notably, the conventional SWCC values obtained in the laboratory were lower than those derived from field measurements (as illustrated

in Figure 2.16). In fact, the majority of the laboratory-determined SWCC data points fell below the 1:1 equality line. It was evident that SWCC outcomes obtained from undisturbed soil samples extracted from ACAP test sections during their initial construction significantly differed from samples collected after being exposed to the natural environment for several years (Aurpa et al. 2022, Latif et al. 2023). Benson et al. (2007) demonstrated that the saturated volumetric water content (Θs) has a propensity to increase over time as soil density diminishes, and soils initially placed at higher Θs levels during construction exhibit minor alterations in Θs values as time progresses.

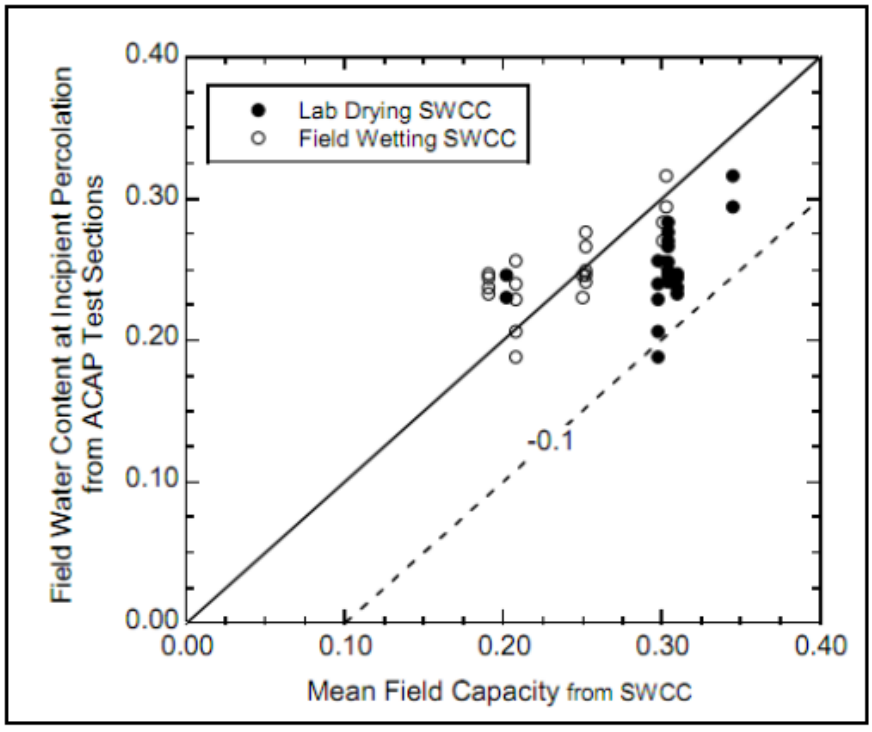

Figure 2.16 Relationship between field capacity water content from SWCCs and the water content at incipient drainage from test section data (Albright et al. 2009)

Over time, the unsaturated hydraulic parameters (α and n) of soils undergo changes due to their exposure to the field environment. Notably, the α parameter tends to increase after a certain

period of field exposure, indicating the development of larger pores within the soil matrix. Conversely, the n parameter generally experiences a decrease at the ACAP sites. Although changes in the n parameter were relatively minor, this is partly due to the inherent range of variability exhibited by n in natural soils.

Utilizing observations regarding alterations in saturated and unsaturated hydraulic parameters across diverse soils at the ACAP sites, Apiwantragoon (2007) formulated a correction approach to facilitate the application of laboratory-based Soil Water Characteristic Curve (SWCC) data in field scenarios. His method involved applying a scaling factor to the van Genuchten (VG) model parameters (α and n) acquired from laboratory derived SWCCs. This adjustment aimed to render the laboratory based SWCC representative of the conditions prevailing in the field environment. Figure 2.17 graphically illustrates the laboratory derived SWCC alongside the SWCC subsequent to the implementation of the correction factor.

For soils with lower plasticity, Apiwantragoon proposed a scaling factor of 1.3, while for high-plasticity soils, a scaling factor of 12.9 was suggested. As for the n parameter, a scaling factor of 1.1 was recommended for less-plastic soils, and a factor of 1.2 was deemed suitable for high-plasticity soils. These corrective factors were designed to bring the laboratory based SWCC data more in line with the actual field conditions, taking into account the evolving hydraulic characteristics of the soils over time.

.

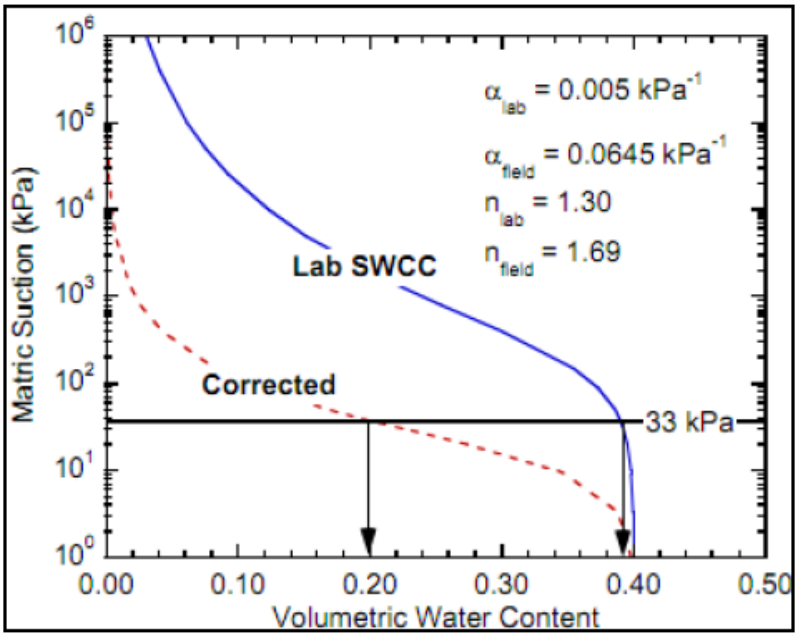

Figure 2.17 Correction procedure applied to a laboratory-based SWCC (Albright 2009)

Figure 2.18 depicts the corrected SWCC, after the scaling factor suggested by Apiwantragoon was applied. Data from field sensors was obtained during the monitoring period for the first two years. The solid line represents the corrected average laboratory SWCC, and the dashed lines correspond to the upper bounds and lower bounds of corrected SWCC from laboratory measurements. A good agreement was found between the field measured SWCCs and the corrected SWCCs. Alam et al. (2017) developed a field-based soil water characteristic curve (FSWCC) to evaluate the percolation of flat and slope section ET cover (Figure 2.18b). Alam et al. (2017) measured the unsaturated hydraulic conductivity based on the FSWCC and assessed percolation relating to the unsaturated hydraulic conductivity. Ahmed et al. (2017) also developed a field-based soil water characteristic curve (FSWCC) to evaluate the moisture distribution in unsaturated subgrade.

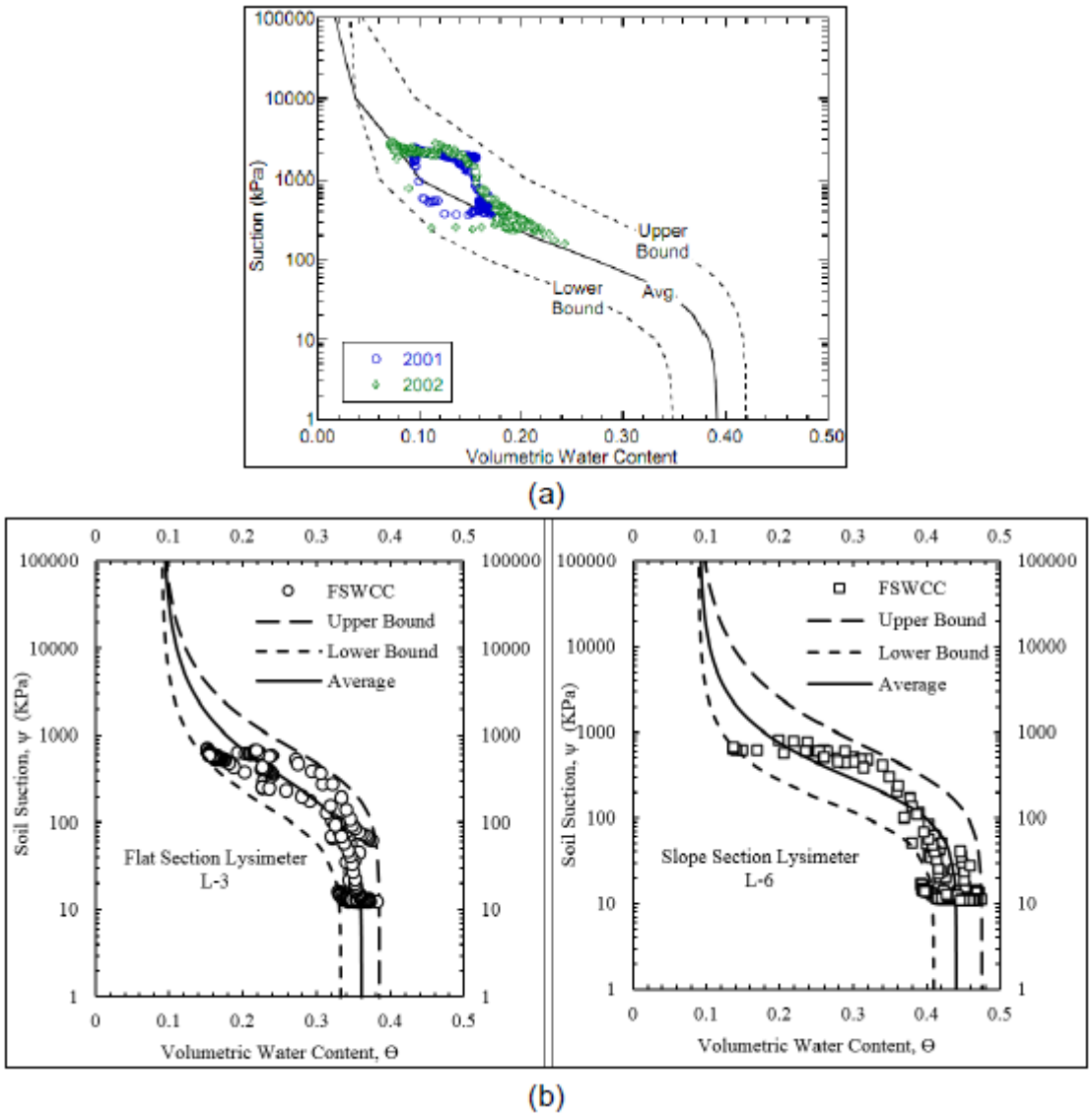

Figure 2.18 (a) Corrected laboratory-measured SWCCs data from co-located sensors in an ACAP site (b) field based SWCC for flat and slope section vegetated lysimeter soil (Alam et al. 2017)

2.6 DETERMINATION OF IN-SITU HYDRAULIC CONDUCTIVITY

The assessment of hydraulic conductivity for soils intended for highway embankments holds significant importance. While it's common to excavate and test soil samples in laboratory settings, evaluating in-situ hydraulic conductivity is essential for accurately gauging its performance in the field. Nevertheless, obtaining dependable results can be challenging, especially when dealing with soils that possess extremely high or low conductivity levels. Additionally, the heterogeneity and anisotropy of the soil can heavily impact the outcomes. Various methods have been developed to measure this soil parameter directly in the field. However, each of these techniques is founded on distinct assumptions concerning the behavior of water flow within the soil medium. In simpler terms, some techniques assume full saturation of the soil, while others presuppose soil isotropy, uniformity, and steady-state flow. The forthcoming sections will elaborate on several of these techniques. (Adapted from Hsin-Yu Shan, DC Watkins et al., 1987).

2.6.1 Guelph Permeameter

This technique capitalizes on Marriotte's principle to determine the saturated hydraulic conductivity of soil. The approach involves conducting a constant-head test, during which the steady-state rate of water recharge from a cylindrical well hole is measured (Reynolds, 1993).

To establish a constant head level within the borehole, adjustments are made to the position of the bottom air-tube located at the center of the permeameter. This manipulation enables water from the reservoir to flow into the borehole, creating a small vacuum above the water level in the reservoir. The vacuum's negative pressure can only be alleviated when bubbles formed due to atmospheric pressure ascend to the reservoir's top. Atmospheric pressure air enters the system through the upper air tube or air inlet tip. As the borehole's water level decreases, air bubbles

emerge and ascend to the vacuumed air space, equalizing the negative pressure and restoring water from the reservoir to the borehole, thereby maintaining a constant head. This equilibrium leads to the formation of a saturation zone or "bulb" around the borehole. Once this saturation zone is fully developed, the flow rate within the water reservoir stabilizes, indicating the determination of the saturated hydraulic conductivity (Reynolds et al., 1986).

Like other permeameters, the Guelph permeameter also relies on the assumptions of isotropic and uniformly saturated soil within the saturation zone, with boundaries extending to infinity. However, it distinguishes itself by offering the ability to measure the matrix flux potential, the α* parameter, and soil sorptivity. Additionally, its tripodal base ensures adaptability to various terrains, such as landfill cover slopes. The instrument's test duration ranges from several hours to a few days, making it suitable for situations involving highly impermeable soil that necessitate multiple tests over a short period. Furthermore, it can assess depths up to 3 feet, providing comprehensive insight into the hydraulic properties of the cover. Although the Guelph permeameter is not suitable for measuring horizontal hydraulic conductivity, its primary function in evaluating vertical hydraulic conductivity aligns well with the critical aspect of landfill cover system performance. Considering these advantages, the Guelph permeameter is the preferred instrument for monthly slope monitoring in the study. Figure 2.19 and Figure 2.20 provides a schematic of the working principles of the Guelph Permeameter.

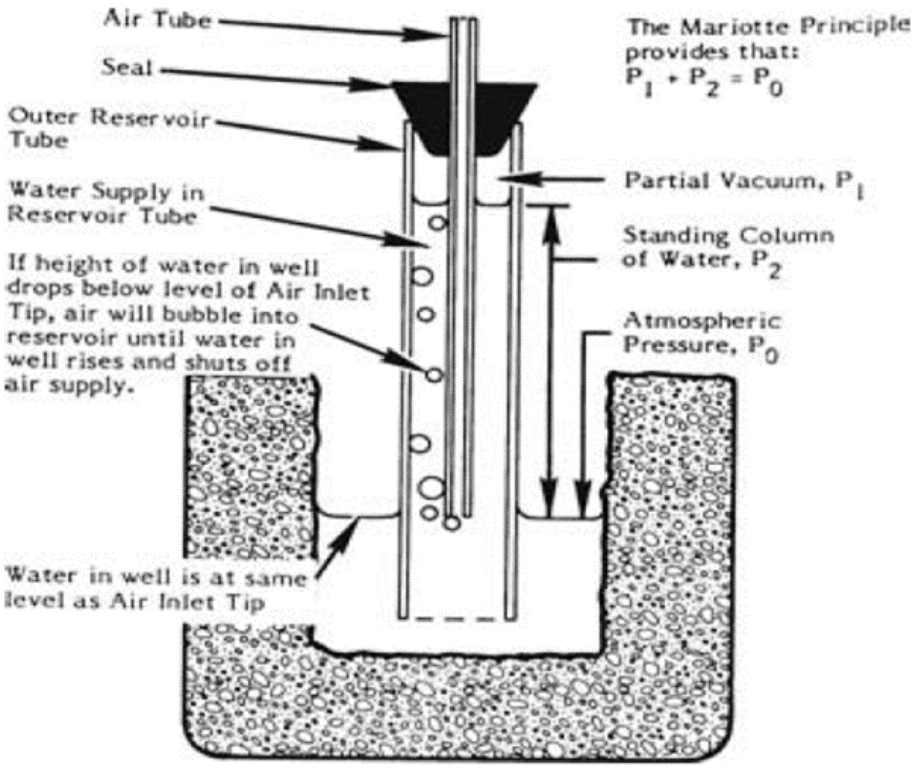

Figure 2.19 In-hole constant head permeameter setup

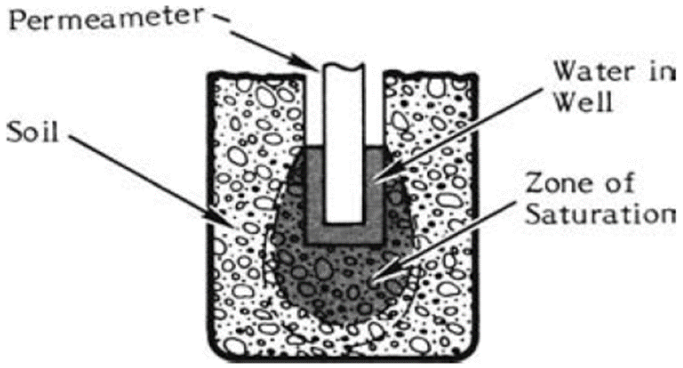

Figure 2.20 Saturated zone around borehole (saturation bulb)

The components of Guelph Permeameter is shown in Figure 2.21.

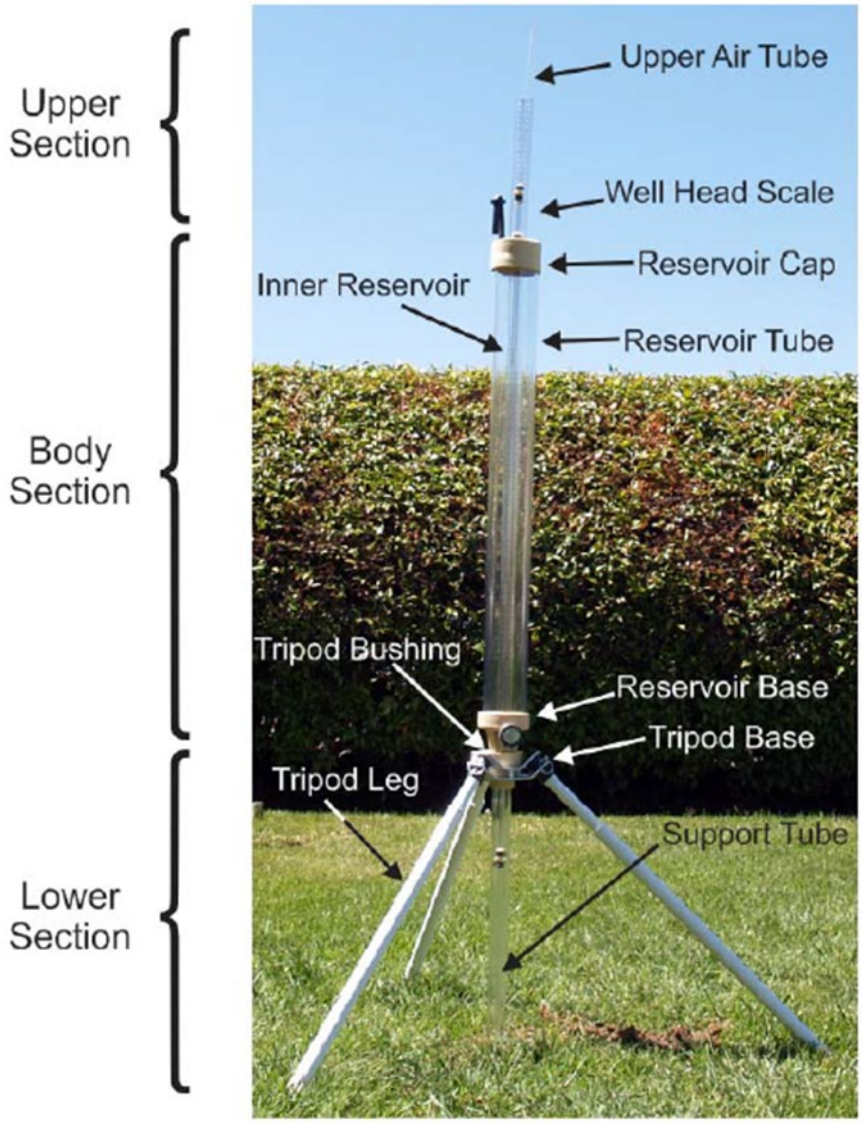

Figure 2.21 Guelph Permeameter main components and field setup

2.6.2 Mini-Disk Infiltrometer

The The Mini Disk Infiltrometer is an ideal tool for conducting field measurements due to its compact size, allowing the necessary water for operation to be easily carried in a personal water bottle. Additionally, it serves practical purposes in laboratory and classroom settings for demonstrating fundamental concepts of unsaturated soil hydraulic conductivity.

The Infiltrometer consists of both upper and lower chambers filled with water. The upper bubble chamber regulates suction, while the lower chamber contains a water volume that infiltrates into the soil at a rate controlled by the selected suction in the bubble chamber. The lower chamber is marked with volume indicators, resembling a graduated cylinder, and features a sintered stainless-steel disk at the bottom that prevents water leakage in open air. The small diameter of this disk enables undisturbed measurements on relatively level soil surfaces.

hen the Infiltrometer is placed on soil, water starts to leave the lower chamber and infiltrate into the soil at a pace dictated by the soil's hydraulic properties. As the water level decreases, its volume is recorded at specific time intervals. The Mini Disk Infiltrometer operates as a tension infiltrometer, gauging the unsaturated hydraulic conductivity of the underlying medium at different applied tensions.

In unsaturated soil, water movement is more complex than in continuously saturated conditions. Air typically occupies macropores, leaving finer pores for water movement. Consequently, hydraulic conductivity heavily depends on pore geometry, water content, and variations in matric potential (Rose, 1966; Brady and Weil, 1999).

The Mini Disk Infiltrometer assesses the hydraulic conductivity of the underlying medium. Its adjustable suction range (0.5 to 7 cm) enables the elimination of macropores with air entry values smaller than the Infiltrometer's suction. This is accomplished by using a slight negative pressure to control infiltration. When water is under tension, it bypasses macropores like cracks or wormholes and instead penetrates further into the soil as determined by the soil's hydraulic forces.

Saturated conductivity occurs when all pores, including larger ones like cracks or wormholes, are filled. However, macropore flow's variability makes it challenging to quantify. Applying tension during infiltration prevents macropores from being filled, resulting in a hydraulic conductivity characteristic of the soil matrix, which exhibits less spatial variability.

Unsaturated soil hydraulic conductivity is influenced by both water potential and water content. The decrease in conductivity as the soil dries is primarily due to air moving into the soil to replace water. This air influx narrows the pathways for water flow between soil particles, making flow more intricate.

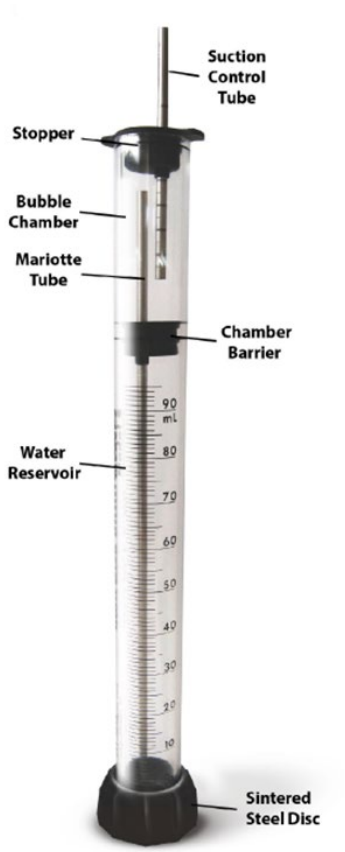

Figure 2.22 Infiltrometer setup and different components

At time zero, the infiltrometer has been placed on the soil surface, assuring that it makes solid contact with the soil surface. The volume of water that infiltrates into the soil has been recorded as a function of time in the record sheet. The procedure has been repeated for a suction head of 0.5 cm set in the MDI. For every repetition, the volume of water (reading in mL) infiltrating into the soil at various intervals of time (in minute) for 1 h is obtained. The square root of time and cumulative infiltration depth (in cm) are calculated. Cumulative infiltration is obtained by dividing the volume of infiltrating water by the area through which water is infiltrating.

A graph is plotted between cumulative infiltration on Y-axis and square root of time on X-axis. The data obtained are then fitted to the two-term equation (Eq. 1) proposed by Zhang (1997a) for describing infiltration under disk infiltrometers and the values of constants C1 and C2 are obtained:

$$I = C_1\sqrt{t} + C_2 t$$

where I is the cumulative infiltration (cm) and t (min) is the time.

Hydraulic conductivity of soil is computed now from the following equation:

$$k = \frac{C_2}{A}$$

where C2 is the slope of the curve of the cumulative infiltration versus the square root of time and A is the value relating the van Genuchten parameters for a given soil type to the suction rate and radius of infiltrometer disk. A is computed from the following equation:

$$A = \frac{11.65\left(n^{0.1}-1\right)\exp\left[2.92\,(n-1.9)\alpha h_0\right]}{(\alpha r_o)^{0.91}} \quad \text{where, } n \geq 1.9$$

$$A = \frac{11.65\,(n^{0.1}-1)\,\exp\,[7.5\,(n-1.9)\alpha h_0]}{(\alpha r_o)^{0.91}} \quad \text{where, } n < 1.9$$

where n and α are the van Genuchten parameters for the soil (Carsel and Parrish 1988), r_o is the disk radius and h_0 is the suction at the disk surface.

2.6.3 Previous studies on determination of hydraulic conductivity

2.6.3.1 Unsaturated Hydraulic Conductivity prediction by Trabelsi and Mabrouk (2018)

In this study a new model was proposed to determine the unsaturated permeability for cracked clay based on the Natural Evaporation Method. The validity and reliability of the model will be evaluated using experimental data to make a comparison with the proposed model. The hydraulic properties of a cracked soil during a drying process change in response to the combination of suction change and cracked volume change. Hence, propagation of cracks will lead to significant change in the coefficient of permeability of the clayey soil and will in turn alter the water infiltration.

First, the evaporation method was used to quantify the hydraulic functions. This method allows the simultaneous measurement of the water retention curve (WRC) and hydraulic conductivity function (HCF) but it contains some limitations, namely the measurement limit of about 70 kPa of the tensiometers and the smaller samples; the cylinder diameter was 80 mm and height 50 mm in Schindler et al. (2010), and the cylinder had a diameter 48 mm and height 50 mm in Garnier et al. (1997).

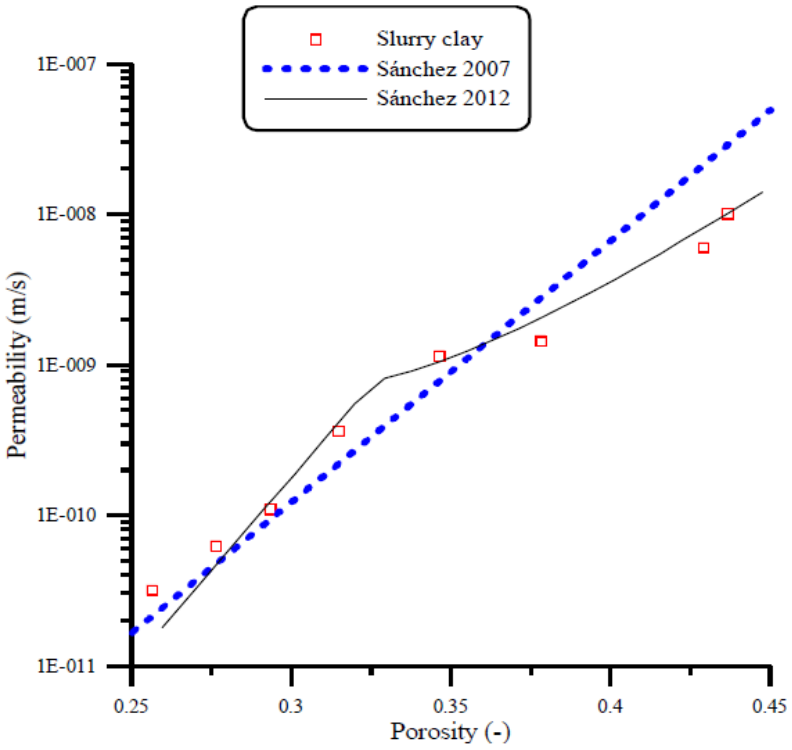

Figure 2.23 Change in saturated permeability as a function of the porosity of slurry clay

The saturated coefficient of permeability is a function of porosity is show in Figure 2.23. The laboratory tests are carried out in a suitably adapted odometer. In the first phase, the sample is saturated, then a hydraulic gradient is applied. The hydraulic head as function of time is evaluated through Darcy law for a falling water head, an exponential law has been fitted to express K_{sat} as a function of porosity.

In Figure 8, water flow is allowed in both domains (matrix and cracks) and the unsaturated flow is controlled by the unsaturated hydraulic conductivity of matrix and cracks domain respectively. We measure the permeability by assuming either hydraulic properties accounting for soil shrinking with a function nc (new model) or a rigid soil with a constant nc (Booth et al. 2014).

The results highlight that cracks connectivity and fissure permeability play an important role in distributing water within a clayey soil. Both the presence of cracks and the change of cracks will significantly affect the hydraulic properties of the cracked soil. The formation of the initial crack is indicated in Figure 2.24. It is well identified that when the suction is more-or-less smaller than the air-entry suction (AEV=360KPa) no desiccation cracks appear.

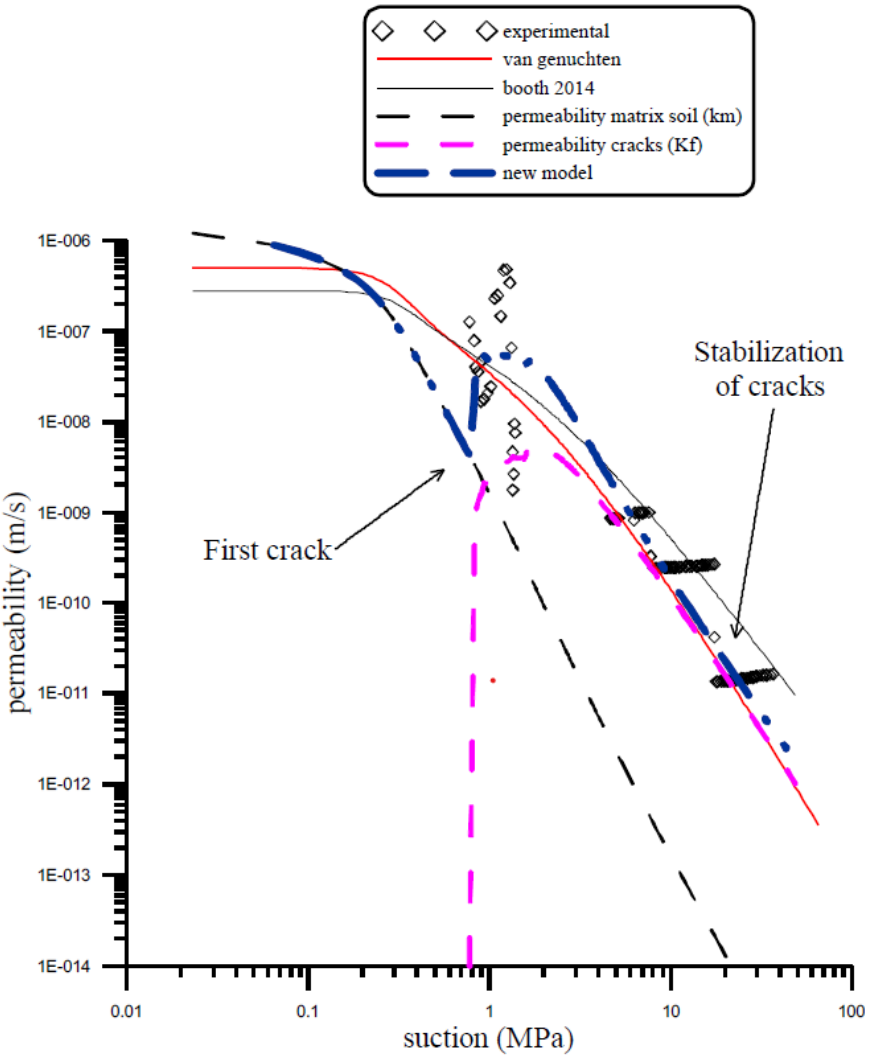

Figure 2.24 variation of unsaturated permeability as a function of the suction of slurry clay and cracked during desiccation.

Here, the first crack appears at a suction around 800 kPa and cracking stabilizes when the cracking no longer changes about 3 MPa. Then, the unsaturated hydraulic conductivity function for cracked clay decreases as the suction increases (or water content decreases) and the hydraulic conductivity remained reasonably the same as the saturated hydraulic conductivity until suction increases to the air-entry value. The results affirm that the permeability is controlled by soil matrix (no cracks appear initially) in the range of low suctions (until reaching AEV) that is generally low. But, when desiccation cracks appear, the permeability of the soil can be dominated by the desiccation cracks and water can flow through the crack network. The new model reproduces well the experimental results.

2.6.3.2 Seasonal variation in field saturated hydraulic conductivity by Messing and Jarvis (1990)

In this study, a simple method (the inversed auger hole method) for measuring field-saturated hydraulic conductivity (K,) was investigated. Measurements were carried out in the spring, summer and autumn at three depths in two Swedish clay soils (Ultuna and Limsta, with clay contents of 45-60%0 and 65-80%, under barley and grass/clover ley respectively). Seasonal fluctuations in Kfs at Limsta were more pronounced and were observed deeper in the profile. This was attributed primarily to larger structural changes due to a higher capacity for swell/shrink (normal shrinkage over the available water range) and an earlier drying up of the soil under grass/clover ley.

Median K_s values for the two soils show that Limsta had lower K_v values than Ultuna in spring and autumn (Table 2.4). In particular, the very low spring values at Limsta (<5 mm h-') reflect the conditions in wet, fully swollen soil. Some of the remaining macropores may have been

smeared by the auger, yielding underestimated K_s values. Thus, the occasional zero-values recorded in the spring at Limsta may reflect negligible infiltration in the clay matrix.

Table 2.4 also shows that at 0.30 m depth K, values at Ultuna and Limsta were respectively one to two, and four orders of magnitude larger in summer than in spring and autumn. This may be attributed to the extensive cracking observed in the surface soil layers during the dry summer period. Large seasonal variations in K_s at 0.5 m depth were apparent only at Limsta. This was presumably owing to a higher capacity for swell/shrink.

Table 2.4 Field saturated hydraulic conductivity for different seasons and depth

Site	Season	Depth (m)	n	Median K_{fs} (mm h^{-1})	[a]s_w (mm h^{-1})	[a]CV_w (%)	[a]w (mm h^{-1})
Ultuna	Spring	0.30	5	34.7	33.2	96	7.7–85.0
		0.50	5	41.1	35.3	86	8.7–90.7
		0.80	5	26.1	38.2	146	20.0–108
	Summer	0.30	5	672	1400	208	67.4–3320
		0.50	5	84.2	35.2	42	49.8–131.6
		0.80	5	60.4	18.3	30	47.3–89.8
	Autumn	0.30[b]	—	—	—	—	—
		0.50	5	45.7	16.0	35	26.9–64.1
		0.80	5	25.3	10.5	42	19.3–43.8
Limsta	Spring	0.30	5	0.0	0.4	200[c]	0.0–1.0
		0.50	5	0.0	1.8	164[c]	0.0–4.3
		0.80	4	2.2	1.1	50	1.2–3.5
	Summer	0.30	5	2680	4280	160	38.5–10 000[d]
		0.50	5	34.8	61.6	177	24.8–168.0
		0.80	5	7.6	6.4	84	3.4–18.2
	Autumn	0.30	5	0.5	1.1	220	0.0–2.9
		0.50	5	0.0	0.9	225[c]	0.0–2.2
		0.80	5	5.8	3.1	53	2.9–10.2

[a]Standard deviation (s_w), coefficient of variation (CV_w) and range (w) as defined in the text. [b]Frozen topsoil. [c]Calculated from anti-logged mean of log K_{fs}. [d]Estimated value. Excessive flow rate.

2.6.3.3 Variability of hydraulic conductivity due to multiple factors by Deb and Shukla (2012)

This study provides a comprehensive review of recent experimental and field investigations focused on the measurement and variability of hydraulic conductivity. It compiles a substantial volume of data available in the literature and delves into potential sources of variability while discussing their implications. Various statistical metrics, such as range, interquartile range, variance, standard deviation, coefficient of variation, skewness, and kurtosis, are employed to express the variability of soil hydraulic conductivity. The study assesses both spatial and temporal variations in hydraulic conductivity and examines how factors like sample support, measurement techniques, soil types, land use, and agricultural practices influence its values.

The research explores disparities in hydraulic conductivity and their changes over time across different land uses (woodland, cropland, pasture, and urban) and soil series (Glenelg, Hagerstown, Joanna, and Morrison) in Pennsylvania. These soil series exhibit diverse textures, structures, and parent materials. Zhou et al. (2008) conducted an investigation at 16 sites encompassing combinations of soil series and land uses. Over the course of May and October from 2004 to 2006, they measured field-saturated and near-saturated hydraulic conductivities using tension infiltrometers. These measurements were taken at various water potentials including -0.12, -0.06, -0.03, -0.02, -0.01, and 0 m. (Figure 2.25).

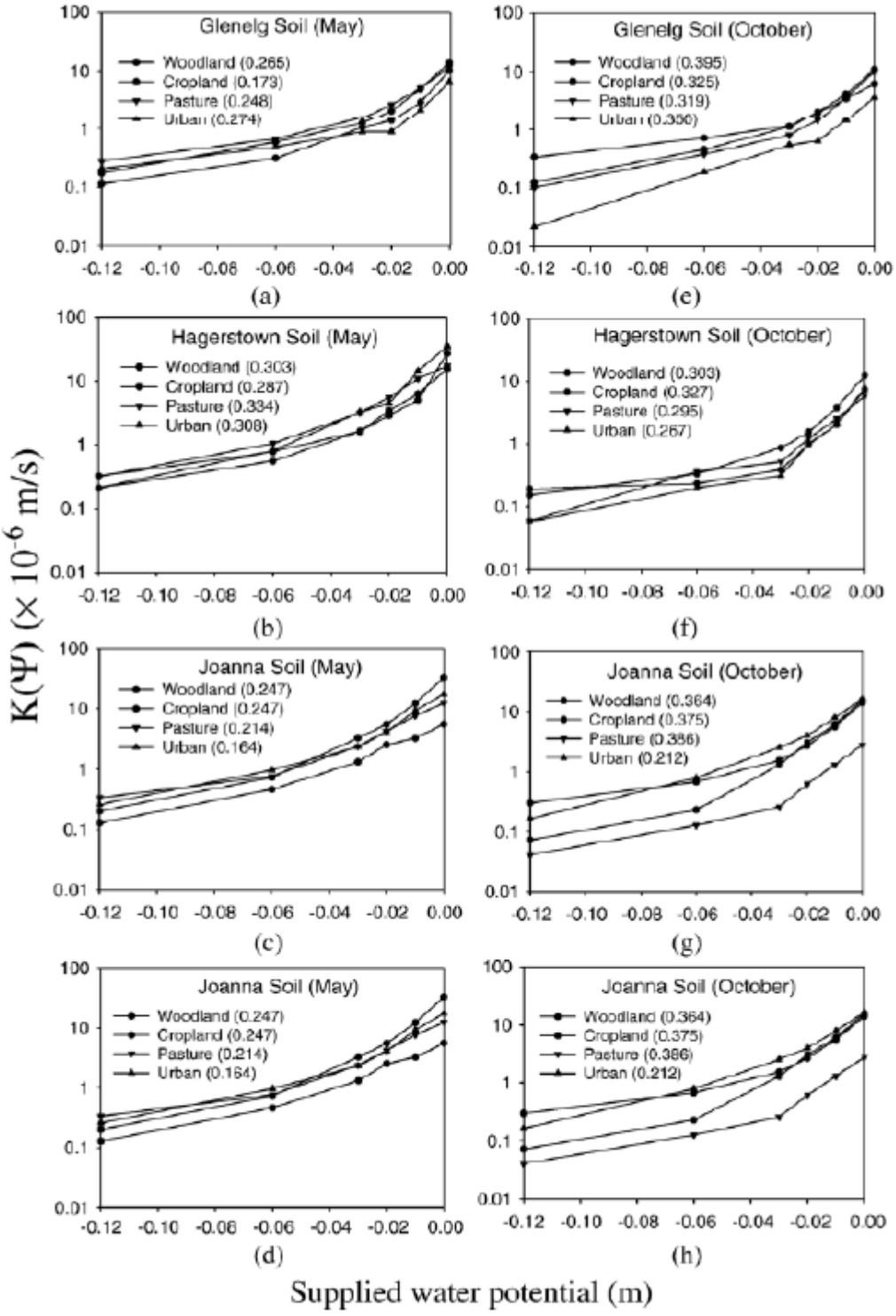

Figure 2.25 Soil hydraulic conductivity as a function of water potential [K (Y)] among the four and uses (woodland, cropland, pasture and urban) within each of the four soil series (Glenelg,

Hagerstown, Joanna and Morrison) measured in May (a-d) and October (e-h), respectively. The number in parenthesis is the averaged initial volumetric soil moisture at each site in May or October (Zhou et al., 2008).

The temporal variability of Ks was determined by several researchers. For example, Scott et al. (1994) studied short- and long-term variability of Ks in four adjacent fields located in Arkansas, USA. One of the fields was under prairie while other three cropped fields had mostly been in a rice-soybean rotation for either 3, 14, or 32 years (Scott et al., 1994). The fields were sampled monthly from March 1989 to March 1990. The Ks was measured on intact soil cores in the laboratory using constant head method and the temporal variability of Ks is presented in Figure 2.26. Scott et al. (1994) defined the variability among fields as long-term and the variability among sampling times within a field as short-term.

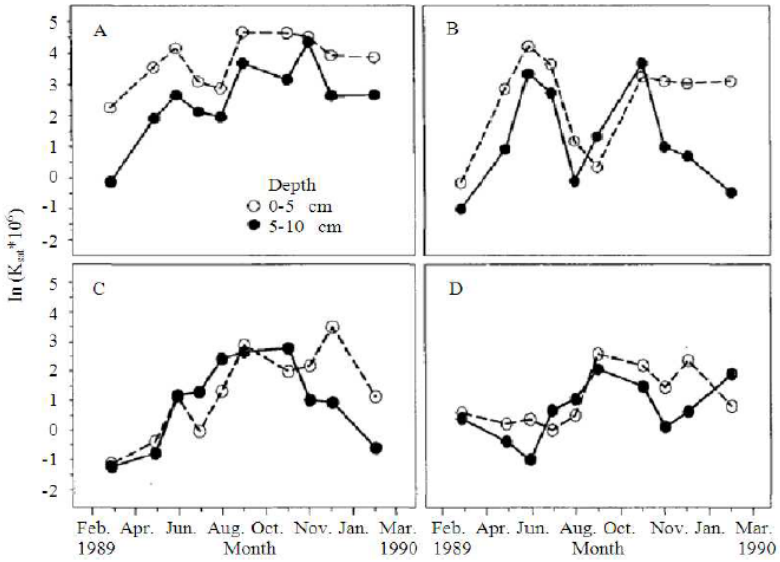

Figure 2.26 Temporal variability of saturated hydraulic conductivity at two soil depths 0-5 cm and 5-10 cm) in (A) prairie and fields with (B) 3, (C) 14 and (D) 32-year of cropping (Scott et al., 1994).

2.6.3.4 Spatial and Seasonal variation in hydraulic conductivity by Gupta et al. (1993)

The objective of this study was to evaluate and quantify the spatial and seasonal variations of hydraulic conductivity estimates, during the spring, fall and summer seasons, obtained by four techniques: Rainfall Simulator, Double Ring Infiltrometer, Guelph Permeameter and Guelph infiltrometer. Three sets of infiltration experiments and hydraulic conductivity measurements were made in three seasons of 1990 and 1991. Summaries of the statistics of K_s estimates determined with the four techniques are presented in Table 2.5 through Table 2.8.

Table 2.5 Statistical properties of saturated hydraulic conductivity (cm/hr) by Double Ring Infiltrometer

Season	N	Mean	Minimum	Maximum	Coefficient of variation (%)
Summer	53	4.26	1.82	12.67	49.47
Fall	50	9.39	5.45	21.34	77.43
Spring	51	8.98	3.62	17.11	79.43

Table 2.6 Statistical properties of saturated hydraulic conductivity (cm/hr) by Rainfall Simulator

Season	N	Mean	Minimum	Maximum	Coefficient of variation (%)
Summer	52	9.17	2.47	15.6	41.62
Spring	51	12.36	3.87	31.68	62.15

Table 2.7 Statistical properties of saturated hydraulic conductivity (cm/hr) by Guelph Permeameter

Season	N	Mean	Minimum	Maximum	Coefficient of variation (%)
Summer	42	4.01	0.85	10.42	60.73
Fall	38	7.83	2.45	27.45	145.74
Spring	39	6.62	0.60	19.42	119.2

Table 2.8 Statistical properties of saturated hydraulic conductivity (cm/hr) by Rainfall Simulator

Season	N	Mean	Minimum	Maximum	Coefficient of variation (%)
Summer	36	11.45	5.53	63.82	83.30
Spring	31	17.81	4.53	73.82	139.20

2.7 FACTORS EFFECTING IN-SITU HYDRAULIC CONDUCTIVITY

The hydraulic conductivity of soil refers to its ability to transmit water through its pores or interstitial spaces. There are various types of intrinsic and extrinsic properties that can affect the soil hydraulic conductivity.

2.7.1 Soil Texture & Structure

Soil texture refers to the proportions of sand, silt, and clay particles present in the soil. Coarse-textured soils, such as sandy soils, typically have higher hydraulic conductivity due to their larger pore spaces, while fine-textured soils, such as clay soils, have lower hydraulic conductivity

due to smaller pore sizes and greater compaction. A promising method to obtain a continuous soil profile is to use electrical resistivity imaging (ERI) (Akhtar et al. 2022, Ahmed 2022).

2.7.2 Porosity

Porosity is the volume of pore spaces in the soil. Higher porosity generally results in higher hydraulic conductivity because there are more interconnected spaces for water to flow through. Factors affecting porosity include soil structure, compaction, and organic matter content.

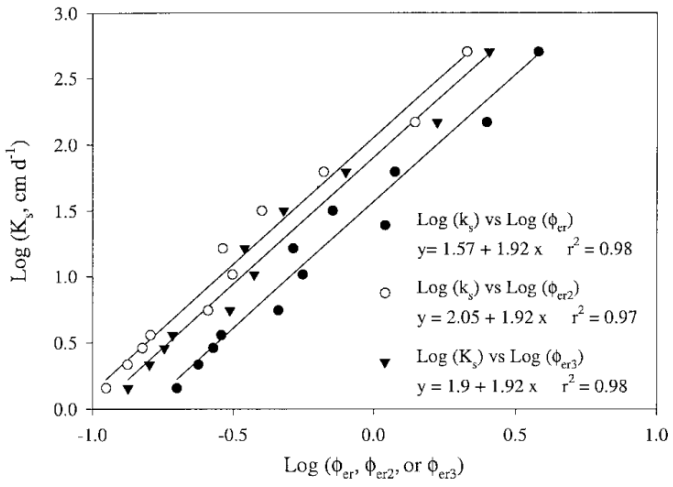

(a)

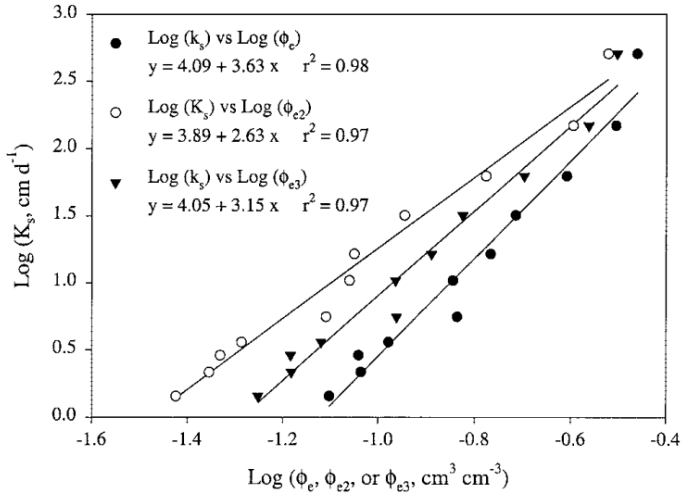

(b)

Figure 2.27 . Log–log relationship of saturated hydraulic conductivity (K_s) with (a) 2 d relative effective porosity (Φ_{er2}), 3 d relative effective porosity (Φ_{er3}), and relative effective porosity (Φ_{er}) (b) Log–log relationship of saturated hydraulic conductivity (K_s) with (a) 2 effective porosity (Φ_{er2}), 3 d effective porosity (Φ_{er3}), and effective porosity (Φ_{er}) for the 11 textural– class mean soils (Rawls et al., 1982)

The plastic treatment enhanced the soil's hydraulic conductivity, and that the degree of this increase was more significant at larger dosages. By mixing plastics with soil, the hydraulic conductivity was increased by approximately 100 times (Tasnim 2022).

2.7.3 Soil Structure

Soil structure refers to the arrangement of soil particles into aggregates or clumps. Well-structured soils with good aggregation tend to have higher hydraulic conductivity because they have larger and well-connected pores. Poorly structured soils, such as compacted soils, may have reduced hydraulic conductivity due to smaller or less connected pore spaces (Islam et al. 2021, Badhon et al. 2023).

2.7.4 Organic Matter Content

Soils with higher organic matter content generally have better soil structure, increased porosity, and improved hydraulic conductivity. Organic matter acts as a binding agent, creating aggregates and improving the soil's ability to hold and transmit water.

2.7.5 Soil Moisture Content

The hydraulic conductivity of soil is typically higher when it is near field capacity (i.e., the moisture content after excess water has drained). As the soil dries out, the hydraulic conductivity

decreases due to reduced water availability and increased soil particle cohesion (Shopnil et al. 2023). Bagarella and Provenzano (1996) used Guelph Permeameter and Constant Head Permeameter to evaluate the influence of moisture content in hydraulic conductivity. From two different analysis, it was found that hydraulic conductivity decreased significantly with the change in moisture content as shown in Figure 2.28

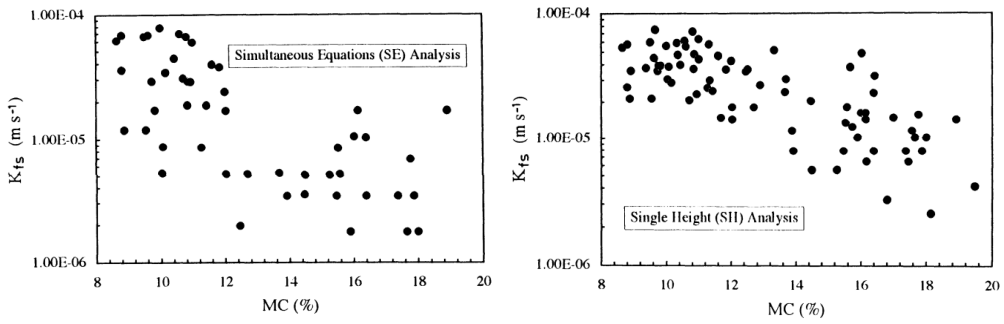

Figure 2.28 Field saturated hydraulic conductivity vs initial moisture content values

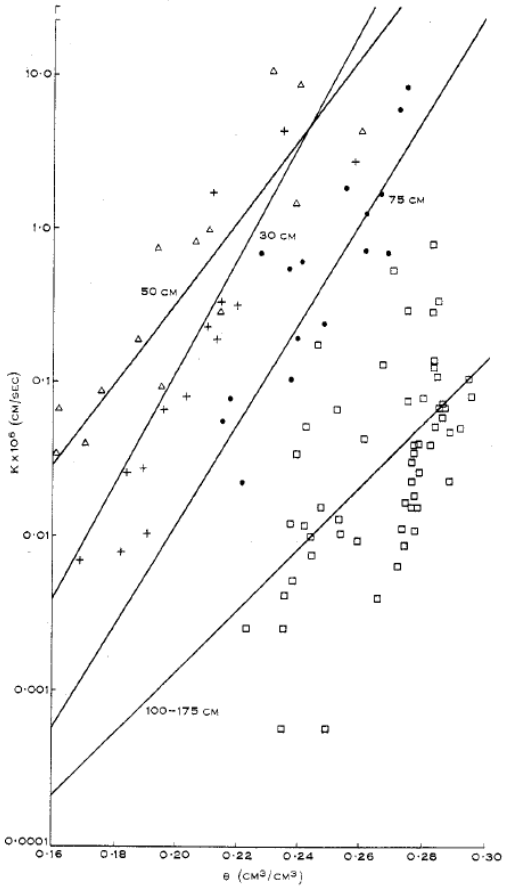

Figure 2.29 Relationship between hydraulic conductivity and volumetric water content

Rose et al. (1965) showed that hydraulic conductivity increases with the increasing volumetric water content for a certain depth. With increasing depth of soil profile, higher water content is required for same hydraulic conductivity (Figure 2.29).

In 2011, Schumann et al., determined the hydraulic conductivity based on soil moisture content in different techniques and for this test, fine grain soils were used. For initial moisture content increase, the unsaturated hydraulic conductivity increased abruptly however, after 10% the increment decreased as shown in Figure 2.30.

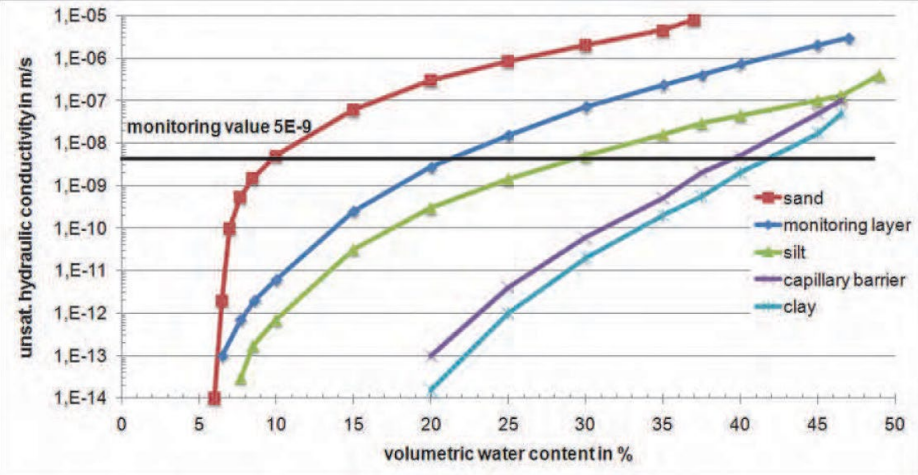

Figure 2.30 Increase in hydraulic conductivity with increasing water content.

2.7.6 Temperature

Temperature can influence the viscosity of water and the soil's physical properties. Higher temperatures generally decrease the viscosity of water, resulting in increased hydraulic conductivity. However, extreme temperatures can also cause freeze-thaw cycles, leading to changes in soil structure and reduced hydraulic conductivity.

Cho et al. (1998) hydraulic conductivities of compacted domestic bentonite increase with increasing temperature, and the hydraulic conductivities at the temperature of 80°C increase up to about 3 times as high as those at 20°C. The permeability is nearly constant within temperature range of 20 to 80°C under the experimental conditions. The effect of temperature elevation up to 80°C on the hydraulic conductivity is not so large, and the hydraulic conductivities are still low enough to inhibit the radionuclide release by advection through buffer.

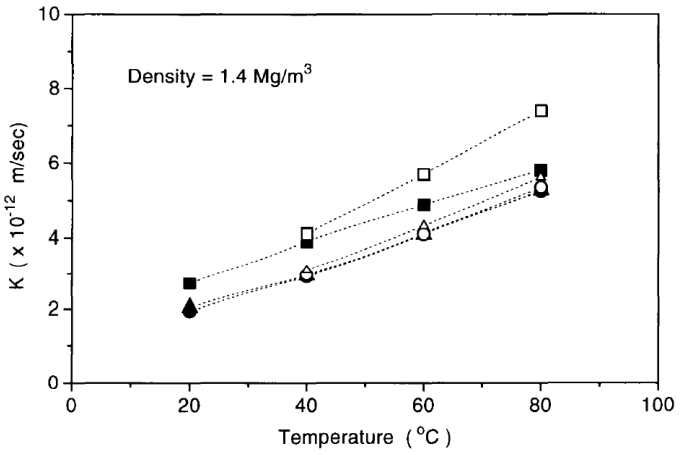

(a)

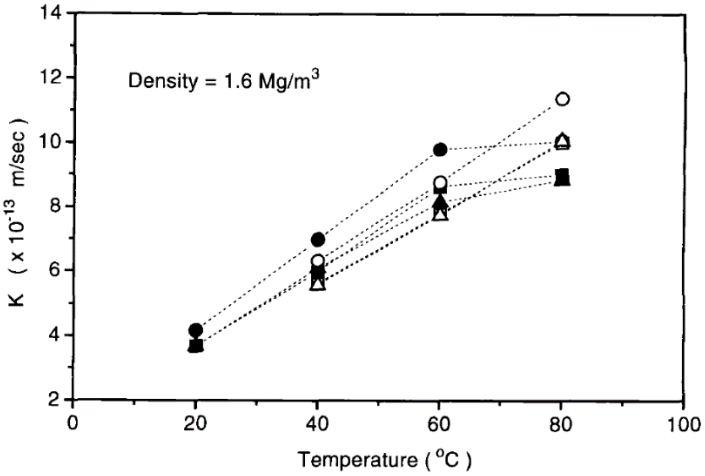

(b)

Figure 2.31 Hydraulic conductivity of compacted bentonite with dry density of (a) 1.4 Mg/m^3 and (b) 1.6 Mg/m^3 at different temperature

Previous studies have suggested that the increase in hydraulic conductivity with temperature, while maintaining a constant water content, can be attributed to a decrease in water viscosity (Haridasan and Jensen, 1972). However, when comparing the experimentally determined conductivity ratios with the corresponding viscosity ratios, Hopmans and Dane (1986a) discovered that measured conductivities exhibited a more rapid increase with temperature than predicted,

especially at higher temperatures and lower water contents. They speculated that the measurement of water conductivity might overestimate its actual value due to the influence of vapor movement, although there was no conclusive evidence supporting this hypothesis. Gupta and Swartzendruber (1964) proposed that the observed difference could be explained by considering the change in volume of entrapped air. However, there is ongoing debate as to whether this mechanism has a significant effect, if any, on hydraulic conductivity.

2.7.7 Compaction

Soil compaction, often caused by heavy machinery or foot traffic, reduces pore spaces and restricts water flow, leading to lower hydraulic conductivity. Compacted soils have increased particle density and decreased total porosity. S. Zhang et al. (2006) showed that hydraulic conductivity decreases with increasing compaction levels. Soil was collected from different levels and for each soil depth, 0%, 10% and 20% level of compaction was used to check the hydraulic conductivity. For every depth, a similar pattern was found.

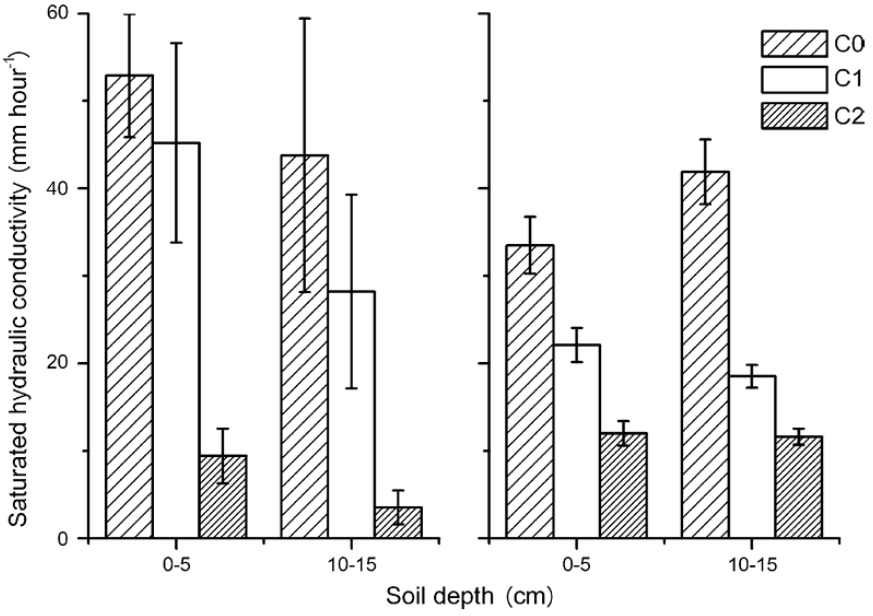

Figure 2.32 Hydraulic conductivity at different levels of compaction (C0, 0%, C1, 10%, C2, 20%)

It is important to note that these factors interact with each other, and their relative importance can vary depending on the specific soil type and environmental conditions.

2.8 PREVIOUS STUDIES ON INVESTIGATION ON HYDRAULIC CONDUCTIVITY AND SHALLOW SLOPE FAILURE

There is numerous research found on the investigation of shallow slope failure. Many researchers have studied the reason behind the slope failure. Previous studies in literature had main focus on rainfall induced failure.

Study by Anastasia et al. (2011)

This study introduces a probabilistic framework designed to evaluate the stability of unsaturated slopes when subjected to rainfall-induced conditions. The primary focus of the research involves investigating how the presence of soil spatial variability influences the likelihood of slope failure, specifically landslides. The consideration of soil spatial variability is achieved through the establishment of a model where the saturated hydraulic conductivity of the soil (referred to as "ks") is represented as a stationary lognormal random field. To estimate the probability of slope failure, the research employs subset simulation coupled with a modified Metropolis–Hastings algorithm. Through this approach, the study assesses the probability of a slope experiencing failure due to rainfall. The findings of the research highlight that incorporating probabilistic analysis that accounts for the spatial variability of ks yields results that can replicate a common mechanism of shallow failure observed in actual rainfall-triggered landslides. This specific type of shallow failure is attributed to the generation of positive pore-water pressures in layers situated near the surface of the ground.

In contrast, when analysis is conducted assuming a uniform soil profile with no spatial variability, the ability to replicate shallow failures is limited. This only becomes possible in instances of extreme conditions where the rate of infiltration flux closely aligns with the value of ks.The changes in pressure head and factor of safety (FS) with time obtained from deterministic seepage and slope stability analyses are depicted in Figure 2.33. The wetting front goes deeper as infiltration progresses, and the factor of safety at the wetted (saturated) zone decreases. In this example, at elapsed time of 1, 4, and 8 days, the minimum FS within the saturated zone is 2.32, 1.57, and 1.28, respectively (as indicated by arrows). As these values are higher than FS at the base, FS_{min} is found at the base of the slope. After 20 days of infiltration, pressure head at the soil reaches steady state. At steady state, the minimum FS is also found at the base of the slope.

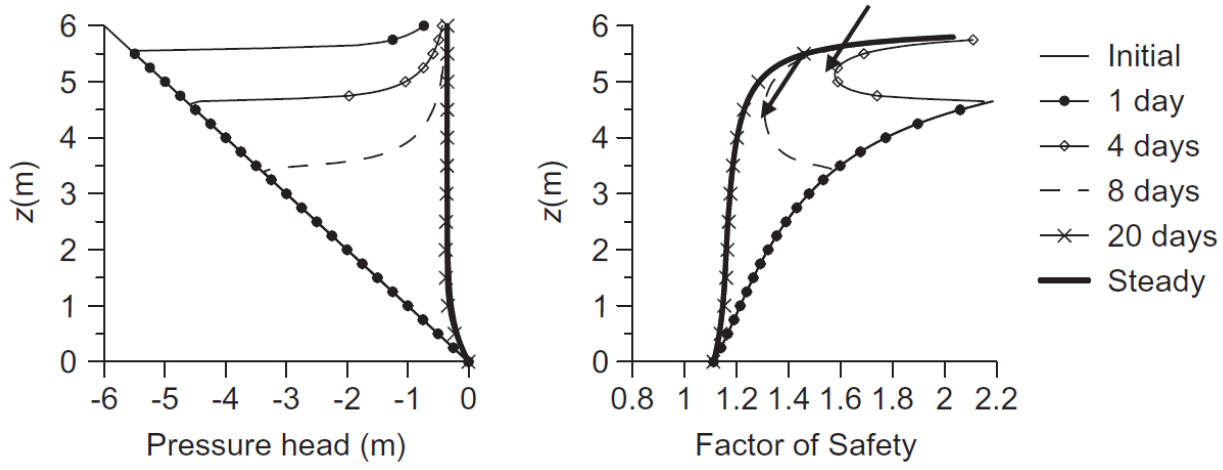

Figure 2.33 Pressure head and factor of safety profile (after Anastasia et al.)

Study by Naik et al. (2018)

The aim of this study is to assess the infiltration characteristics of an area encompassing four distinct soil types: sand, loamy sand, loam, and silt. To achieve this, a practical mini disk infiltrometer was utilized to quantify cumulative infiltration. Based on these measurements, near-

saturated hydraulic conductivity values were determined. To validate the accuracy of the results, simulations were conducted using HYDRUS 2D/3D, a software solution that employs Van Genuchten's model to solve Richard's equation. Notably, the findings reveal that the simulated outcomes provided by HYDRUS are particularly accurate for loamy sand soil. However, in the case of sandy and loamy soils, the numerically simulated results tend to underestimate the observed values. Conversely, for silt soil, the simulated outcomes overestimate the experimental data. This variability in results primarily stems from discrepancies in the parameters employed for the numerical simulations. To address this, an inverse simulation was performed using HYDRUS, aiming to derive optimized values for the hydraulic parameters.

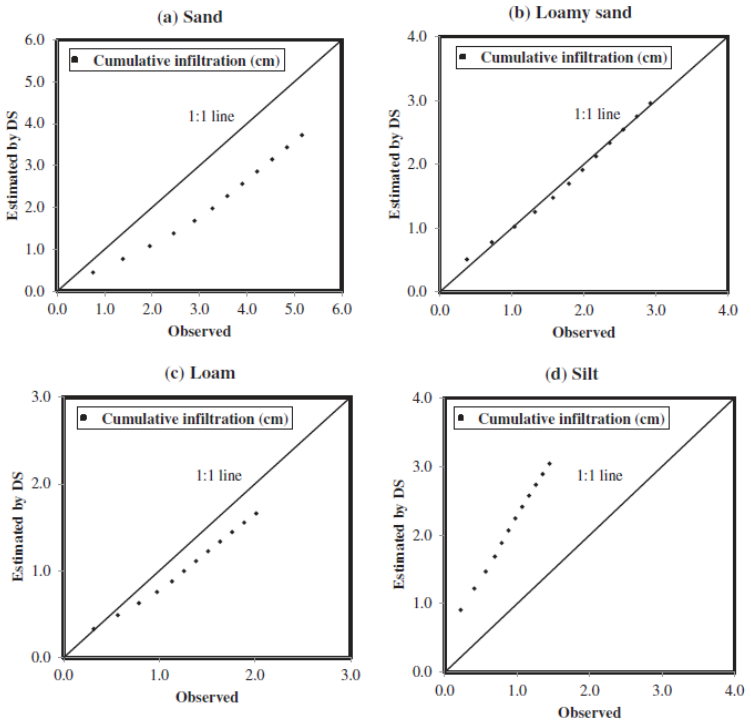

Figure 2.34 Comparison of cumulative infiltration obtained using observed ad predicted by DS using HYDRUS (after Naik et al. 2018)

The figure clearly illustrates a substantial disparity between the experimental and predicted cumulative infiltration values. The observed field data and the DS (Direct Simulation) results from HYDRUS diverge significantly, except in the case of loamy sand soil. Specifically, for sand and loam soils, the simulated cumulative infiltration measurements fall below the observed values, whereas for silt soil, the simulated measurements exceed the experimental data. These discrepancies between the modeled and field results can likely be attributed to the utilization of soil hydraulic parameters α and n, which are contingent on the soil texture.

In terms of statistical analysis, it was determined that the Root Mean Square Error (RMSE) values obtained for DS results across all sites were notably higher compared to the RMSE values obtained from inverse modeling (IS) results. For instance, at sites 1 and 4, RMSE values of 1.186 and 1.225 were recorded for DS, respectively, whereas the corresponding IS values were significantly lower at 0.424 and 0.025. This suggests that the employment of optimized hydraulic parameters in modeling cumulative infiltration has substantially contributed to reducing errors. Additionally, the Nash-Sutcliffe Efficiency (NSE) assessment of the results exhibited a considerably negative value of 10.208 for DS at site 4, in contrast to the favorable value of 0.995 obtained for IS results at the same location.

Study by Dong et al. (2012)

This paper presents a numerical procedure to explore how hydraulic conductivity anisotropy and strength anisotropy affect the stability of stratified, poorly cemented rock slopes. Neglecting the hydraulic conductivity anisotropy of a slope with horizontal layers leads to a 40% overestimation of the safety factor. For a dip slope with inclined layers with h = 30_, including the

strength anisotropy caused a 25% reduction of the safety factor compared to the cases which isotropic strength is assumed.

Figure 2.35 The influence of hydraulic conductivity anisotropy on the factor of safety of slopes

It was observed that the low strength of the bedding planes of a dip slope dominates the slope stability and that plane failures occur more frequently than circular failures. Notably, for a gentle dip slope composed of poorly cemented sedimentary rocks, even with flattened layers, the inherent anisotropy (including hydraulic conductivity and strength) also plays a very important role in its stability.

Study by Muhammad Suradi (2016)

In this study a parametric study was carried out at typically residual soil slopes with two distinctively different types of hydraulic conductivity, high ($ks=10^{-4}$ m/s) and low ($ks=10^{-6}$ m/s) conductivity. It was found in particular, spatial variability of hydraulic conductivity noticeably affected rainfall-induced failuresof both high and low-conductivity slopes when the slopes were subjected to sufficiently intense rainfall.

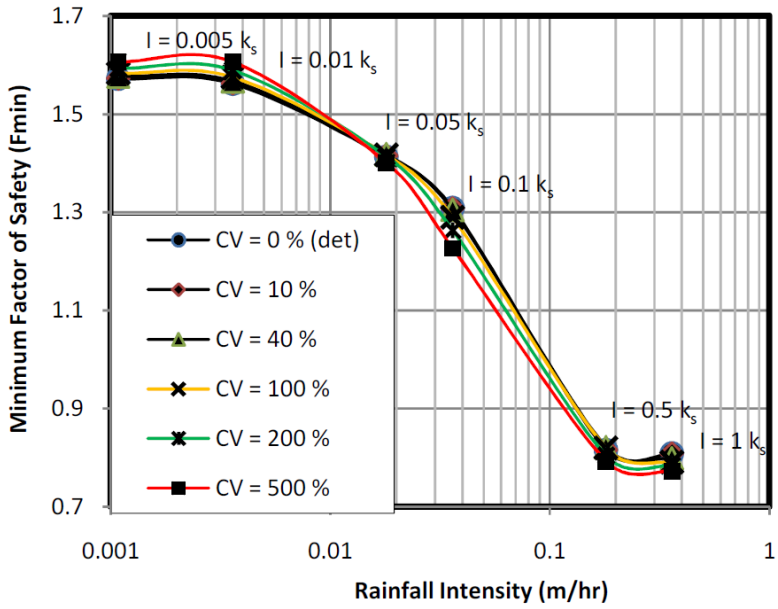

(a)

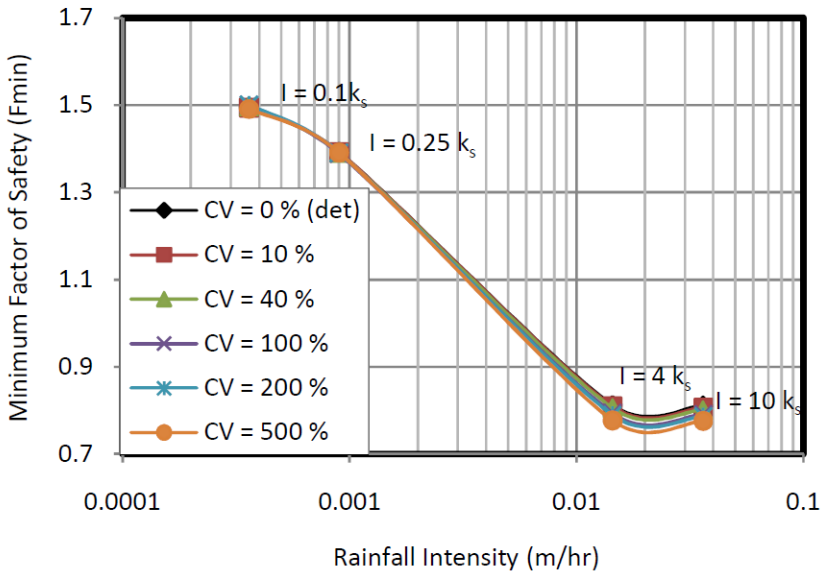

(b)

Figure 2.36 Minimum factor of safety of (a) high and (b) low hydraulic conductivity in different rainfall intensity

The higher the spatial variability of hydraulic conductivity, the lower minimum safety factors of slope were triggered by rainfall as shown in Figures 4 and 6. Then, the factors of safety resulting from the higher spatial variability recovered much more slowly since rainfall stopped and eventually converged long after the cessation of rainfall for the high- conductivity slope but tended to diverge since rainfall ceased for the low conductivity slope.

Study by Rahardjo et al. (2007)

In this study, the relative importance of soil properties, rainfall intensity, initial water table location and slope geometry in inducing instability of a homogenous soil slope under different rainfall was investigated through a series of parametric studies. Soil properties and rainfall intensity were found to be the primary factors controlling the instability of slopes due to rainfall, while the initial water table location and slope geometry only played a secondary role.

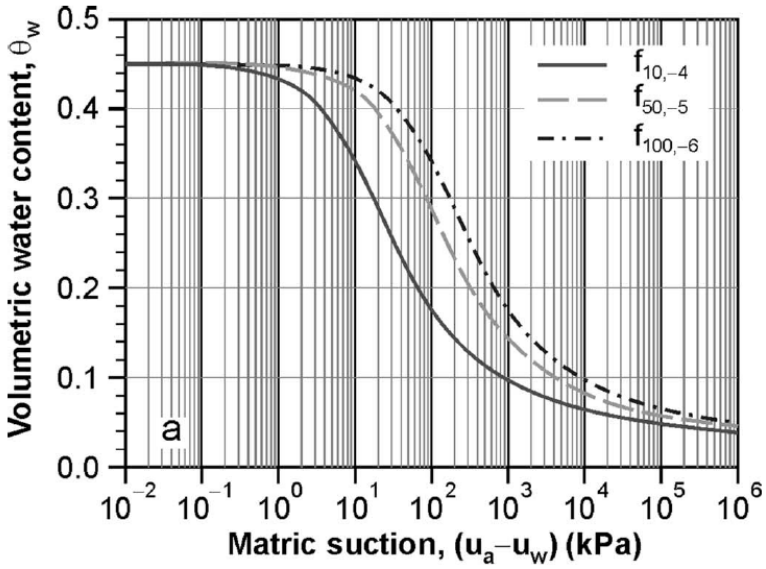

(a)

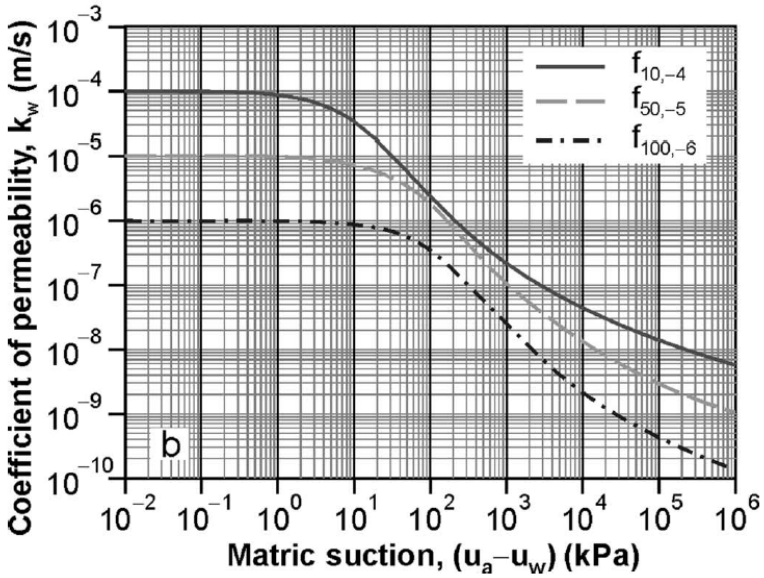

(b)

Figure 2.37 (a) Soil-Water Characteristics Curve and (b) permeability function

In this study, the factor of safety along with time with different rainfall intensities were analyzed. Figure 2.38 shows that after a rainfall event starts, the factor of safety will drop regardless of the soil type or the rainfall intensity applied to the slope. The magnitude and rate of reduction in factor of safety is directly proportional to the magnitude of intensity of rainfall. The higher the intensity, the faster the factor of safety decreases with time. It also suggests the possibility of the existence of threshold rainfall intensity which will cause the maximum reduction in Fs of a homogeneous soil slope.

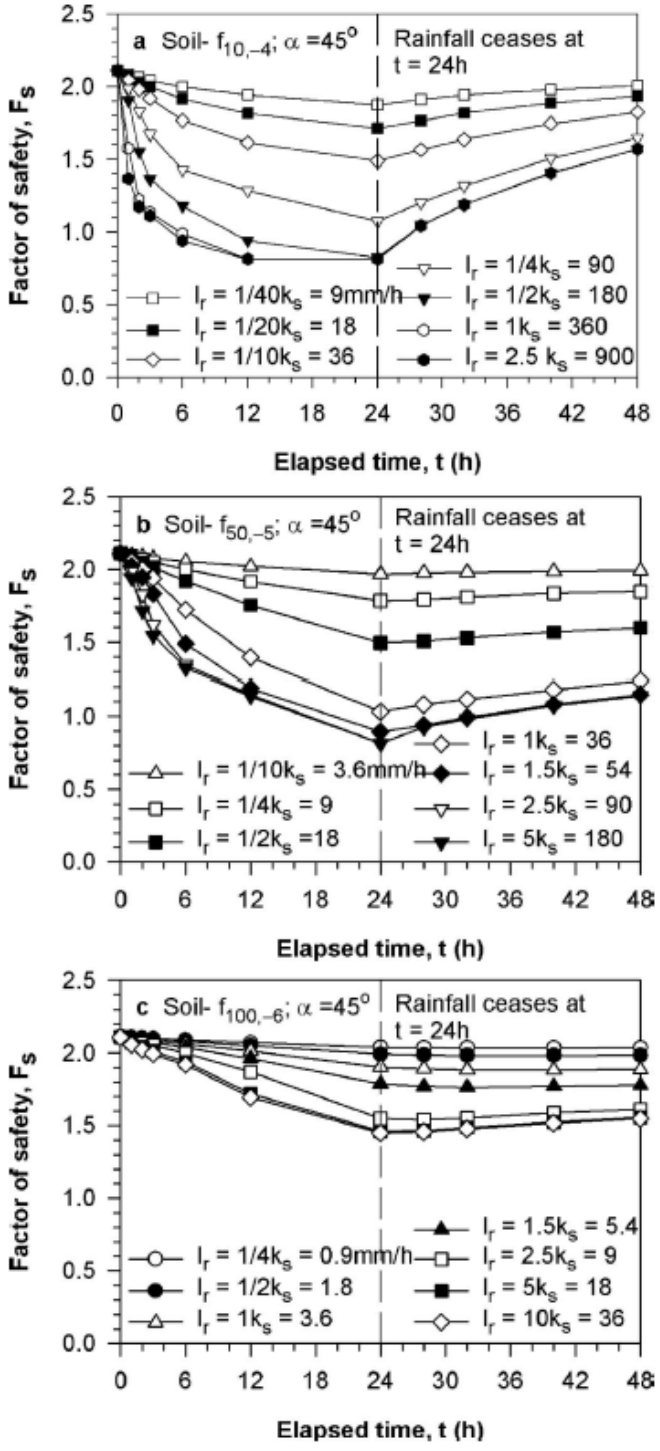

Figure 2.38 Effect of rainfall intensity on variation of factor of safety

for homogeneous soil slope

Study by Harris et al. (2011)

To validate the numerical models employed in the development of an early warning system for rainfall-induced landslides, a retrospective analysis of a roadside embankment near State Highway 1 in Silverdale, New Zealand, was conducted. The study involved the use of volumetric water content sensors and a rainfall gauge to record the soil's real-time response to rainfall events during the winter of 2010. The investigation encompassed saturated and unsaturated seepage analyses, utilizing empirically derived soil parameters to replicate the fluctuations in monitored volumetric water contents. These analyses were coupled with a slope stability assessment to determine the slope's factor of safety.

To assess the impact of a specific rainfall event that triggered the slope failure, the corresponding rainfall record was incorporated into the model. The hourly rainfall data from 2008 was then applied to the finite element model, and limit equilibrium analyses were performed at discrete time intervals. The same constant-level negative flux between rainfall events, as observed in the 2010 data, was considered.

The factor of safety (FOS), which indicates the stability of the slope, was computed for the 2008 rainfall scenario and plotted against time. The resulting FOS-time graph demonstrated distinct trends. Notably, each significant rainfall event coincided with a sudden decrease in the factor of safety. Subsequent to these events, the FOS exhibited a gradual recovery over time. For instance, there was a gradual increase in the factor of safety between approximately 1,500 to 2,500 hours, followed by a rapid decrease during the next significant rainfall event.

The FOS graph indicated that the factor of safety reached a nadir of around 0.85 at an elapsed time of 5,000 hours. This analytical finding aligns with observations made by Transfield

Services (New Zealand) Ltd. in 2008, which reported the initial signs of movement at the site after approximately 4,400 hours. However, the complete progression of failure, including the time from initial movement to full slope failure, remained uncertain. Consequently, there might be a disparity between the timing of failure in the analyses and the actual observations on-site. In the analysis, the factor of safety dropped to unity just after this observed failure time, possibly indicating a slight mismatch between the two timings.Based on the time of failure in the report from Transfield Services (New Zealand) Ltd. (2008), it would appear that the rainfall event circled in Figure 2.39 was the cause of the slope failure; however, this analyses indicates that it was the large rainfall event following this which caused the slope failure.

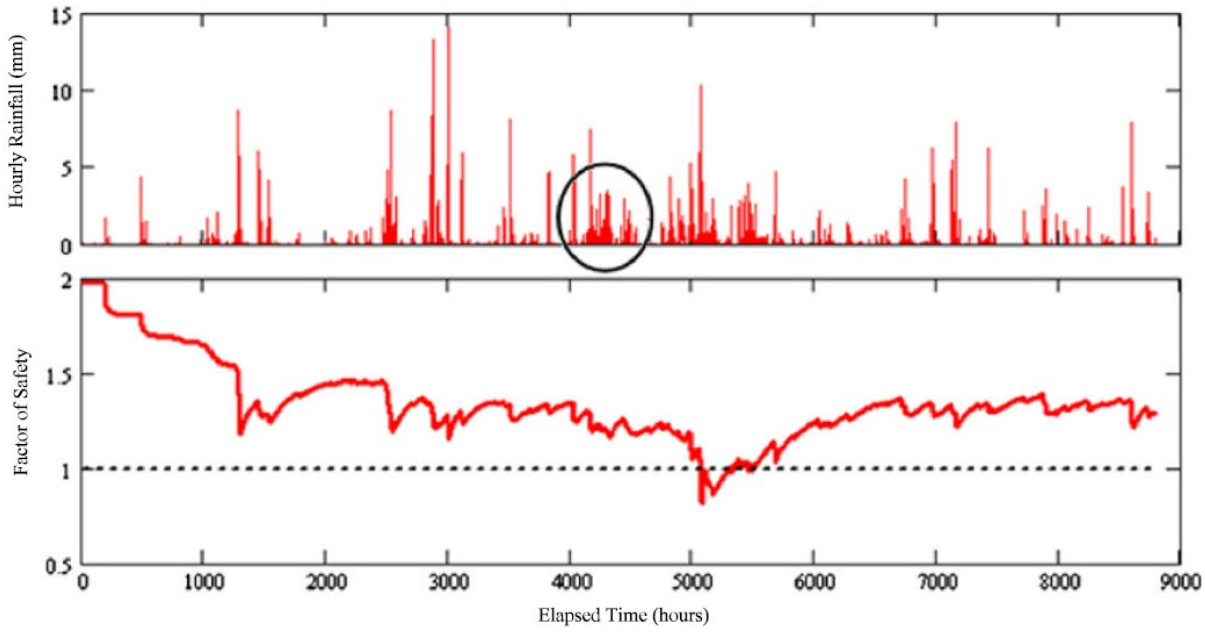

Figure 2.39 Rainfall events in 2008 and corresponding factor of safety

Study by Fathiyah and Erly (2017)

This research focused on the effect of rainfall pattern on the FS of unsaturated slope with low or high hydraulic conductivity of the soil. The analyses were conducted with SEEP/W for the seepage and SLOPE/W for the slope stability. To know whether different hydraulic conductivity affect the change of FS on normal rainfall pattern at 30° slope angle, there will be three different hydraulic conductivities used in this section. The three different hydraulic conductivities noted as Initial (1 x 10^{-6} m/s) which represents the hydraulic conductivity used on the beginning of this study, Low (1x10^{-7} m/s), and High (1x10^{-5} m/s). The Initial conductivity represents the value in between the Low and High conductivities. The results are shown in Figure 2.40 .

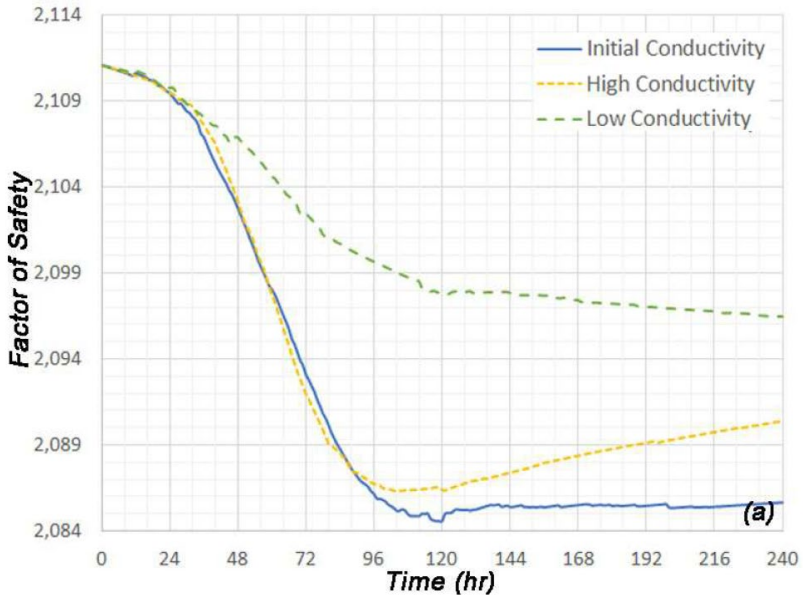

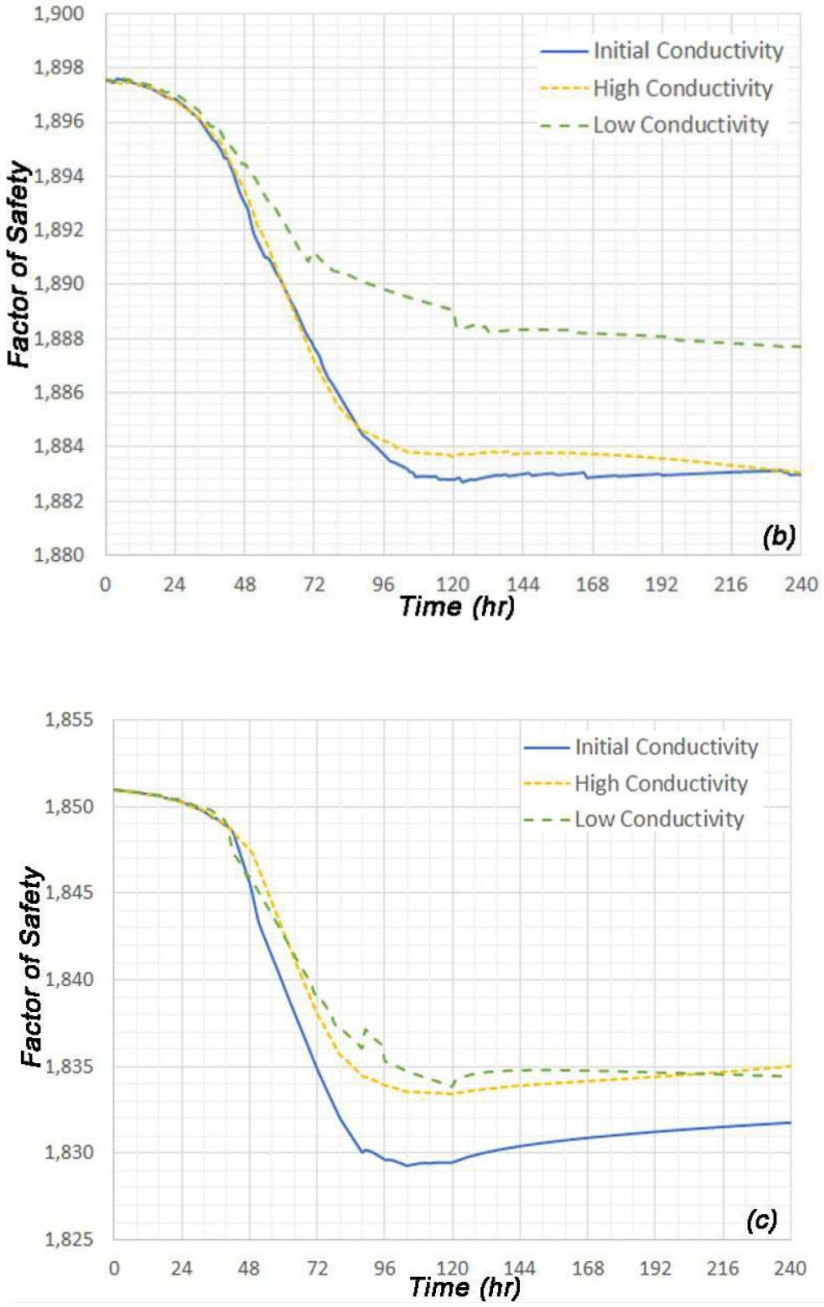

Figure 2.40 FS vs Time on different hydraulic conductivity for (a) 30º, (b) 45º, and (c) 60º

From Figure 2.40, it is shown that for the three slope angles, 30º, 45º, and 60º, the Low conductivity always gives the least FS reduction. The largest difference of FS reduction between the Low conductivity and the Initial or High conductivities is shown at the 30º slope. This means

that the effect of infiltration is significant to the reduction of FS since the low conductivities slowing down the infiltration of rainfall through the slope. Compared to at 30^{o} slope angles for different hydraulic conductivity, which is High (1 x 10^{-5} m/s) and Low (1 x 10^{-6} m/s), it is known that the least reduction of FS is obtained at High. As for this research, the same behaviour corresponds at Initial (1 x 10^{-6} m/s) and High (1 x 10^{-5} m/s) for the normal rainfall pattern.

2.9 PREVIOUS STUDIES ON EARLY WARNING SYSTEM OF SLOPE FAILURE

An early warning system for shallow slope failures comprises various components that work together to detect and alert people to potential slope failures before they happen. The system includes monitoring equipment such as inclinometers, piezometers, and ground-based radar, which measure slope movements, groundwater levels, and pore pressure changes. These instruments collect data in real-time, which is then analyzed using algorithms and models to detect patterns or anomalies associated with slope instability. Upon identifying potential risks, the system generates warnings or alerts based on predefined thresholds. These alerts are communicated through an alert system, which can include SMS alerts, sirens, mobile apps, and email notifications, ensuring that relevant authorities, emergency responders, and communities receive timely information. To enhance preparedness, public awareness campaigns educate individuals about the early warning system, signs of slope instability, and appropriate actions to take when receiving a warning. Regular maintenance and calibration of monitoring equipment, along with collaboration with geotechnical experts, ensure the system's reliability and effectiveness. By implementing such an early warning system, communities can be better prepared to respond and mitigate the risks associated with shallow slope failures. Literature denotes that there have been studies conducted in several places like China, India and Singapore to develop a early warning system for shallow slope failure.

Chae and Kim (2011) involved the installation of a real-time monitoring system to observe physical property changes in soils in a valley during rainfall events. This monitoring included the measurement of volumetric water content, which was compared with the results of laboratory flume tests to identify landslide indicators in the soils. Although no landslide occurred, the field monitoring results showed a directly proportional relationship between the effective cumulative rainfall and the gradient of volumetric water content per unit time (t/t_{max}). This preliminary study thus related slope failure to the volumetric water content gradient as a function of rainfall.

Laboratory results showed that a high amount of rainfall and a high gradient of volumetric water content could induce slope failure. Based on these results, it is possible to suggest a threshold value of the volumetric water content gradient demarcating the conditions for slope stability and slope failure.

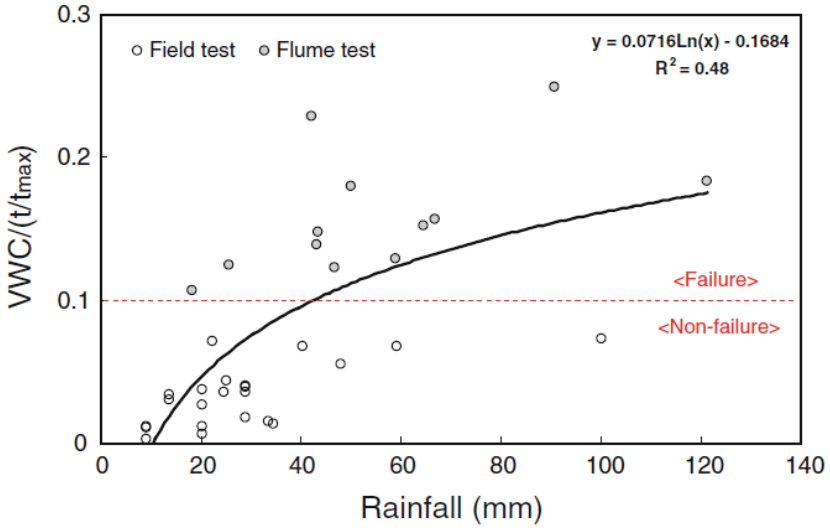

Figure 2.41 Relationship between volumetric water content gradient and rainfall based on the data from field monitoring and laboratory flume tests (after Chae and Kim 2011)

Figure 2.41 showed a comparison of the changes in volumetric water content gradient with rainfall amount based on the data from the field monitoring and the laboratory flume tests. The volumetric water content gradient was steep for low rainfall amounts and became gentle with an increase in rainfall amount. This phenomenon is related to the low initial volumetric water content of unsaturated soil, indicating a slow infiltration of rainfall under high volumetric water content conditions induced by the antecedent rainfall. In a similar mechanism, rainfall infiltration was nearly uniform or slightly decreased even as the cumulative rainfall amount increased. In the case of the laboratory flume tests with slope failures, the gradient of volumetric water content is plotted in a range between 0.107 and 0.249. Conversely, field monitoring results without slope failure from June to August in both 2008 and 2009 show a range of volumetric water content gradients between 0.003 and 0.073. The results show that a large rainfall amount and a high gradient of volumetric water content contribute to slope failures. Based on the the results of the preliminary study, Chae and Kim (2011) suggested a threshold for the volumetric water content gradient marking the point between slope failure and stability. This threshold could provide a baseline for the early warning of landslides that are triggered by rainfall. Comparison of the results for the volumetric water content gradient showed that a landslide tends to be triggered at volumetric water content gradient of over 0.1 in the case of the granitic gneiss weathered soil of the Deoksan test site.

Chen and Jiang (2020) developed an early warning system integrating the time-of-failure analysis. The study aimed to investigate the prediction of the slope failure time and establish alert procedure. historical slope

failure database was first established containing 50 failure cases and 50 non-failure cases to study our methods. A dimensionless inverse velocity method (DINV) was proposed to provide

a general solution framework for calculating the time of failure. Additionally, linear and non-linear DINV trends were used to establish a failure time window to evaluate the potential failure time frame. For the alert procedure, two proposed dimensionless indicators were used to define a series of threshold levels. These two indicators could be combined as a potential tool for determining whether a slope with acceleration will eventually fail. The system adopted dimensionless processing methods and considered different slope failures with similar acceleration patterns.

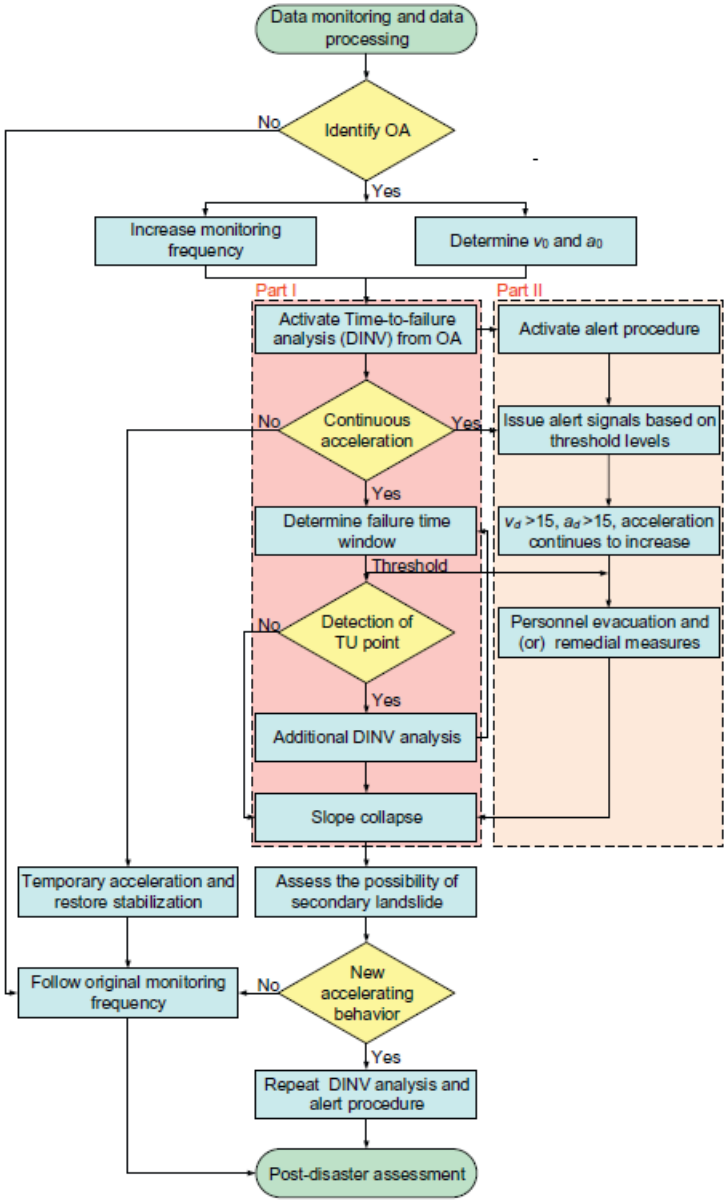

Figure 2.42 Flowchart by Chen and Jiang for the early warning system

Aleotti (2004) developed a critical threshold by establishing a relation between duration and normalized critical rainfall as shown in Figure 2.43.

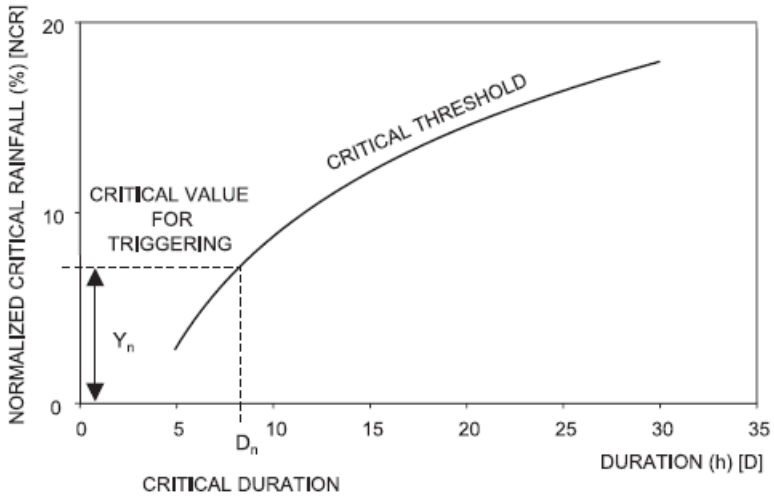

Figure 2.43 Relationship between Duration (D) and normalized critical failure (NCR)

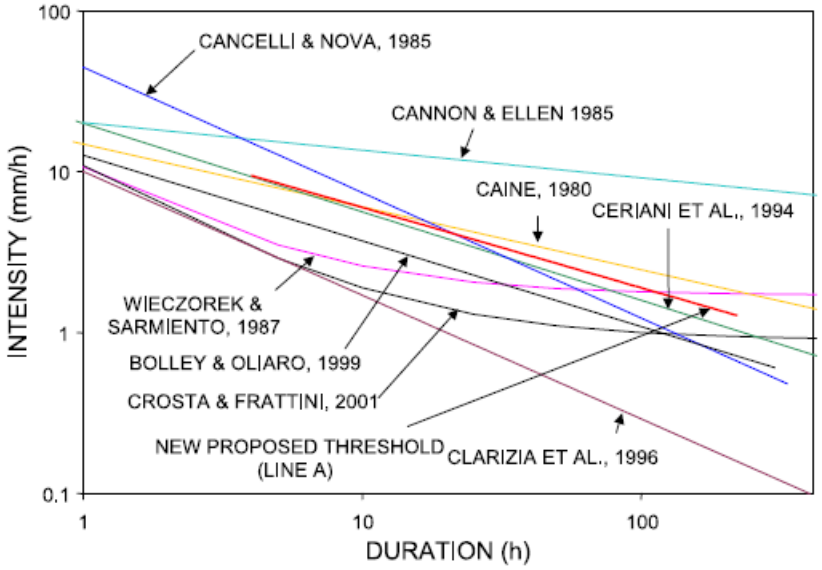

Figure 2.44 Comparison of the triggering threshold in graph I –D with those reported in the literature.

Figure 2.44 showed the thresholds proposed by Caine (1980) and Crosta and Frattini (2001) are prepared by using all the data available at the date for the world; the thresholds by Cancelli and Nova (1985), Ceriani et al. (1994) and Clarizia et al. (1996) are referred to wide areas with different soil, morphologic and rainfall characteristics. The threshold proposed by Bolley and Oliaro (1999) was calculated for the upper Susa Valley.

Islam (2021) developed an early warning system based on different rainfall intensities and duration. In this study empirical thresholds were developed based on historical rainfall and slope failure studies in Texas. The empirical thresholds were validated by slope failure event. Intensity-Duration, Event rainfall-Duration and Event Rainfall-Intensity thresholds were developed in this study.

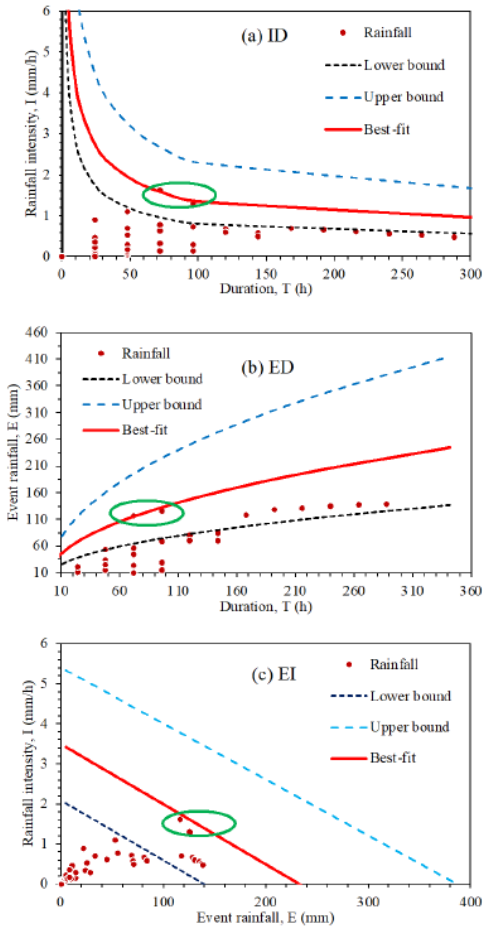

Figure 2.45 (a) Intensity- Duration, Event Rainfall-Duration and Event Rainfall-Intensity thresholds

CHAPTER 3

MONITORING SEASONAL VARIATION OF IN-SITU HYDRAULIC CONDUCTIVITY ON HIGHWAY EMBANKMENT

3.1 ABSTRACT

Highway embankments are frequently constructed using locally available materials, and in North Texas, the primary material used is high plasticity clay, which undergoes cyclic shrinkage and swelling during dry and wet periods, respectively. Saturation condition changes as it undergoes cyclic change and therefore it is necessary to study the hydraulic conductivity of the soil to understand the failure mechanism of the slope. The objective of the study is to evaluate the seasonal variation of in-situ hydraulic conductivity on a highway slope in Midlothian, Texas. The change in Hydraulic conductivity was measured monthly using Mini-Disk Infiltrometer (on the surface) and Guelph Permeameter (at 2ft depth) with different rainfall events. A cyclic pattern was observed over the years with precipitation and changes in volumetric water content. The average hydraulic conductivity was found to be highest in summer (3.8×10-6 cm/s) using the Guelph method. Using Mini-Disk Infiltrometer, hydraulic conductivity was found higher in Summer as well. Mini-Disk Infiltrometer showed a 10 to 100 times higher value than Guelph permeameter due to numerous desiccation cracks and pores on the surface.

Keywords: Embankment, hydraulic conductivity, seasonal variation, Guelph Permeameter, Mini-Disk Infiltrometer.

3.2 INTRODUCTION

Shallow slope failures commonly occur in embankments constructed with high plastic clay. The primary cause of these failures is the decline in shear strength. Various factors influence the shear strength of compacted cohesive soil, including soil water content, gradation, dry density, soil

structure, thixotropy, and normal effective stress. It's worth noting that the impact of water content on shear strength goes beyond just the initial molding water content; subsequent changes after placement also play a role (Langfelder and Nivargikar, 1967). Failures typically manifest following prolonged rainfall, leading to a reduction in soil strength (Sapkota, 2019). Shallow slope failures often occur at depths ranging from 3 to 6 feet (Loehr et al., 2007). During the summer, the upper soil layer undergoes drying, and over several years with minimal rainfall, the depth of the dry soil zone gradually increases. This period might witness the emergence of extensive surface cracks, providing a preferential pathway for rainwater flow. Water content fluctuations are mostly confined to the surface soil, remaining relatively stable below the zone of annual fluctuation (Loehr et al., 2007). The strength loss of expansive clay over time is influenced by the seasonal variations in rainfall and temperature. Rainwater infiltrates voids and cracks, making it essential to assess seepage rates across different seasons, sense soil permeability, and predict potential slope failure probabilities (Islam and Hossain, 2021).

The hydraulic conductivity of soil is influenced by various parameters, encompassing climatic conditions and soil physical properties like compaction degree and pore size distribution. This property can exhibit varying extents of change across different seasons, following cyclical patterns corresponding to spring, summer, fall, and winter weather. During dry seasons, expansive soil develops cracks that can serve as conduits for water. In wet clay soil, saturated hydraulic conductivity (Ks) closely relates to macropore volume (Bouma and Wösten, 1979). Unsaturated hydraulic conductivity, on the other hand, is influenced by volumetric water content. While laboratory testing is common for excavated soil, in-situ hydraulic conductivity assessments are crucial for accurate geotechnical evaluations. However, producing reliable results can be challenging for soils with extremely high or low conductivity. Soil homogeneity and anisotropy

can also significantly impact the assessment's validity. Numerous researchers have investigated the effect of soil hydraulic conductivity on rainfall-induced slope failures. However, the majority, if not all, employed deterministic methods for their studies (Keery et al., 2007). Furthermore, Stephen S. Boynton and David E. Daniel (1985) highlighted variations in results between different permeameters, attributed to differences in equipment and testing procedures (Boynton, 1987). Despite several laboratory tests conducted to determine hydraulic conductivity, limited field studies have been conducted on highway slopes.

The change in permeability with the change of season in a slope has not been extensively monitored in previous studies. Specifically, no significant research has been conducted to compare the variation of the permeability near the surface and at any depth below the surface. Thus, this study aims to investigate spatial and temporal variations in in-situ soil permeability through extensive field monitoring using a Guelph Permeameter and a Mini Disk infiltrometer.

3.3 SITE LOCATION

Two highway slope sites were selected and investigated for this task. They are:

1. Slope-1: US-287 (Midlothian)

2. Slope-2: I-20 and Parks Springs Blvd (Arlington)

The first slope was located over highway US 287 near Midlothian, TX (Figure 3.1). The selected 79.2 m (260 ft) long highway section was constructed over an embankment slope of 3H: 1V. The slope section underwent repetitive failures from its construction. The shoulder portion experienced many severe longitudinal edge cracks due to the downward slope movement. After each failure incidence, the slope was repaired, and in 2017 one part of the slope was reinforced

with Recycled Plastic Pin (RPP) with combining Modified Moisture Barrier (MMB)(Sapkota 2019). The amount of total precipitation in September and October 2018 were 15.3 and 13.39 inches, and one part of the slope failed in October 2018. This time, the length of the surficial slope failure was about 100 ft, the starting of the slip circle was just 5 ft below the pavement, and there was a massive bulge at the middle of the slope (Figure 3.2).

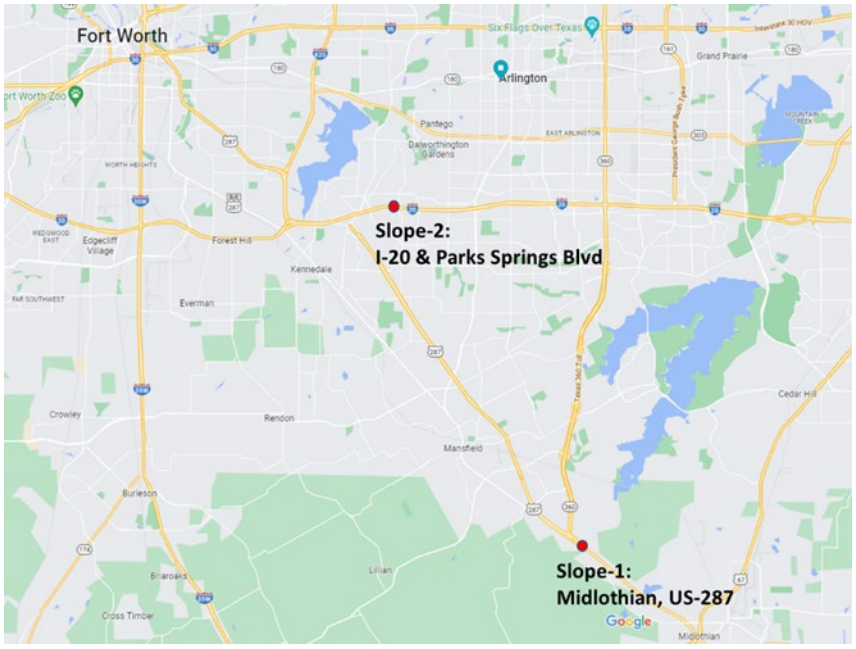

Figure 3.1 Map showing failed slopes along with the current project site.

A comprehensive site investigation program was undertaken, involving soil boring and resistivity imaging. The results of this investigation revealed the presence of two distinct soil layers in the subsurface: highly plastic clay soil and shale. Upon analyzing the Standard Penetration Test-N value, the uppermost layer was further subdivided into two sections: soft clay (0 to 10 feet) and medium-stiff clay (10 to 22 feet). The prevailing soil type was predominantly high plastic clay, known for its susceptibility to shrinkage and swelling behavior. The cyclic nature of this shrinkage-swelling behavior led to a decrease in the shear strength of the plastic clay, eventually reaching its fully softened strength (Saleh and Wright, 1997; Wright, S.G., 2005).

Also, penetration of rainwater significantly deteriorates the condition which further causes the movement and shallow failure of slopes.

Figure 3.2 The failed sections at US-287 (after Islam 2021)

The second slope is located at the intersection of Eastbound Interstate Highway 20 & Park Springs Blvd. The slope has a geometry of 3 (H): 1 (V). The length of the failure is about 120 ft and 61 ft wide. It was classified as shallow slope failure based on the failure depth of about 2 to 3 ft (Figure 3.3). After site reconnaissance, a slope stabilization scheme using modified moisture barrier (MMB) and recycled plastic pins (RPP) was implemented in September 2019. A modified moisture barrier was installed in a 60 ft long section followed by a 60 ft long section reinforced with recycled plastic pins. Lastly, a 60 ft long control section was established next to the reinforced section. The control section was a well compacted and stable slope that had not experienced failure.

Figure 3.3 The failed section at I-20 and Parks Springs Blvd

3.4 LABORATORY TEST RESULTS

For laboratory testing, disturbed and undisturbed samples were collected at different depths from both sites. Soil physical, shear strength and hydraulic properties were determined in the laboratory.

For slope-1, Moisture content examinations were conducted to monitor the moisture fluctuations at different depths. The gravimetric moisture content test adhered to the ASTM D2216 Standard Test Methods for Laboratory Determination of Water (Moisture) Content of Soil and Rock by Mass. Depicting the moisture content profiles concerning the depths of soil samples collected from four boreholes, Figure 3.4 provides an overview. The outcomes illustrated a range of gravimetric moisture content from 22% to 42%. Furthermore, significant moisture variations were particularly noticeable within the upper 8 feet (Sapkota 2019).

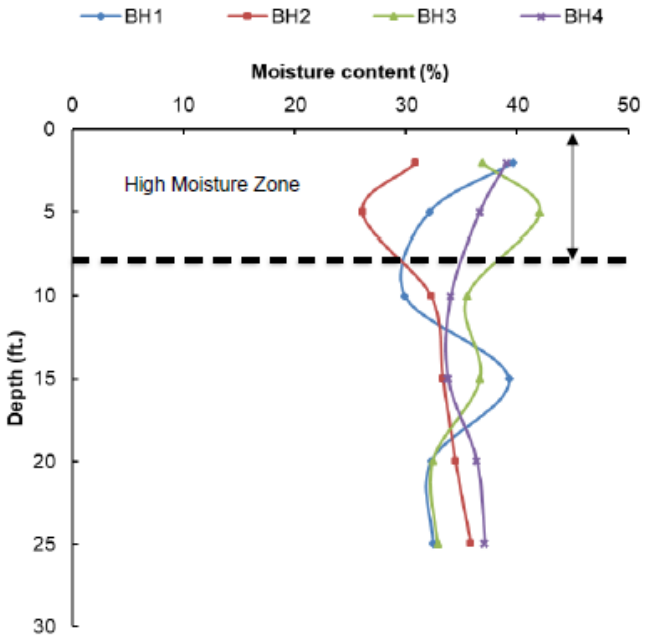

Figure 3.4 Moisture profile with respect to depth (after Sapkota 2019)

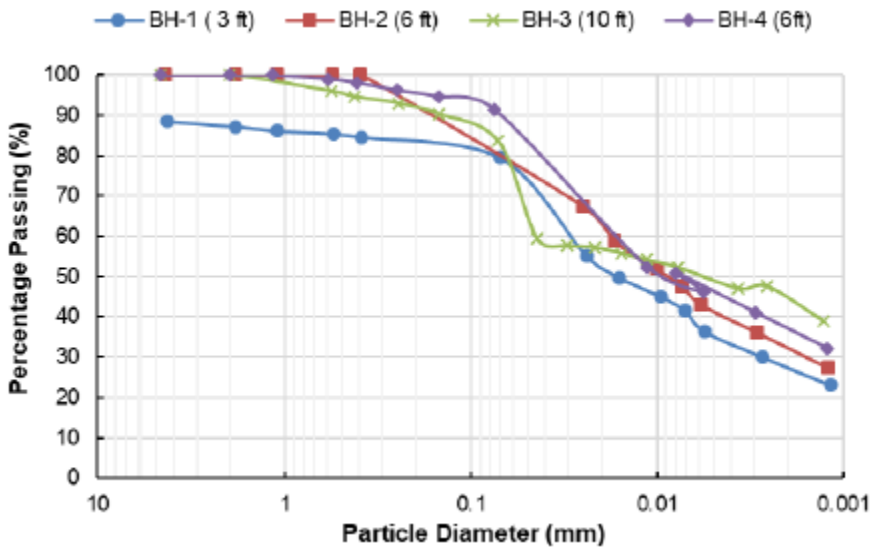

Figure 3.5 Grain size distribution curve (after Sapkota 2019)

The results of the grain size distribution test showed that the fine fraction of the collected soil samples passing through a #200 sieve ranged from 75 to 95%, indicating fine-grained soils.

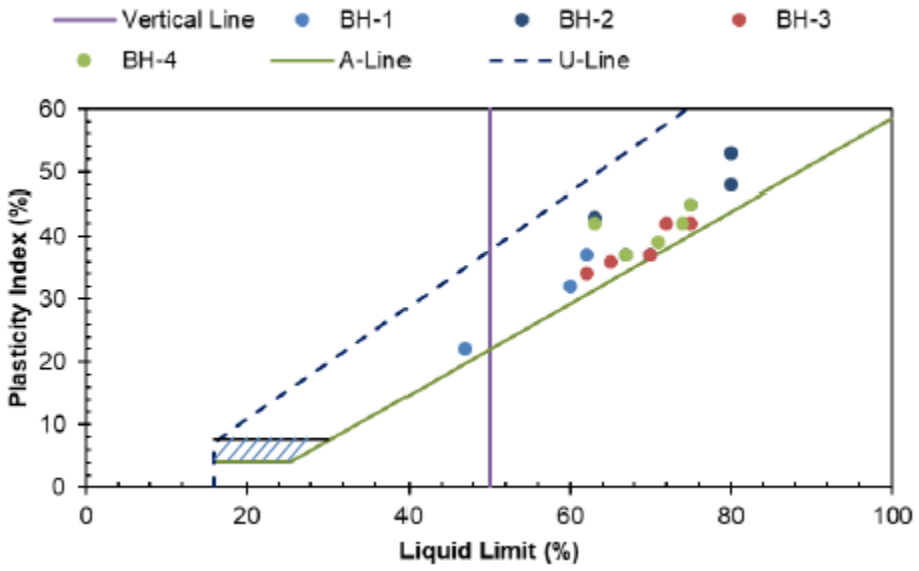

Figure 3.6 Plasticity chart from collected soil samples.

The liquid limit for collected samples ranged from 47 to 80%, while the plastic limit ranged from 30 to 55%. The plasticity chart of the soil samples is presented in Figure 3.6. The results of

the Atterberg limit tests and grain size distribution tests showed that the collected soil samples were high plasticity clay, based on the Unified Soil Classification System (USCS).

For slope-2, moisture content varied between 8% to about 20%. The liquid limits and plasticity indices of the samples ranged from 30% to 48% and 9% to 32% respectively.

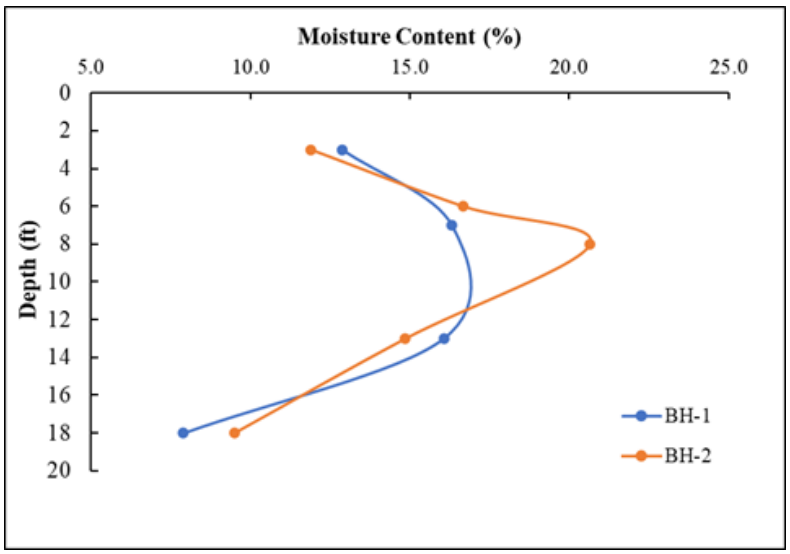

Figure 3.7 Moisture profile at different depth

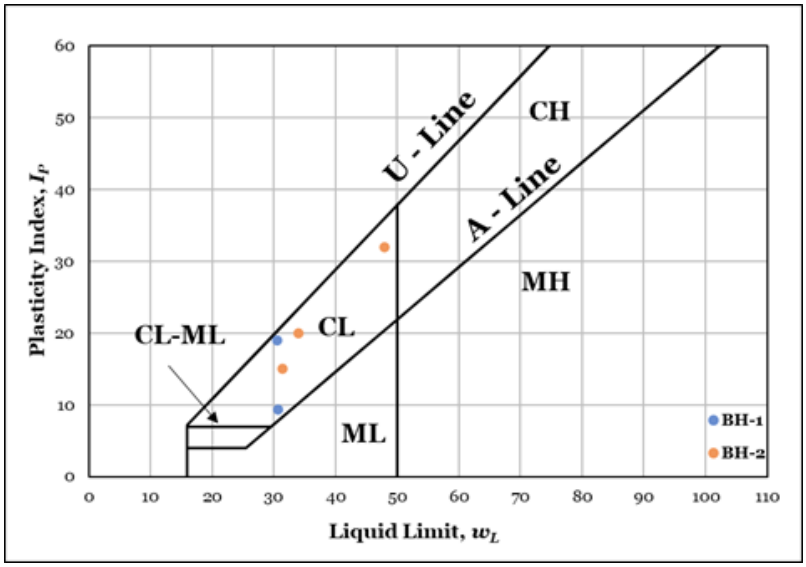

Figure 3.8 Plasticity chart from selected soil samples

Grain size distribution test was performed using both mechanical sieve and hydrometer analyses to obtain the full-range grain size distribution curve following ASTM D7928 Code. The results of the test have been tabulated below in Table 3.1.

Table 3.1 Grain Size Distribution Results.

Depth(ft)	% Gravel	% Sand	% Silt or Clay	Classification
3-4	0.71	76.58	23.42	Clayey Sand
18	12.47	70.82	29.18	Clayey Sand

Shear strength properties

The undisturbed samples were used to evaluate the shear strength properties through laboratory testing. For slope-1, shear test results are tabulated in Table-1.

Table-1: Shear Strength properties of soil from Slope-1 (after Islam 2021)

Boring No.	Sample Depth (m)	Specimen	Test Type	Cohesion (kPa)	Friction Angle
BH-1	1.5	Undisturbed	Direct Shear	5.31	11.6
BH-1	4.5	Undisturbed	Triaxial CU	1.63	21.06
BH-1	7.6	Undisturbed	Triaxial UU	214.3	0

For slope-2, direct shear test (ASTM D3080) was performed on a sample collected from 8 ft depth and it showed the following parameters:

Table-2: Shear Strength properties of soil from Slope-2

Boring No.	Sample Depth (m)	Specimen	Test Type	Cohesion (kPa)	Friction Angle
BH-1	2.5	Undisturbed	Direct Shear	11.7	14.5

3.5 FIELD INSTRUMENTATION

The test slope sections were instrumented using moisture sensors and soil water potential sensors to observe volumetric moisture content and metric suction at site.

Slope-1: US-287 (Midlothian)

In October 2019, the instrumentation for the project was carried out. This instrumentation consisted of soil water potential probes and soil moisture sensors. Water content data solely cannot give the unsaturated condition of the soil. The combination of a water content sensor and soil water potential sensor provides the ground's current situation. Thus, soil water potential sensors were also installed during instrumentation. In this study, commercially available TEROS 12 sensors were used to measure volumetric water content and TEROS 12 Soil Water Potential sensors were used to measure the soil metric suction.

These sensors were installed at 0.91 m (3 ft), 1.52 m (5 ft), 2.1 m (7 ft), and 3.0 m (10 ft) depth and 3.048 m (10 ft) away from the shoulder (Figure 3.9).

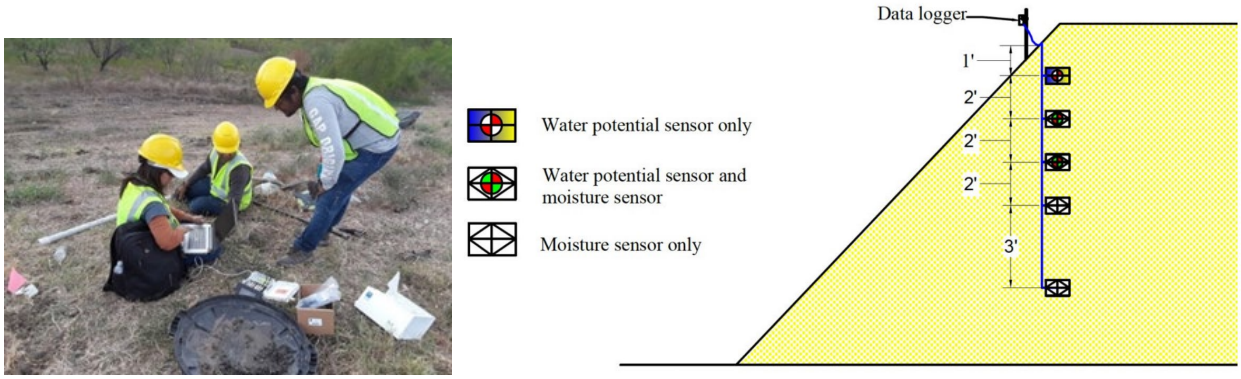

Figure 3.9 Instrumentation process and layout at US-287 site

Slope-2: I-20 and Parks Springs Blvd (Arlington)

In this slope section, the Meter Group moisture-temperature sensors (Teros 12) and suction sensors (Teros 21) were installed to monitor the moisture fluctuation. Two 10 ft. deep boreholes were drilled at the MMB section and at the control section to install the moisture and suction sensors at varying depth. A total of 8 sensors (4 moisture sensors and 4 suction sensor) were installed at each borehole at 4 different 0.91 m (3 ft), 1.52 m (5 ft), 2.1 m (7 ft), and 2.74 m (9 ft) depth. Proper care was taken while compacting the soil after each sensor was installed to avoid any damage to the sensors. The sensors were then connected to a data logger (Figure 3.10).

A new set of sensors were installed in the control section in March 2021 at 0.3048 m (1 ft) and 0.6096 m (2 ft) depth to monitor the volumetric water content at shallow depth.

Figure 3.10 Installation of the sensors at Parks Springs site

Data acquisition

The moisture-temperature sensors, and water potential sensors were connected to the data logger. For receiving and storing the field data, ZL6 model data loggers were used. The data logger

was used to store the recorded hourly readings for all sensors. The measurement interval was set to 60 minutes, which allowed storing 24 data per day. Rainfall data were obtained from the National Oceanic and Atmospheric Administration (NOAA) website.

3.6 FIELD EXPERIMENTAL PROGRAM

As shear strength fluctuates most at the crest of slope (Sakib et al., 2022), two points were chosen at the crest of the slope to assess changes in soil permeability across different seasons, as shown in Figure 3.11. The hydraulic conductivity was determined monthly on the points and average values were taken. The tests were conducted using Guelph permeameter and Mini Disk Infiltrometer. Using Guelph Permeameter, the hydraulic conductivity was measured at a depth of 2 feet, whereas the Mini Disk Infiltrometer measured the hydraulic conductivity on the surface.

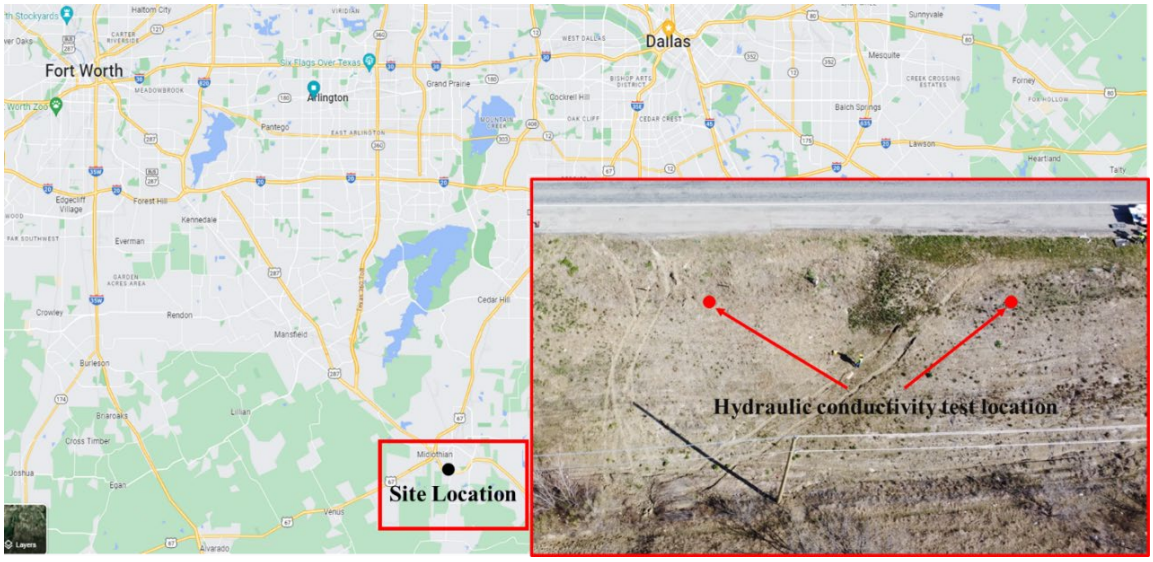

(a)

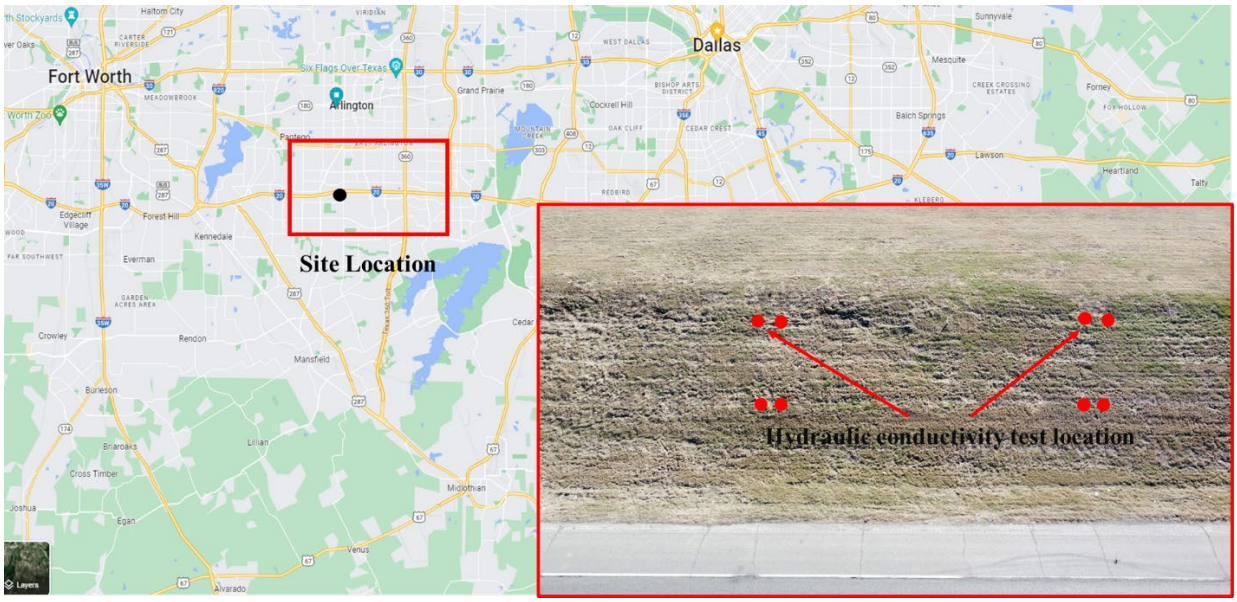

(b)

Figure 3.11 Location of selected section for field investigation at (a) US287 and (b) I20 and Parks Springs Blvd

The detailed instrumental setup of the Guelph permeameter is shown in Figure 3.12. The method involves measuring the steady-state rate of water recharged into unsaturated soil from a cylindrical well hole, in which a constant depth (head) of water is maintained. Before the test, a borehole was prepared using the soil auger so that the surface was plain and free of any debris. Then the instrument was assembled with all the components and placed in the hole. The reservoir of the instrument is then filled with water, and the whole setup is made sure that it is air tight. A clamping ring was tied to the nylon tube, and a fill plug was placed into the water inlet hole to make it air tight. A head of 10 cm was then provided at the well head scale, and water was allowed to flow. The reading from the inner reservoir of the permeameter was recorded, and the hydraulic conductivity was calculated using a set of equations developed by Zang et al. (1998).

$$Q_1 = \bar{R}_1 \times 2.16 \qquad (1)$$

$$C_1 = \left[\frac{H_2/a}{2.081 + 0.0121(H_2/a)}\right]^{0.672} \quad (2)$$

$$K_{fs} = \frac{C_1 \times Q_1}{2\pi H_1^2 + \pi a^2 C_1 + 2\pi\left(\frac{H_1}{a^*}\right)} \quad (3)$$

Where, K_{fs} is soil saturated hydraulic conductivity (cm/s); C is dimensionless shape factor; R is steady state rate of fall of water in reservoir (cm/s); H is steady depth of water in boring; a is the radius of well; H_1 is the first head of water established in borehole (cm); H_2 is the second head of water established in borehole (cm); a^* is the microscopic capillary length parameter: 0.01 for compacted structureless clayey materials, 0.04 for fine-grained unstructured clay, 0.12 structure soil and unstructured medium to fine sand, 0.36 for coarse-grained sand and gravel, highly structured soil with large cracks.

Figure 3.12 Instrumental setup of Guelph Permeameter

Mini Disk Infiltrometer is a tension Infiltrometer and measures the medium's unsaturated hydraulic conductivity at different applied tensions. A plain surface was prepared where the instrument would be placed. Then the bubble chamber was filled three quarters full down the suction control tube or removing the upper stopper. Once the upper chamber is full, the suction control tube slides down. The water reservoir was filled with water by inverting the infiltrometer and removing the bottom elastometer with the porous disk. Then the position of the end of the Mariotte tube with respect to the porous disk was set to ensure a zero suction offset while the tube bubbles. Then the suction rate was adjusted to 2 cm, following the instruction for clay soil. The infiltrometer was placed on the prepared surface, ensuring good contact between the soil and the infiltrometer as shown in Figure 3.13.

Figure 3.13 Instrumental setup of Mini Disk Infiltrometer

In this study, the volumetric water content data were collected from NASA POWER (Prediction of Worldwide Energy Resources) website and used to establish a relationship with hydraulic conductivity. Since, the soil was in unsaturated condition, it was very important to

monitor the volumetric water content over time. The saturated and unsaturated flow through a medium is defined by the following equations:

Darcy's Law (for saturated condition): $q = -K_s \frac{dh}{dL}$;

q=rate of water flow, K_s=saturated hydraulic conductivity, $\frac{dh}{dL}$=hydraulic gradient

Darcy-Buckinghum Law (for unsaturated condition) : $q = -K(\Psi)[\frac{d(\Psi)}{dz} + 1]$;

Ψ=metric potential, K=unsaturated hydraulic conductivity, $\frac{d(\Psi)}{dz}$=gradient for metric potential

The unsaturated flow is clearly a function of metric potential or the volumetric water content. The relationship between hydraulic conductivity and volumetric water content was tried to comprehend and explained in this study.

3.7 RESULTS AND DISCUSSION

In this study, monthly variation was monitored for slope-1 in two designated spots using the Guelph Permeameter and Mini Disk Infiltrometer, respectively, at 2 ft depth and on the surface. The designated spots were at the crest of the slope in two different sections, as mentioned earlier. At first the volumetric water content data from the POWER Website were plotted and a relationship was established in Figure 3.14.

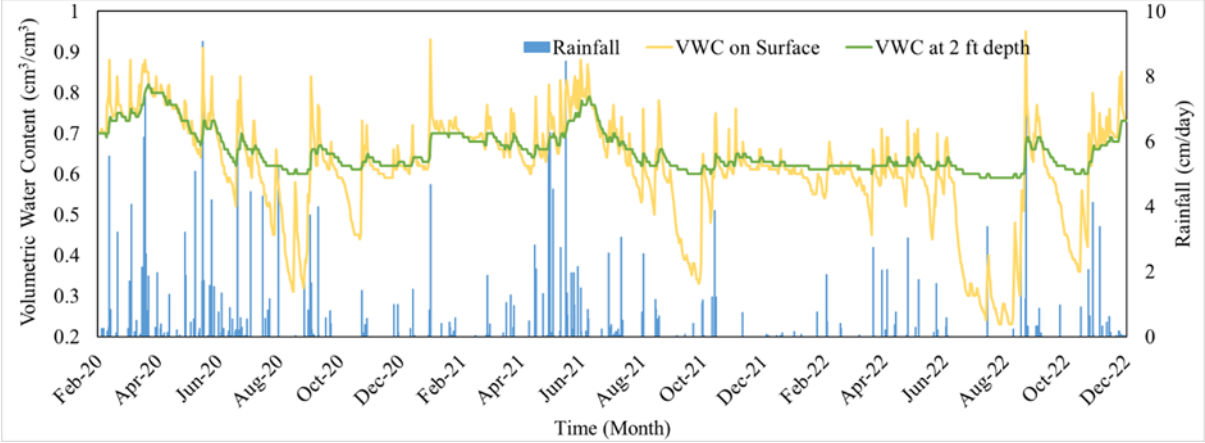

Figure 3.14 The variation in Volumetric Water Content with Rainfall using on surface and at 2ft depth.

Figure 3.14 shows the change in daily volumetric water content (VWC) with rainfall on surface and at 2ft depth from February 2020 to December 2022. The monthly precipitation data for Midlothian, TX, were collected from the NOAA website. It was evident that the rainfall events are liable for the change in VWC. Typically, following a precipitation event, a portion of the rainfall is channeled as surface runoff, while the remainder infiltrates the soil. Therefore, the changes are prominent after the rainfall events. However, the result shows that the VWC on surface fluctuates more than at 2ft depth. The VWC on surface can be as high as 0.95 and as low as 0.23 which also indicates fluctuation. At 2ft depth, the VWC ranged from 0.61-0.82. In every year, during August, when the air temperature was very high and the rainfall depth was, a steep drop in VWC was observed on the surface. The Figure 3.15 shows that the standard deviation at 2ft depth was 62% less than that of on the surface. The coefficient of variation was also found to be 21% on the surface whereas only 8% at 2ft depth.

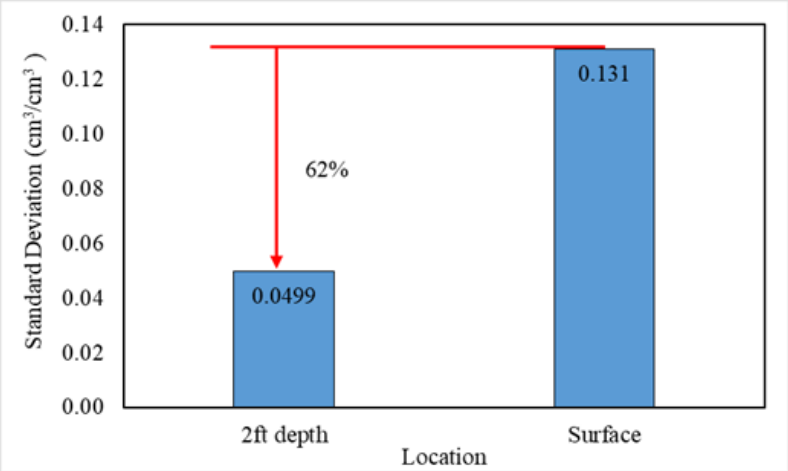

Figure 3.15 Standard Deviation in Volumetric Water Content at different depth

3.7.1 Hydraulic Conductivity results

The hydraulic conductivity results were collected and presented graphically in Figure 3.16. The observed trend indicates various changes with time with the changing volumetric water content which resulted due to different precipitation events.

The Guelph permeameter test results show the condition at 2ft depth. variation can be elucidated through an examination of volumetric water content data. Typically, following a precipitation event, a portion of the rainfall is channeled as surface runoff, while the remainder infiltrates the soil. The precipitation events augment the volumetric water content within soil pore spaces. It was observed that rainfall events led to an increased volume of water within soil pores. The flow of water through pore spaces is governed by capillary forces, and heightened water content within these spaces results in increased hydraulic conductivity. Pore spaces filled with water act as channels for water flow. In short, the volumetric water content increases, more pores are filled with water, and the water can flow more easily through the soil, resulting in higher hydraulic conductivity (Rose et al., 1965).

Nonetheless, exceptions to this trend may arise due to partially unsaturated conditions. According to Darcy's law of flow through any soil media, in fully saturated conditions, all pore spaces are interconnected, facilitating ease of water flow. However, under partially saturated or unsaturated conditions, air voids do not contribute to water flow, leading to reduced hydraulic conductivity which follows Darcy-Buckingham's law. From the Figure 3.16(a), such discrepancies were observed during February 2020 and January-February 2021. Despite high VWC, the hydraulic conductivity was low. This may happen if the fine-grained soils possess a layer of adsorbed water strongly attached to their surface, which is not free to move under gravity even under high moisture (Arora, 2008), which eventually leads to the decrease of hydraulic conductivity.

For the Mini Disk Infiltrometer, a similar variation was found on a monthly basis (Figure 3.16(b)). Macropores generally fill with air, leaving only the finer pores to accommodate water movement. Therefore, the hydraulic conductivity of the soil is strongly dependent on the detailed pore geometry, water content, and differences in matric potential (Brady and Weil, 1999). After heavy rainfall, the soil water content increases which results in increasing hydraulic conductivity (similar to Guelph permeameter). In this case, in certain instances, high hydraulic conductivity was found even in low moisture content. During dry days, expansive soil forms cracks and the air inside is connected to the atmospheric air which is easily to be replaced by flow of water (unlike entrapped air) and so, the ease of water flow increases the hydraulic conductivity. This also can be explained by the fact that there is a good infiltration rate due to the continuity of pores in the soil, as stated by Costa et al. (2016).

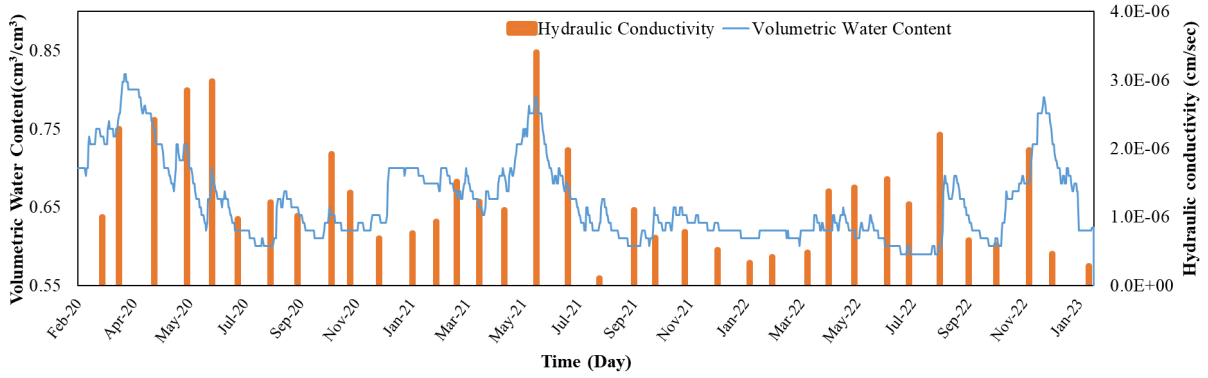

(a)

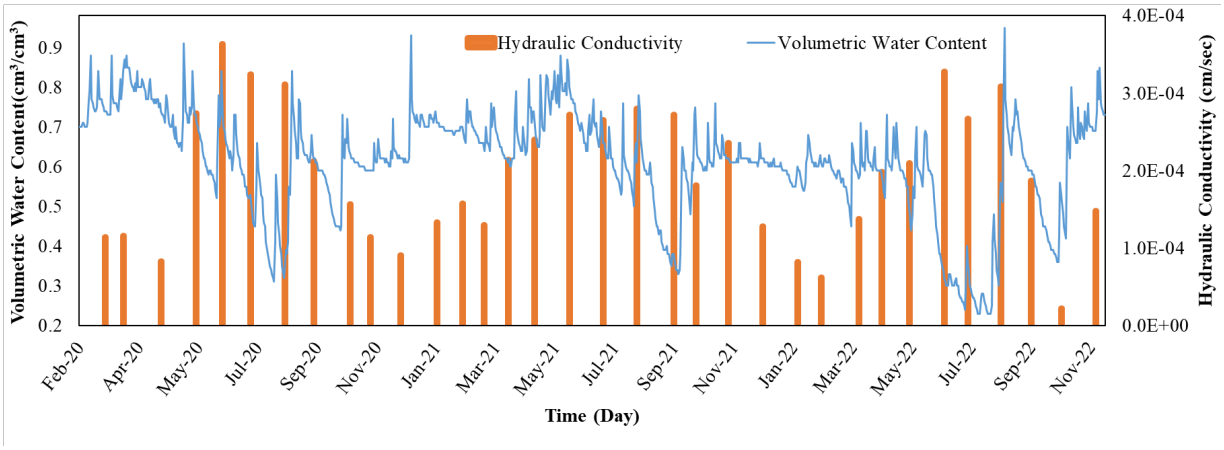

(b)

Figure 3.16 Variation in hydraulic conductivity with VWC using (a) Guelph Permeameter and (b) Mini Disk Infiltrometer

3.7.2 Seasonal Variation in hydraulic conductivity

The seasonal variation in hydraulic conductivity was observed as a part of this study. March-May, June-August, September-November and December-January were defined as Spring, Summer, Fall and Winter season. For every three months, average values were considered, and a seasonal trend was found as shown in Figure 3.17. The results obtained from both instruments

showed that highest and lowest hydraulic conductivity was observed during Summer and Winter respectively. A possible reason for the higher conductivity in summer is the cracks formed due to high temperature. And due to this crack, the rainwater can infiltrate easily filling up the pores which makes the water flow path and ease the flow of water during the test.

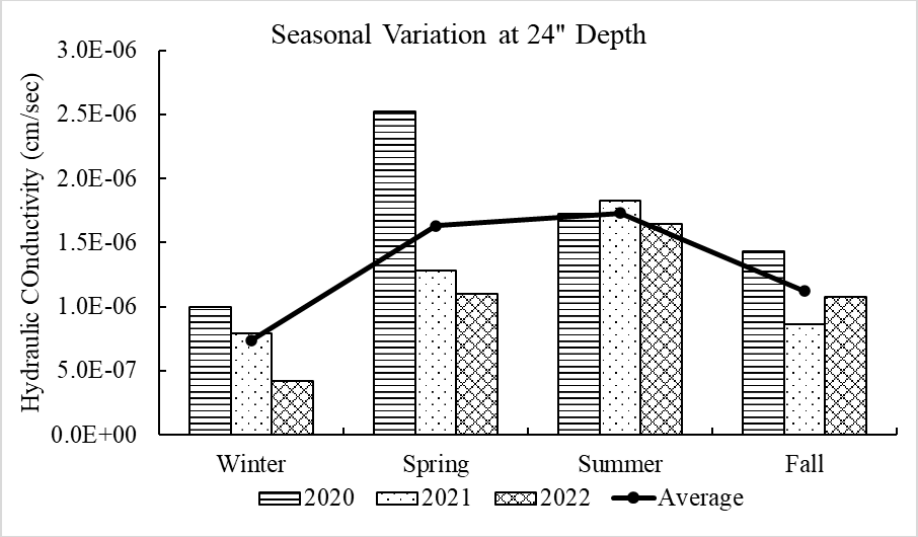

(a)

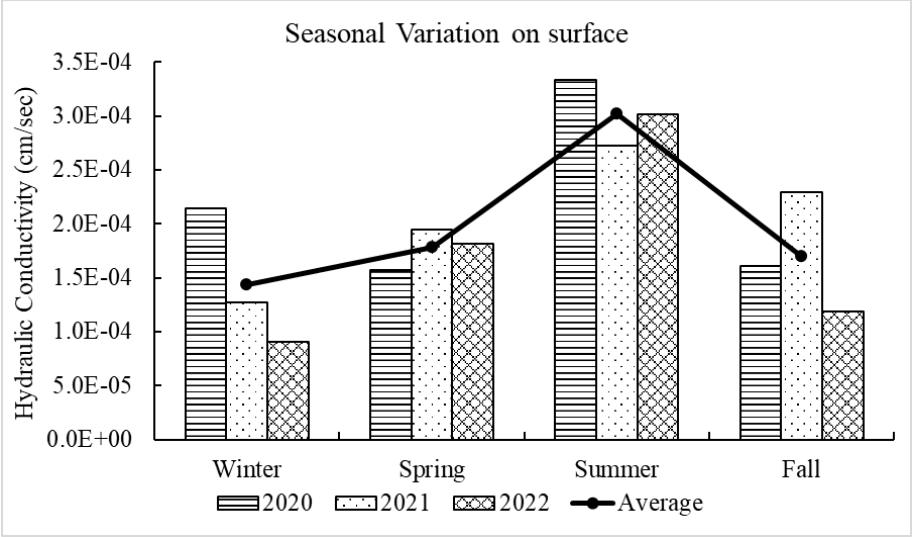

(b)

Figure 3.17 Seasonal Variation monitored using (a) Guelph Permeameter and (b) Mini-Disk Infiltrometer

In summer, the high soil temperature can lead to higher microbial activities which can alter soil and increase hydraulic conductivity. In contrast, colder temperatures in winter can reduce these processes, leading to lower hydraulic conductivity. In winter, freeze and thaw cycle can affect the hydraulic conductivity since the soil is high plastic clay. During Spring and fall, the moisture retention, the evapotranspiration process, the plant activity increases which results in hydraulic conductivity higher than winter and lower than summer. The average decrease in hydraulic conductivity for all three years with respect to summer is shown in Table 3.2.

Table 3.2**.** The decrease in hydraulic conductivity from Summer

	Winter	**Spring**	**Fall**
Guelph Permeameter	57%	6%	36%
Mini-Disk Infiltrometer	52%	42%	44%

3.7.3 Comparison between Guelph Permeameter and Mini-Disk Infiltrometer

The discrepancy between the two instruments signifies the variance in hydraulic conductivity at the surface level and at a depth of 2 feet. The alteration pattern in hydraulic conductivity is notably similar for both instruments. As displayed in Figure 3.18, the hydraulic conductivity at the surface, determined via the Mini Disk Infiltrometer, was found to be up to 100 times higher than that at a depth of 2 feet, as assessed using the Guelph Permeameter. This discrepancy can be attributed to visible surface desiccation cracks during dry seasons, which lead to augmented hydraulic conductivity. These cracks, however, do not extend to the 2-foot depth,

resulting in the lower hydraulic conductivity measurements using the Guelph Permeameter. Even during the rainy season, the hydraulic conductivity remains elevated compared to the 2-foot depth readings. Factors contributing to this disparity include surface disturbances and increased compaction at the 2-foot depth, leading to reduced pore size and subsequently lower hydraulic conductivity. These factors encompass shallow root growth and cracking instigated by worms or ants, ultimately causing an overestimation of surface hydraulic conductivity, as noted by Silva et al. (2019). The diminished hydraulic conductivity at the 2-foot depth can be attributed to trapped air hindering the free flow of water through voids. Similar patterns of short-term variability, as observed by Scott et al. (1994), reinforce this trend, indicating higher hydraulic conductivity in the top layer compared to the lower layer.

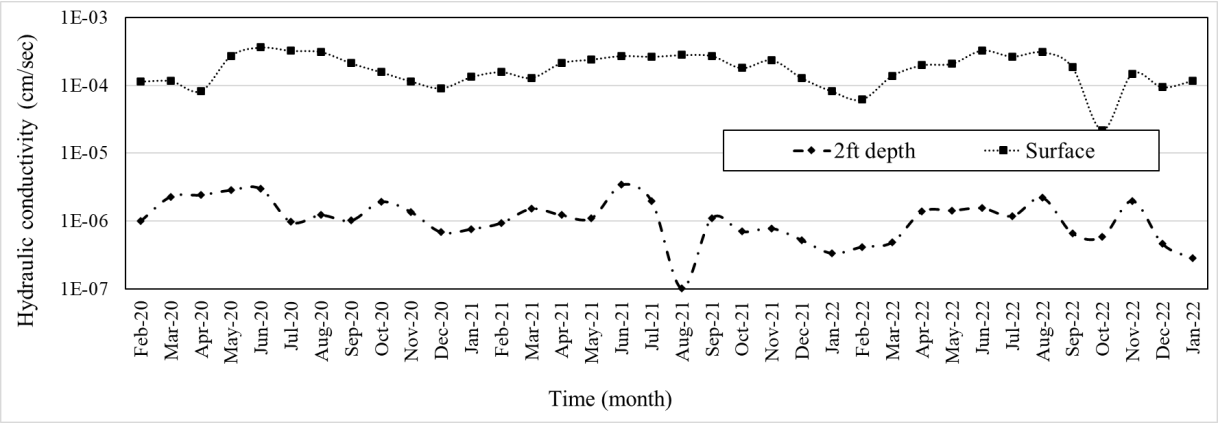

Figure 3.18 Difference in hydraulic conductivity results between at different depth

The differences in hydraulic conductivity between two instruments are quantified below in **Error! Reference source not found.**. The co-efficient of variation shows that Guelph permeameter result varies more seasonally. This is due to the change in substructural properties inside the soil such as soil temperature, volumetric water content, soil porosity etc. However, the

standard deviation is high in Mini-Disk infiltrometer due to surficial cracks caused by high temperature, and shallow root activities of plants.

Table 3.3 The statistical data by two different instruments

	Guelph Permeameter	**Mini-Disk Infiltrometer**
Mean (cm/sec)	1.3×10^{-6}	1.9×10^{-4}
Median (cm/sec)	1.1×10^{-6}	1.8×10^{-4}
Standard Deviation (cm/sec)	8.0×10^{-7}	8.7×10^{-5}
Co-efficient of Variation (%)	63	46
Maximum (cm/sec)	3.4×10^{-6}	3.6×10^{-4}
Minimum (cm/sec)	1.02×10^{-7}	2.2×10^{-5}

3.8 CONCLUSION

This paper contains the field investigation of hydraulic conductivity and its variation in different climatic & subsurface conditions on a slope in the US287 highway located at Midlothian, Texas. The investigated results can be summarized as follows:

- The standard deviation in VWC was 62% less at 2ft depth.

- It was evident from the field test that, with higher precipitation, the volumetric water content increased and hence the hydraulic conductivity increased.
- Despite some inconsistencies, hydraulic conductivity was found highest in Summer due to the desiccation cracks formed in expansive clay.
- In the statistical comparison, it was observed that the results at the surface level were 100 times higher than that of the results at 2 feet depth. The soil at 2 feet depth is more compacted and has fewer cracks, and contains a significant number of air pockets, which are the reasons behind low hydraulic conductivity.

CHAPTER 4

DEVELOPMENT OF A PREDICTION MODEL BASED ON IN-SITU HYDRAULIC CONDUCTIVITY

4.1 ABSTRACT

In this chapter, a prediction model was developed based on the in-situ hydraulic conductivity. To develop the predictive model, the numeric computing software MATLAB was used. Antecedent rainfall, volumetric water content and soil temperature were used as independent variables and hydraulic conductivity was considered as output in this program. The regression learner application was used to build this model. 3-years of monthly in-situ hydraulic conductivity data were used as input to train the model. Based on the training data, a prediction was developed. The test data were calculated based on the new data collected from another site and output hydraulic conductivity were validated with the field data. Based on the model, an investigation on slope failure from real-time data was carried out and the threshold hydraulic conductivity was evaluated for the slopes in Fort-Worth.

4.2 INTRODUCTION

A hydraulic conductivity prediction model based on soil temperature, volumetric water content, and antecedent rainfall is a valuable tool in hydrogeology and environmental science. The model leverages the relationships between these key parameters to estimate the hydraulic conductivity of soil accurately. Soil temperature influences the viscosity and flow of water through the soil matrix, while volumetric water content indicates the amount of water present in the soil pores, affecting its ability to transmit water. Antecedent rainfall, representing previous precipitation events, plays a role in soil moisture levels and can affect the saturated hydraulic conductivity. By integrating these variables into a prediction model, researchers and engineers can

gain insights into the dynamic behavior of soil water movement. This information is crucial for various applications, such as groundwater recharge estimation, flood forecasting, and irrigation management. The model enables the assessment of soil water dynamics, allowing for better decision-making in predicting shallow slope failure.

Machine learning has become increasingly important in various fields, including geotechnical engineering. Machine learning algorithms can analyze large datasets containing geotechnical information, historical data, and sensor readings to develop highly accurate predictive models. These models can help anticipate potential failures, landslides, settlement, and other geotechnical issues, enabling engineers to take proactive measures and avoid costly damages. Machine learning (ML) is an empirical approach where a computer program learns from a dataset without the need to code the problem and a procedure to solve it. However, there are limited studies in Geotechnical engineering where machine learning algorithms are used to predict based on historical data.

Several ML applications can already be found in the geotechnical engineering literature. For example, Mustafa et al. (2013) evaluated the performance of four ANN training algorithms for modelling the dynamics of soil pore water pressure (PWP) in response to rainfall variations using multilayer perceptron (MLP) ANN. The results showed that the network performance (training time and prediction accuracy) is related to the type of training algorithm.

Gordan et al. (2015) used artificial neural network (ANN) and particle swarm optimization (PSO)–ANN models to predict the factor of safety (FOS) of homogenous slopes during earthquakes. A dataset including 699 FOS values for different slope geometries, soil properties and peak ground accelerations was obtained using the Geostudio software package.

In this study, in-situ hydraulic conductivity tests were conducted on monthly basis using two instruments: Guelph Permeameter and Mini-Disk Infiltrometer. From February 2020, monthly data were collected till May 2023 from US287 Midlothian Site. And these data were used for training the model. Another site was selected at I30 and Perks Springs Blvd to collect data for validation. This developed model was used to predict threshold hydraulic conductivity and historical slope failure sites were used to validate the threshold results.

4.3 REGRESSION LEARNER APP

Regression Learner is a module of MATLAB that can be used to train regression models including linear regression models, regression trees, Gaussian process regression models, support vector machines, kernel approximation, ensembles of regression trees, and neural network regression models. In addition to training models, it can be used to explore data, select features, specify validation schemes, and evaluate results. The model can be exported to the workspace to use the model with new data or generate MATLAB code to learn about programmatic regression.

Training a model in Regression Learner consists of two parts:

Validated Model: Train a model with a validation scheme. By default, the app protects against overfitting by applying cross-validation. Alternatively, holdout validation can be chosen. The validated model is visible in the app.

Full Model: Train a model on full data, excluding test data. The app trains this model simultaneously with the validated model. However, the model trained on full data is not visible in the app. If a regression model is chosen to export to the workspace, Regression Learner exports the full model.

The app displays the results of the validated model. Diagnostic measures, such as model accuracy, and plots, such as a response plot or residuals plot, reflect the validated model results. One or more regression models can be automatically trained, compared validation results, and choose the best model that works for regression problem. If a model is chosen to export to the workspace, Regression Learner exports the full model. Because Regression Learner creates a model object of the full model during training, there is no lag time when exporting the model. The exported model can be used to make predictions on new data.

4.4 INPUT DATA PREPARATION

The hydraulic conductivity data were collected and corresponding soil temperature, volumetric water content and 10 days antecedent data were collected from National Oceanic and Atmospheric Administration (NOAA) official site and NASA Prediction of Worldwide Energy Resources (POWER) website. Data were obtained both surficial data and at 2 ft depth to incorporate with Mini-Disk Infiltrometer and Guelph Permeameter data respectively. 40 sets of data were used to train the model.

4.4.1 Guelph Permeameter

The input variable and corresponding hydraulic conductivity data were prepared as shown in Table 4.1.

Table 4.1 Input data for Guelph Permeameter

Soil Temperature (ºC)	**VWC (cm^3/cm^3)**	**Antecedent Rainfall (cm/day)**	**Hydraulic Conductivity (cm/sec)**

13.2	0.7	1.3	9.98E-07
24.54	0.77	3.3	2.28E-06
26.6	0.75	4.7	2.42E-06
28.9	0.77	5.1	2.85E-06
29.6	0.78	4.21	2.98E-06
28.55	0.62	2.24	9.67E-07
26.45	0.7	3.01	1.22E-06
25.49	0.65	1.1	1.02E-06
19.9	0.68	2.98	1.92E-06
18.19	0.62	3.4	1.35E-06
10.94	0.64	0.68	6.84E-07
7.95	0.7	0.65	7.60E-07
8.4	0.68	0.12	9.36E-07
18.9	0.67	3.4	1.52E-06
20.3	0.65	2.36	1.22E-06
17.46	0.69	3.94	1.10E-06

30.55	0.79	4.66	3.40E-06
27.06	0.68	2.66	1.97E-06
16.77	0.63	0	1.02E-07
18.44	0.65	0.19	1.10E-06
26.5	0.64	1.16	6.99E-07
16.66	0.64	0.29	7.78E-07
8.33	0.63	0.1	5.22E-07
4.64	0.61	0.05	3.34E-07
5.44	0.62	0	4.15E-07
8.6	0.62	1.09	4.85E-07
23.19	0.62	2.23	1.37E-06
21.2	0.62	4.2	1.43E-06
26.5	0.7	3.6	1.55E-06
26.66	0.74	1.33	1.18E-06
30.57	0.75	2.73	2.20E-06
27.73	0.64	0	6.59E-07

11.63	0.61	0.36	5.89E-07
20.11	0.68	2.3	1.98E-06
3.84	0.66	0.39	4.59E-07
4.08	0.61	1.34	2.82E-07
9.2	0.62	0.13	4.98E-07
13.65	0.68	1.56	7.22E-07
19.66	0.65	1.55	5.49E-07
24.5	0.71	2.88	1.49E-06

A simple linear regression analysis was performed with each variable and hydraulic conductivity and strong relationship was found between each relation. The Figure 4.1, Figure 4.2, Figure 4.3 show the relation of hydraulic conductivity with 10-days antecedent rainfall, volumetric water content and soil temperature. It was found that volumetric water content has the best R-squared value of 0.72 which means that 72% of the data can be explained with the governing equation between hydraulic conductivity and volumetric water content. In-situ geotechnical properties can vary temporarily and spatially. Hence, with respect to that statement, it has a good fit.

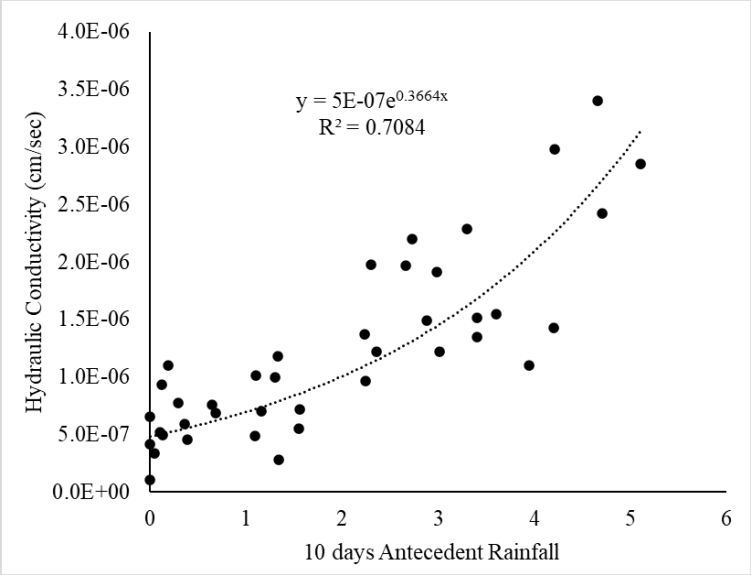

Figure 4.1 Relation between soil hydraulic conductivity with 10 days antecedent rainfall

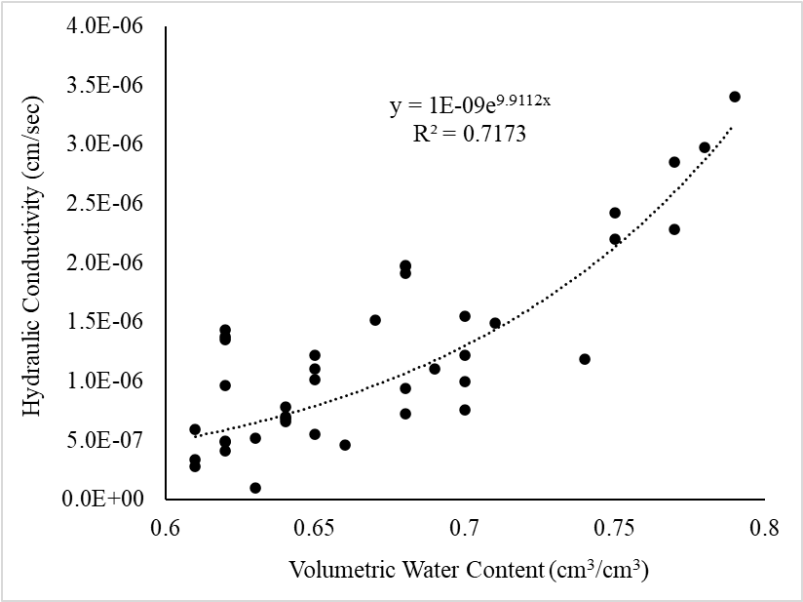

Figure 4.2 Relation between soil hydraulic conductivity with volumetric water content

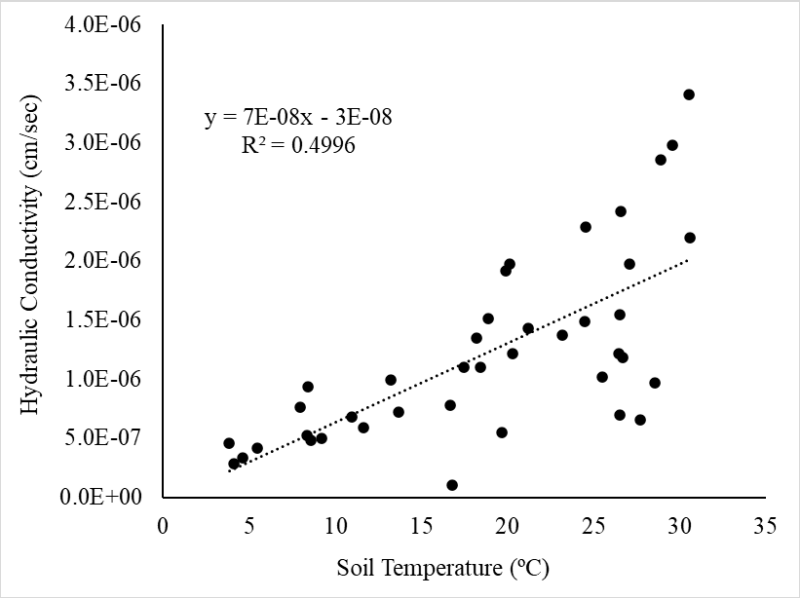

Figure 4.3 Relation between soil hydraulic conductivity with soil temperature

4.4.2 Mini-Disk Infiltrometer

The input variable and corresponding hydraulic conductivity data were prepared as shown in Table 4.2.

Table 4.2 Input data for Mini-Disk Infiltrometer

Soil Temperature (ºC)	**VWC (cm^3/cm^3)**	**Antecedent Rainfall (cm/day)**	**Hydraulic Conductivity (cm/sec)**
5.48	0.23	0.33	1.14E-04
15.74	0	0.54	1.16E-04
19.95	0.7	0.44	8.26E-05
23.25	4.8	0.73	2.74E-04

26.29	3.89	0.73	3.63E-04
29.3	2.24	0.75	3.24E-04
32.49	3.01	0.77	3.11E-04
22.97	1.1	0.62	2.12E-04
12.62	2.98	0.63	1.57E-04
18.21	1.4	0.59	1.14E-04
9.49	0.68	0.62	9.08E-05
8.37	0.65	0.51	1.33E-04
17.08	0.12	0.7	1.57E-04
15.74	3.4	0.64	1.30E-04
20.37	2.36	0.61	2.14E-04
18.1	3.94	0.7	2.40E-04
26.73	4.66	0.8	2.72E-04
27.84	2.66	0.66	2.66E-04
30.28	3.4	0.72	2.80E-04
23.04	3.19	0.68	2.72E-04

21.87	1.16	0.66	1.81E-04
20.19	3.29	0.62	2.36E-04
8.22	0.1	0.62	1.28E-04
9.01	0.05	0.6	8.18E-05
4.42	0	0.31	6.18E-05
11.11	1.09	0.57	1.37E-04
23.51	2.23	0.58	1.98E-04
24.44	4.2	0.48	2.09E-04
33.51	3.6	0.72	3.28E-04
28.99	2.3	0.56	2.67E-04
30.56	2.73	0.75	3.09E-04
28.26	1.8	0.59	1.87E-04
18.65	0.36	0.3	2.19E-05
15.26	2.3	0.69	1.48E-04
5.24	0.39	0.48	9.43E-05
3.93	1.34	0.42	1.17E-04

8.6	0.13	0.44	9.08E-05
11.66	1.56	0.48	1.33E-04
18.96	3.55	0.77	3.07E-04
21.36	2.88	0.48	1.30E-04

A simple linear regression analysis was performed with each variable and hydraulic conductivity and strong relationship was found between each relation. The Figure 4.4, Figure 4.5 and Figure 4.6 show the relation of hydraulic conductivity with 10-days antecedent rainfall, volumetric water content and soil temperature. It was found that volumetric water content has the best R-squared value of 0.65 which means that 65% of the data can be explained with the governing equation between hydraulic conductivity and volumetric water content. In-situ geotechnical properties can vary temporarily and spatially. Hence, with respect to that statement, it has a good fit.

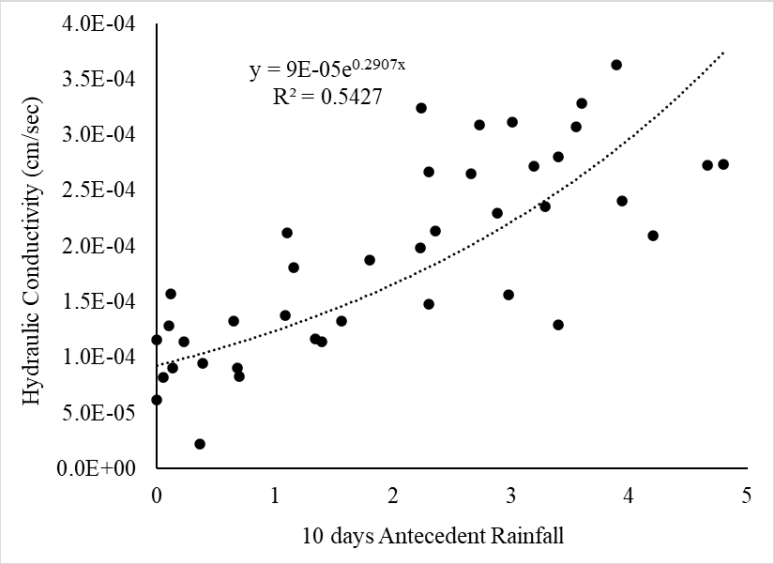

Figure 4.4 Relation between soil hydraulic conductivity with 10 days antecedent rainfall

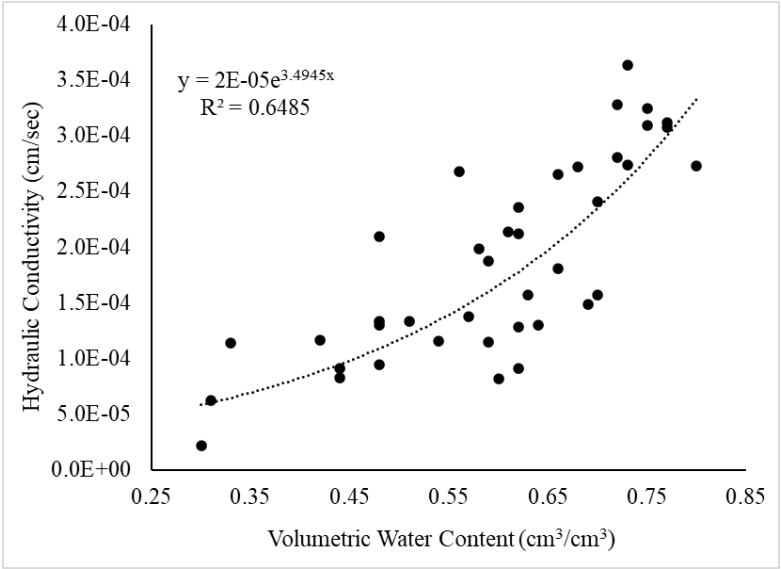

Figure 4.5 Relation between soil hydraulic conductivity with volumetric water content

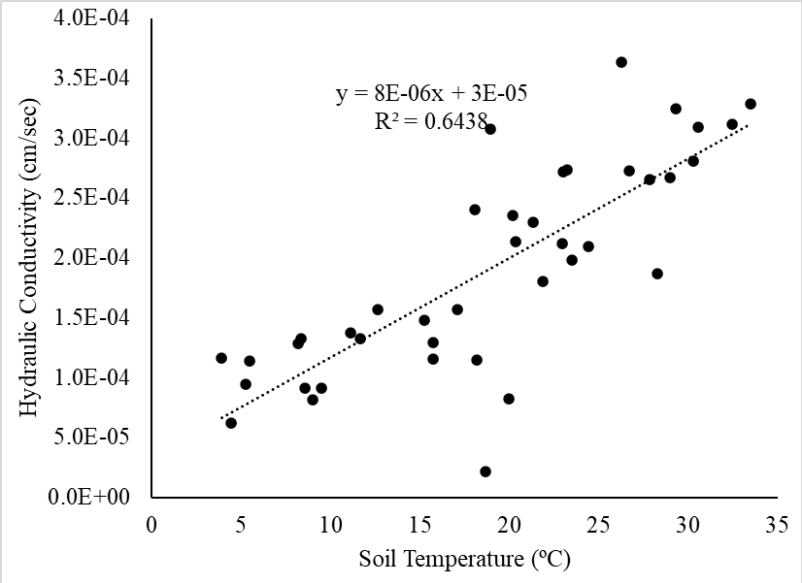

Figure 4.6 Relation between soil hydraulic conductivity with surface soil temperature

4.5 TRAINING DATA

In this Regression Learner Session in MATLAB, the training data consists of 40 observations with three predictors: Soil Temperature, VWC (Volumetric Water Content), and 10 Day Antecedent Rainfall. The goal of the prediction model is to estimate the Hydraulic Conductivity based on these three predictors.

The training process will use 5-fold cross-validation, a common technique to evaluate the model's performance. In 5-fold cross-validation, the dataset is randomly divided into five subsets (or "folds"). The model will be trained five times, each time using four of the folds for training and one-fold for validation. This helps to ensure that the model's performance is robust and not influenced by the specific data split.

By using the Regression Learner App in MATLAB, the relationships between the predictors (Soil Temperature, VWC, and 10 Day Antecedent Rainfall) and the response variable (Hydraulic Conductivity) can be explored to build a regression model. The app will automatically handle data preprocessing, algorithm selection, and model evaluation, making it easier to find the best model for predicting hydraulic conductivity based on the given predictors. After the training process, the model's accuracy can be assessed using various performance metrics obtained from the 5-fold cross-validation results.

4.5.1 Guelph Permeameter

The dataset obtained from Guelph permeameter was trained using different algorithms and the summary is tabulated below:

Table 4.3 Summary of the algorithms

Model Type	Status	RMSE (Validation)	MSE (Validation)	R-Squared (Validation)	MAE (Validation)
Tree	Trained	4.79E-07	2.30E-13	0.6350	3.57E-07
Linear Regression	Trained	3.38E-07	1.14E-13	0.8185	2.69E-07
Linear Regression	Trained	3.33E-07	1.11E-13	0.8242	2.65E-07
Linear Regression	Trained	3.39E-07	1.15E-13	0.8179	2.73E-07

Stepwise Linear Regression	Trained	3.26E-07	1.07E-13	0.8308	2.60E-07
Tree	Trained	4.79E-07	2.30E-13	0.6350	3.57E-07
Tree	Trained	5.73E-07	3.29E-13	0.4780	4.36E-07
Tree	Trained	7.93E-07	6.30E-13	0.0000	6.27E-07
SVM	Trained	4.27E-07	1.83E-13	0.7101	3.57E-07
SVM	Trained	4.48E-07	2.01E-13	0.6812	3.90E-07
SVM	Trained	7.87E-07	6.20E-13	0.0154	5.41E-07
SVM	Trained	6.71E-07	4.50E-13	0.2858	5.14E-07
SVM	Trained	3.88E-07	1.50E-13	0.7613	3.11E-07
SVM	Trained	4.70E-07	2.21E-13	0.6487	3.64E-07
Ensemble	Trained	4.84E-07	2.34E-13	0.6276	3.63E-07
Ensemble	Trained	4.69E-07	2.20E-13	0.6513	3.58E-07
Gaussian Process Regression	Trained	7.93E-07	6.30E-13	0.0000	6.27E-07

Gaussian Process Regression	Trained	7.93E-07	6.30E-13	0.0000	6.27E-07
Gaussian Process Regression	Trained	7.93E-07	6.30E-13	0.0000	6.27E-07
Gaussian Process Regression	Trained	7.93E-07	6.30E-13	0.0000	6.27E-07
Neural Network	Trained	9.26E-03	8.58E-05	-136310849.7395	3.92E-03
Neural Network	Trained	2.40E-02	5.78E-04	-918245067.9885	1.48E-02
Neural Network	Trained	1.65E-02	2.72E-04	-431277834.1634	1.23E-02
Neural Network	Trained	2.69E-02	7.22E-04	-1146101908.6447	1.25E-02

Neural Network	Trained	8.79E-03	7.73E-05	-122767056.7567	4.12E-03
Kernel	Trained	5.58E-07	3.11E-13	0.5057	4.16E-07
Kernel	Trained	7.93E-07	6.30E-13	0.0000	6.27E-07

The table represents the results of various machine learning models that were trained to predict hydraulic conductivity based on three predictors: Soil Temperature, VWC (Volumetric Water Content), and 10 Day Antecedent Rainfall. Each row in the table corresponds to a specific model, and the columns provide information about the model type, training status, Mean Squared Error (MSE), Root Mean Squared Error (RMSE), R-squared (R2) value, and Mean Absolute Error (MAE) for that model.

The best result among the models is the one with the lowest values for MSE, RMSE, and MAE, and the highest R-squared (R^2) value. These metrics indicate the accuracy and performance of the model in predicting hydraulic conductivity. It was observed from the Stepwise linear regression is a variable selection technique used in multiple linear regression to choose the most relevant predictors from a larger set of potential predictor variables. The goal is to build a model that includes only significant predictors while achieving good predictive performance and avoiding overfitting. The stepwise linear regression process involves the following steps:

Initialization: Start with an empty model or a model with all potential predictors included.

Step 1: Forward Selection: In this step, one predictor variable with the highest impact on the response variable is added to the model. This is done by fitting a simple linear regression model

for each potential predictor variable against the response and selecting the predictor with the lowest p-value (i.e., the most statistically significant) to include in the model.

Step 2: Backward Elimination: Once the first predictor is included, the algorithm proceeds to check the contribution of the other predictors. One by one, each predictor is removed from the model, and the impact on the model's overall performance is assessed. If removing a predictor result in a significant drop in model performance, that predictor is kept in the model. This process continues iteratively until no more predictors can be removed without a significant decrease in model performance.

Step 3: Stepwise Refinement: After the forward selection and backward elimination steps, the model may not be fully optimized. Stepwise refinement is carried out by iteratively adding or removing predictors one at a time and checking the impact on the model's performance.

Final Model Selection: The stepwise process continues until no more predictors can be added or removed to improve the model significantly. The final model is selected based on some criterion, such as the Akaike Information Criterion (AIC) or the Bayesian Information Criterion (BIC), which balance model complexity and predictive accuracy.

Stepwise linear regression can be a useful approach for variable selection, but it is essential to exercise caution and not rely solely on automated techniques. Overfitting and model instability can occur when using stepwise regression, so it is crucial to validate the selected model's performance on an independent dataset and consider domain knowledge and prior research in the selection of predictors.

From the provided table, the best model appears to be the "Stepwise Linear Regression" model with the following metrics:

- MSE: 3.26E-07
- RMSE: 1.07E-13
- R^2: 0.8308
- MAE: 2.60E-07

The low values of MSE, RMSE, and MAE indicate that the model's predictions are very close to the actual hydraulic conductivity values. The R-squared value of 0.8308 indicates that approximately 83.08% of the variability in the hydraulic conductivity can be explained by the predictor variables, which is a relatively good fit. Root mean square value is also very low which attests to the mentioned statement. Figure 4.7 Predicted response vs true response of the training data. Figure 4.7 and Figure 4.8 shows the predicted response vs true response and the residual plot of the training data respectively.

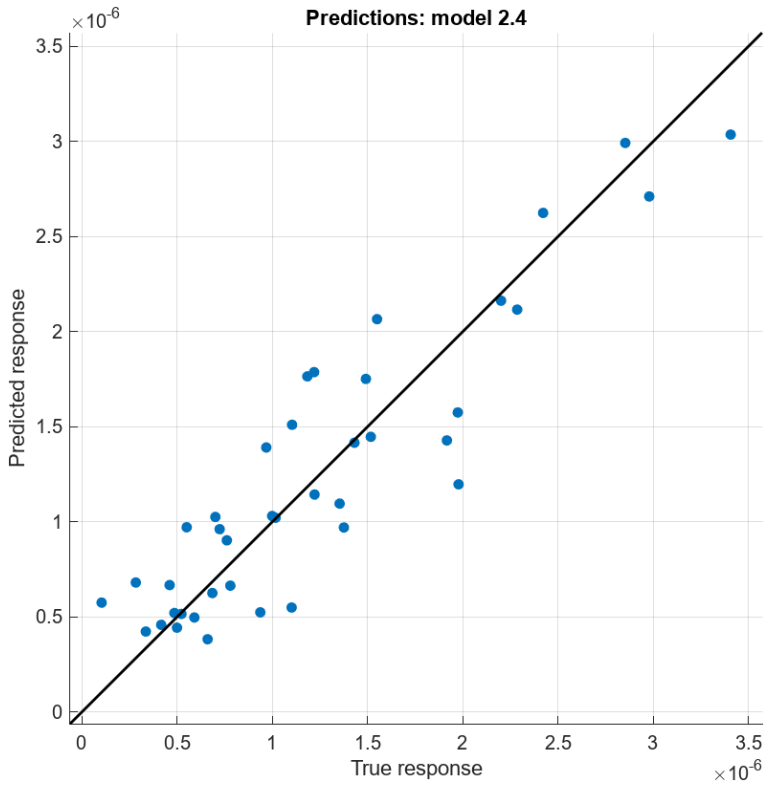

Figure 4.7 Predicted response vs true response of the training data

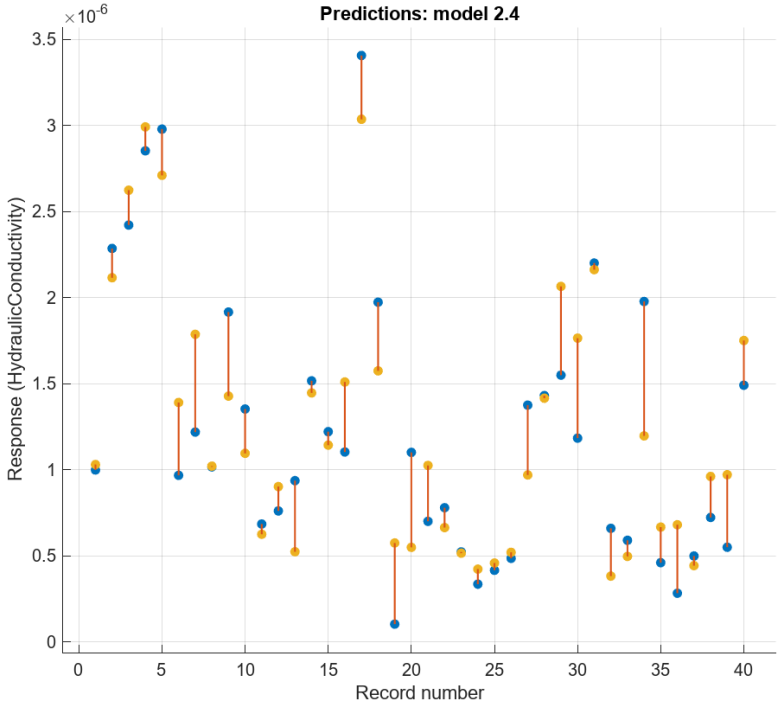

Figure 4.8 Residual plot of the training data

4.5.2 Mini-Disk Infiltrometer

The dataset obtained from Mini-Disk Infiltrometer was trained using different algorithms and the summary is tabulated below:

Table 4.4 Summary of different algorithms

Model Type	Status	RMSE (Validation)	MSE (Validation)	R-Squared (Validation)	MAE (Validation)
Tree	Trained	5.68E-05	3.23E-09	0.5815	4.21E-05
Linear Regression	Trained	4.14E-05	1.72E-09	0.7777	3.45E-05
Linear Regression	Trained	3.80E-05	1.45E-09	0.8125	2.87E-05
Linear Regression	Trained	4.16E-05	1.73E-09	0.7760	3.49E-05
Stepwise Linear Regression	Trained	3.86E-05	1.49E-09	0.8071	2.95E-05
Tree	Trained	5.68E-05	3.23E-09	0.5815	4.21E-05
Tree	Trained	7.49E-05	5.61E-09	0.2729	5.59E-05
Tree	Trained	8.78E-05	7.72E-09	0.0000	7.66E-05

SVM	Trained	4.83E-05	2.33E-09	0.6975	4.09E-05
SVM	Trained	4.11E-05	1.69E-09	0.7806	3.33E-05
SVM	Trained	6.17E-05	3.80E-09	0.5071	4.94E-05
SVM	Trained	7.26E-05	5.27E-09	0.3176	6.06E-05
SVM	Trained	4.42E-05	1.95E-09	0.7473	3.55E-05
SVM	Trained	4.36E-05	1.90E-09	0.7539	3.36E-05
Ensemble	Trained	4.20E-05	1.76E-09	0.7717	3.52E-05
Ensemble	Trained	4.61E-05	2.12E-09	0.7250	3.48E-05
Gaussian Process Regression	Trained	8.78E-05	7.72E-09	0.0000	7.66E-05
Gaussian Process Regression	Trained	8.78E-05	7.72E-09	0.0000	7.66E-05
Gaussian Process Regression	Trained	8.78E-05	7.72E-09	0.0000	7.66E-05

Gaussian Process Regression	Trained	8.78E-05	7.72E-09	0.0000	7.66E-05
Neural Network	Trained	1.53E-02	2.34E-04	-30286.2164	4.39E-03
Neural Network	Trained	1.88E-02	3.54E-04	-45859.9259	1.27E-02
Neural Network	Trained	1.84E-02	3.38E-04	-43813.6342	1.18E-02
Neural Network	Trained	2.16E-02	4.66E-04	-60330.7715	1.37E-02
Neural Network	Trained	1.23E-02	1.52E-04	-19637.7716	5.91E-03
Kernel	Trained	6.91E-05	4.78E-09	0.3811	4.75E-05
Kernel	Trained	5.40E-05	2.92E-09	0.6219	4.17E-05

The table represents the results of various machine learning models that were trained to predict hydraulic conductivity based on three predictors: Soil Temperature, VWC (Volumetric Water Content), and 10 Day Antecedent Rainfall. Each row in the table corresponds to a specific model, and the columns provide information about the model type, training status, Mean Squared Error (MSE), Root Mean Squared Error (RMSE), R-squared (R2) value, and Mean Absolute Error (MAE) for that model.

The best result among the models is the one with the lowest values for MSE, RMSE, and MAE, and the highest R-squared (R2) value. These metrics indicate the accuracy and performance of the model in predicting hydraulic conductivity.

From the provided table, the best model appears to be the "Stepwise Linear Regression" model with the following metrics:

- MSE: 3.80E-05
- RMSE: 1.45E-09
- R^2: 0.8125
- MAE: 2.87E-05

The model explains about 81.25% of the variance in Hydraulic Conductivity. This is a relatively good fit to the data, indicating that the model captures a significant portion of the relationship between predictors and the response.

For each observation in the dataset, the model's predicted value for Hydraulic Conductivity may be higher or lower than the true value by approximately 3.80E-05 on average. This value represents the average error or discrepancy between the model's predictions and the actual values in terms of Hydraulic Conductivity.

A smaller average deviation (or error) is generally desirable because it indicates that the model's predictions are closer to the true values. In this case, with an average deviation of 3.80E-05, the "Linear Regression" model provides relatively accurate predictions for Hydraulic Conductivity. However, it's crucial to consider this value in the context of the problem's requirements and the scale of the Hydraulic Conductivity values being predicted. For some applications, a deviation of 3.80E-05 might be acceptable, while for others, it may not meet the required level of accuracy.

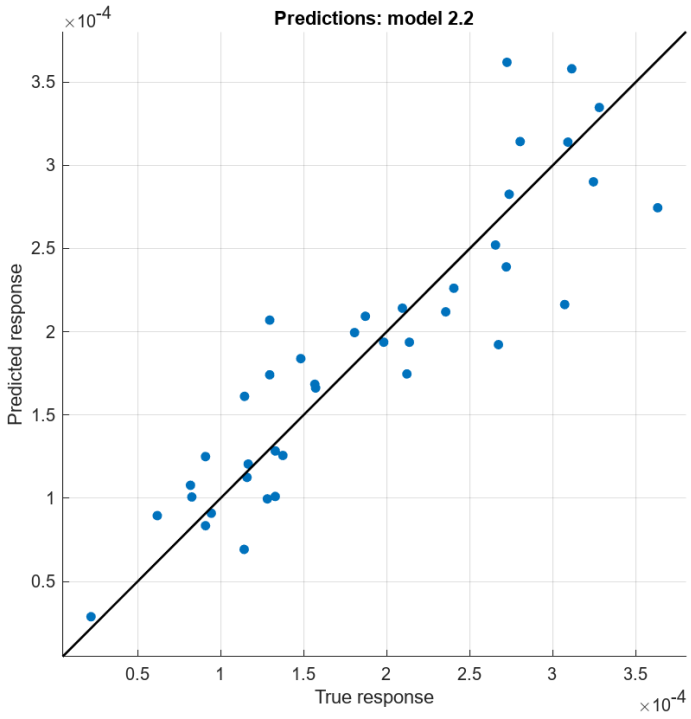

Figure 4.9 Predicted response vs true response of the training data

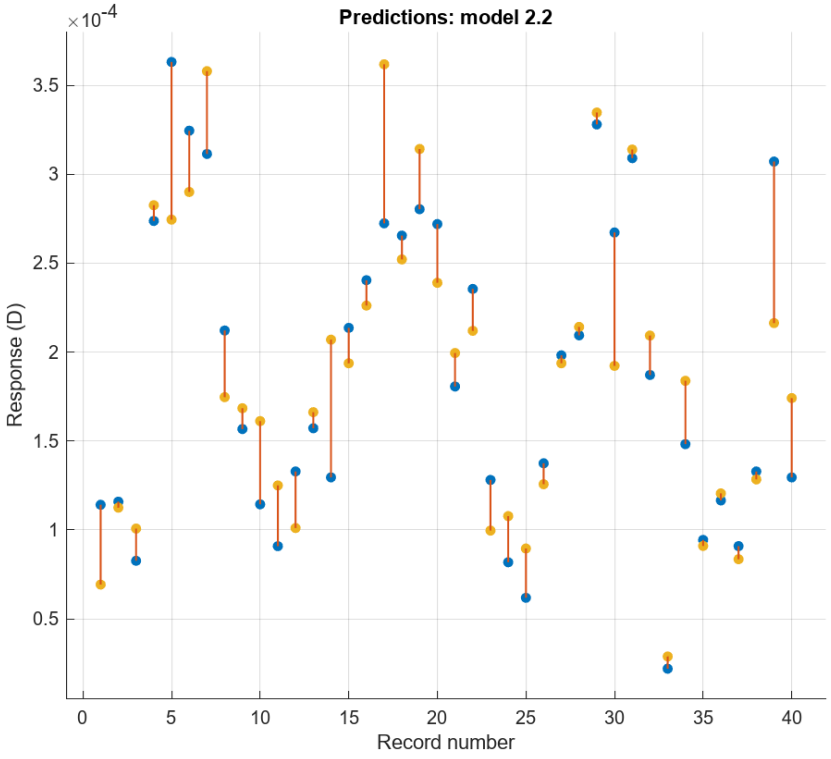

Figure 4.10 Residual plot of the training data

Figure 4.9 and Figure 4.10 shows the predicted response vs true response and the residual plot of the training data respectively.

4.6 DATA VALIDATION

To validate the data from prediction model, the data obtained from slope-2 at Parks Springs Blvd were used. The volumetric water content, 10 days antecedent rainfall and soil temperature data on surface and at 2 ft depth were collected and using the prediction model, the corresponding hydraulic conductivity data were determined. The calculated hydraulic conductivity data were compared with the in-situ hydraulic conductivity data and data comparison are tabulated below:

Table 4.5 In-situ and predicted value using both instruments.

Guelph Permeameter		**Mini-Disk Infiltrometer**	
In-situ hydraulic conductivity	**Predicted hydraulic conductivity**	**In-situ hydraulic conductivity**	**Predicted hydraulic conductivity**
5.68E-07	6.13E-07	9.10E-05	1.14E-04
3.60E-06	5.41E-06	9.88E-05	1.08E-04
5.55E-06	6.06E-06	6.26E-05	8.83E-05
3.90E-06	4.39E-06	1.02E-04	1.17E-04
2.15E-06	4.56E-06	1.13E-04	1.59E-04
2.90E-06	2.14E-06	1.49E-04	1.75E-04

3.00E-06	3.52E-06	2.16E-04	2.47E-04
3.50E-06	4.32E-06	9.82E-05	1.07E-04
3.60E-06	3.76E-06	5.01E-05	7.05E-05
8.00E-07	7.12E-07	7.21E-05	6.01E-05
1.50E-06	1.35E-06	1.27E-04	2.14E-04
3.00E-06	5.19E-06	7.87E-05	1.03E-04
9.87E-07	1.12E-06	8.10E-05	1.23E-04
3.94E-07	3.94E-07	7.67E-05	8.22E-05
4.23E-06	5.36E-06	9.12E-05	1.37E-04
9.01E-07	9.01E-07	1.18E-04	1.63E-04
8.86E-07	1.09E-06	1.11E-04	1.28E-04
2.66E-07	4.69E-07	1.26E-04	1.30E-04
2.12E-06	3.29E-06	2.42E-04	3.39E-04

To interpret the data, linear regression analysis was performed, and the R-squared values were calculated as 0.8466 and 0.8863 in Guelph permeameter and Mini-Disk Infiltrometer result. It can be explained that in 85% and 89% cases, the data were interpretable as shown in Figure 4.11 and Figure 4.12.

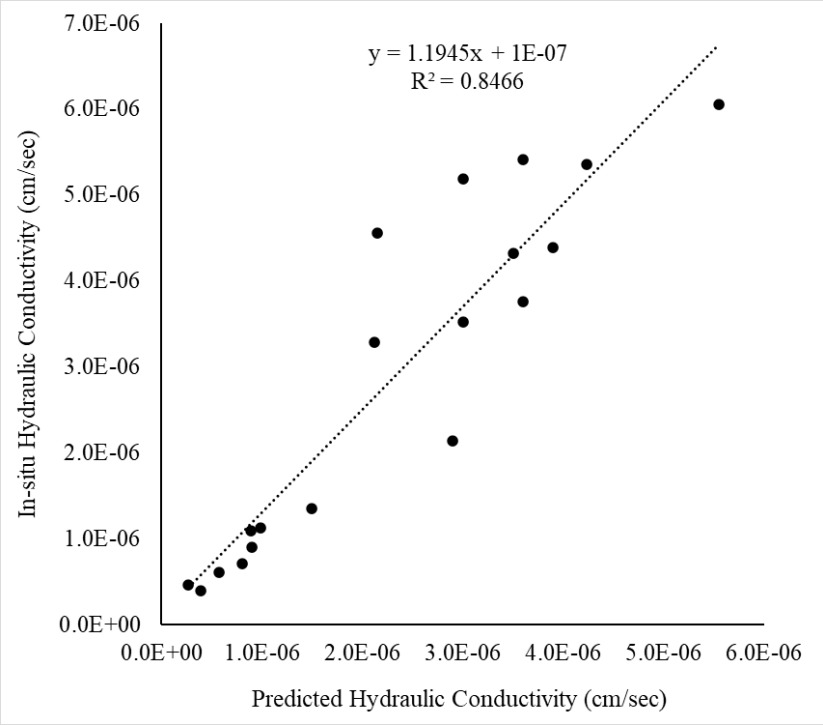

Figure 4.11 Regression analysis for Guelph Permeameter

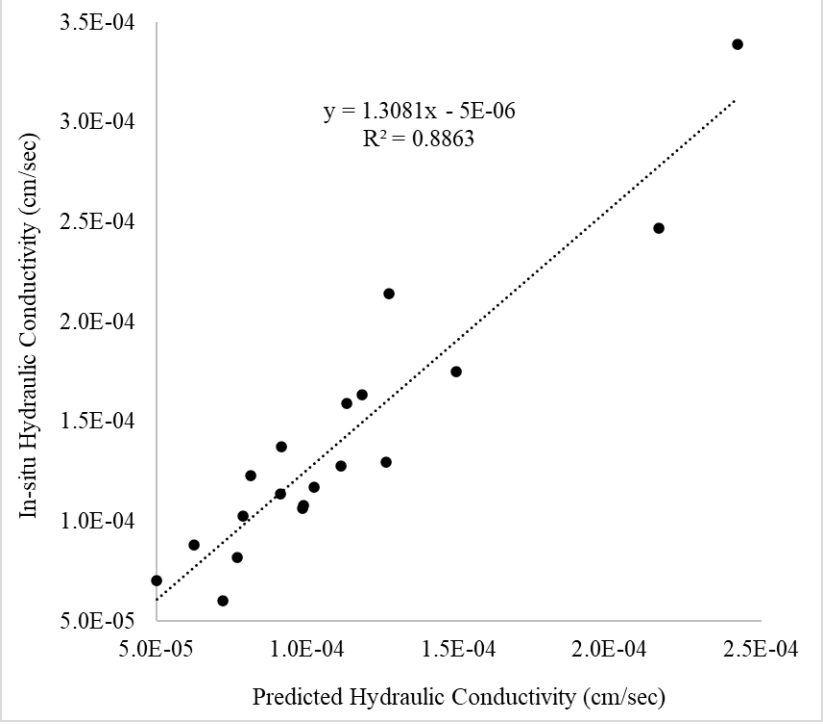

Figure 4.12 Regression analysis for Mini-Disk Infiltrometer

Furthermore, an independent two-sample t-test with unequal variance was conducted to assess whether there were significant differences between the actual and predicted moisture increase values. The decision to use an independent test was based on the assumption that the two sets of values were not dependent on each other.

The test compared the mean of the predicted values against the mean of the observed values. The analysis was performed at a 90% confidence level, which corresponds to a significance level of 0.1. However, due to using a two-tailed test, the significance level was adjusted to 0.05 (from the initial 0.1) to account for the possibility of differences in either direction.

The null hypothesis (H_0) for the two-sample t-test stated that there was no significant difference between the means of the predicted and observed values of hydraulic conductivity. The alternative hypothesis (H_a) suggested that there was a statistically significant difference between the two means. By conducting the t-test, we aimed to evaluate whether the observed differences in the means were likely due to random chance or if they were genuinely meaningful. The basic hypothesis of the two-sample t-test can be described as follows:

H_0: $m_1 - m_2 = 0$

H_a: $m_1 - m_2 \neq 0$

where,

m_1= mean of the actual hydraulic conductivity

m_2= mean of the predicted hydraulic conductivity

Table 4.6 Summary of two-tailed T- test

		Mean	Std. Dev	Variance	t-value	P-value
Guelph Permeameter	In-situ	2.31E-06	1.53E-06	2.35E-12	-0.9848	0.3313
	Predicted	2.88E-06	1.99E-06	3.97E-12		
Mini-disk Infiltrometer	In-situ	1.11E-04	4.83E-05	2.33E-09	-1.5553	0.1295
	Predicted	1.40E-04	6.71E-05	4.5E-09		

From Table 4.6, it was observed that the P-value was 0.3313 and 0.1295 for Guelph Permeameter and Mini-Disk Infiltrometer. That explains that P-value is way higher than the significance level (0.05) and it fails to reject the null hypothesis. That means there is not enough evidence to conclude that there is a significant difference between the in-situ and predicted hydraulic conductivity based on the data or there is no significant difference in in-situ hydraulic conductivity and predicted hydraulic conductivity.

Also, in hypothesis testing, the t-value is used to determine if there is a statistically significant difference between the two-sample means. The magnitude of the t-value indicates the size of the difference between the means, and its sign (+ or -) indicates the direction of the difference.

A t-value of -0.9848 and -0.1533 means that the in-situ hydraulic conductivity values tend to be lower than the predicted hydraulic conductivity values. Therefore, from the predicted value, we can calculate the in-situ value using the following equations as per regression analysis:

Guelph Permeameter: In-situ HC (cm/s) = 1.1945*Predicted HC (cm/s) + 1×10^{-7}

Mini-Disk Infiltrometer: In-situ HC (cm/s) = 1.3081*Predicted HC (cm/s) + 5×10^{-6}

4.7 CONCLUSION

In this chapter, a dataset collected from slope-1 was used to train the data. For testing and validating the data, another dataset from slope-2 was used. From this study, it can be concluded that:

1. In the training data, using machine learning algorithms, Linear regression model and stepwise linear regression model showed the best possible outcome having R-squared value of 0.81 and 0.83 for Mini-Disk Infiltrometer and Guelph permeameter respectively.
2. The predicted function showed a very similar pattern as the in-situ results as the regression analysis between predicted and in-situ values showed 89% and 85% similarity for Mini-Disk Infiltrometer and Guelph Permeameter.
3. It was observed that the P-value was 0.3313 and 0.1295 for Guelph Permeameter and Mini-Disk Infiltrometer. That explains that P-value is way higher than the significance level (0.05) and it fails to reject the null hypothesis. That means there is not enough evidence to conclude that there is a significant difference between the in-situ and predicted hydraulic conductivity based on the data or there is no significant difference in in-situ hydraulic conductivity and predicted hydraulic conductivity.
4. A t-value of -0.9848 and -0.1533 means that the in-situ hydraulic conductivity values tend to be lower than the predicted hydraulic conductivity values.

CHAPTER 5

ANALYTICAL EVALUATION OF THRESHOLD HYDRAULIC CONDUCTIVITY FOR SHALLOW SLOPE FAILURE

5.1 ABSTRACT

Shallow slope failure is a common incident in Texas during prolonged period of heavy rainfall. During heavy rainfall water seeps into the ground, saturating the upper layers of soil. Porewater pressure develops and reduces the shear resistance of the soil and becomes the reason for shallow slope failure. The objective of the study is to determine a threshold value of hydraulic conductivity which leads to saturation of the soil due to prolonged rainfall and causes slope failure using Green-Ampt model. The whole Texas region is divided into three areas (West Texas, Central Texas and East Texas) according to rainfall intensity and it was estimated that East Texas had 100% more rainfall depth than West for 50 years return period. Based on the model, it was found that, the threshold value of hydraulic conductivity varies from 10-5 to 10-7 cm/s depending on the rainfall intensity and interval of rainfall recurrence. On the other hand, this study also predicts the depth of the slope failure and concludes that the slope with low hydraulic conductivity fails at 3-6ft depth depending on the cohesion of the soil.

5.2 INTRODUCTION

Slope failure and landslides are major disasters all over the world and cause substantial economic loss and fatalities (Wright et al. 2005). These failures occur in both natural slopes and human-made slopes. The problem is periodic in areas where the highway embankment is constructed on high plastic clay. High plastic clay has enough strength to hold the slope in a dry condition, but it is susceptible to cyclic swelling and shrinkage under weather loading like precipitation and evapotranspiration (Estabragh et al. 2015; Abbey et al. 2019). The soil tends to

soften over time, reducing the effective shear strength and reducing the factor of safety (McCormick and Short 2006; Wright et al. 2007). Moreover, shrinkage cracks that develop on slopes act as a conduit for rainfall infiltration, providing a potential flow path for the water to seep through.

When seepage occurs on a slope, the hydraulic conductivity of the material governs the velocity and direction of water flow. It determines the rate at which water can infiltrate or move through it. Materials with high hydraulic conductivity allow water to flow more easily, while those with low hydraulic conductivity impede the movement of water. Therefore, the hydraulic conductivity of the slope material directly influences the seepage characteristics and patterns within the slope. The minimum hydraulic conductivity required for seepage-induced instability or failure to occur within a slope is referred to as threshold hydraulic conductivity. When the hydraulic conductivity of a slope material exceeds the threshold conductivity, seepage can initiate or accelerate various failure mechanisms. Moreover, seepage flow can cause erosion or piping within the slope material. Fine particles can be carried away by the flowing water, gradually weakening the slope and creating voids or preferential flow paths. The erosion of slope material can lead to localized failures or progressive failure mechanisms, compromising the overall stability of the slope. Therefore, to determine the failure condition, it is important to evaluate the threshold hydraulic conductivity of the soil. In this study, threshold hydraulic conductivity was assessed depending on rainfall condition in three different parts in Texas.

5.3 BACKGROUND AND THEORY

After a heavy or prolonged rainfall on a highway embankment, a part of the precipitation drains as surface runoff and another part contributes to the seepage inside the soil. The seepage rate is governed by hydraulic conductivity which determines the time and depth of saturation.

Before failure due to the seepage parallel to the face of the slope can occur, the soil must reach saturation. The minimum requirements to reach saturation are:

1. Rainfall intense enough to exceed the infiltration rate of the material.

2. Rainfall long enough to saturate the slope up to a depth of z_w (Figure 5.1).

Consider the slope section shown in Figure 5.1. It is assumed that the soil is initially unsaturated, and the surface is wet due to rainfall.

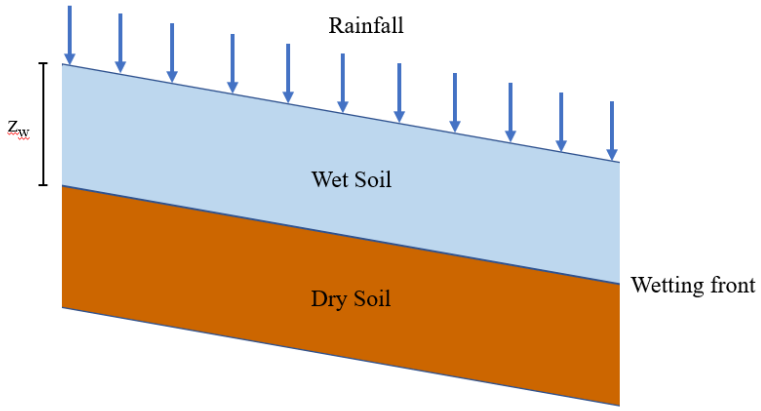

Figure 5.1 Cross section showing wetting process by rainfall.

The rate at which the unsaturated soil will wet up is critical to the surficial stability of the slope. Because of the complexity of the mechanism of moisture retention and transmission, numerous researchers have investigated the equations governing unsaturated flow, e.g. Wallace (1977).

A simple model for infiltration, based on Darcy's Law, was proposed by W. Heber Green and G.A. Ampt which is known as Green-Ampt model. The assumptions made in the model are:

1. The soil surface is wet.

2. There is a distinct wetted front as shown in **Error! Reference source not found.**.

3. The co-efficient of permeability in the wetted zone, k_w does not change over time.

4. There is a constant negative pressure just above the wetting front.

According to the model, time necessary to saturate soil:

$$T_w = \frac{\mu}{k_w}[z_w - Sln\left(\frac{S+z_w}{S}\right)] \ldots\ldots\ldots\ldots\ldots (1)$$

where, μ = the wettable porosity (volume of fillable pore space/total volume of the soil), μ can be expressed as the difference between the volumetric water content (volume of water/total volume) before and after wetting, (θ_w-θ_i). Hence, the effect of initial moisture content θ_i on μ is very important and has major influence on T_w (Pradel, 1993), S = the wetting front capillary suction. Typical values for S range from 2.6 ft for coarse soil and 4.6 ft for clays (Moore 1939). k_w and z_w denotes the permeability and depth of failure of the slope.

$$\text{Now, } k_w = \frac{\mu}{T_w}[z_w - Sln\left(\frac{S+z_w}{S}\right)] \ldots\ldots\ldots\ldots\ldots (2)$$

The infiltration rate, υ_i, is the rate at which the water enters the soil surface. The Green-Ampt model predicts:

$$\upsilon_i = k_w \frac{z_w+S}{z_w} \ldots\ldots\ldots\ldots\ldots (3)$$

To reach the failure criteria, the soil must reach saturation. The first condition to reach the saturation requires that the rainfall intensity, I, must be greater than the infiltration rate, υ_i, the

second condition requires that the precipitation must last longer than the time required for saturation, T_w. Therefore,

$$I_{min} \geq \upsilon_i \ldots\ldots\ldots\ldots (4)$$

$$\text{And, } T_{min} \geq T_w \ldots\ldots\ldots\ldots (5)$$

Combining (2), (3), (4) and (5), it is obtained,

$$I_{min} = \frac{\mu}{T_{min}}\left[z_w - Sln\left(\frac{S+z_w}{S}\right)\right]\left(\frac{z_w+S}{z_w}\right) \ldots\ldots\ldots\ldots\ldots (6)$$

It is to be mentioned that the aforementioned equation does not consider the effect of surface runoff and evapotranspiration. Hence, to produce saturation, higher intensity rainfall is required. Combining (3) and (6), the following expression of the threshold hydraulic conductivity is obtained:

$$k_{lim} = I_{min}\left(\frac{z_w}{z_w+S}\right) = \frac{\mu}{T_{min}}\left[z_w - Sln\left(\frac{S+z_w}{S}\right)\right] \ldots\ldots\ldots\ldots (7)$$

where, k_{lim} = the maximum permeability that will allow saturation to the depth z_w. Since the aforementioned equation does not consider the effect of surface runoff and evapotranspiration, the soil with hydraulic conductivity well above k_{lim} may not become saturated due to rainfall.

5.4 LABORATORY EXPERIMENTAL WORK

A laboratory experimental test was performed to determine the wettable porosity of the soil. The wettable porosity is the ratio of volume of the fillable pore space and total volume of the soil sample. To determine wettable porosity, triaxial test setup were used. Undisturbed soil samples were collected from the test location. The test section was located at a highway embankment beside

US-287 at Midlothian, Texas. The undisturbed samples were collected following the process shown in Figure 5.2. Six undisturbed samples were collected and taken to the laboratory for testing. Samples of 5 inches of height and 2.5 inches of diameter were prepared to perform the test.

Figure 5.2 Undisturbed samples were collected from site.

The laboratory test setup is shown in Figure 5.3. Using the triaxial cell apparatus, back pressure was applied to saturate the sample. When the sample was 100% saturated, the test was stopped. In Triaxial test, Skempton's pore water pressure parameter, B is denoted as the ratio of change in pore water pressure and change in cell pressure.

$$B = \frac{\Delta u}{\Delta \sigma};$$

Where, Δu = difference in pore water pressure, $\Delta \sigma$ = change in axial pressure.

An initial cell pressure was applied which gradually increased. With the increase in axial cell pressure, the pore water pressure was also monitored in the control panel.

Figure 5.3 Laboratory test setup of Triaxial apparatus.

The axial cell pressure, Δσ was increased at certain intervals until B = 1 was obtained which denoted that the change in pore water pressure and cell pressure were equal. The initial burette reading, and the final burette reading were noted. The change in burette reading denoted the volume of water required to saturate the sample. Therefore, this volume of water also denoted the volume of pore space that was replaced by the water. The wettable porosity was tabulated in Table 5.1.

Table 5.1 The wettable porosity

Soil sample	Volume of the soil sample (cm^3)	Cross-sectional area of the burette, A (cm^2)	Difference in burette reading, B (cm)	Volume of water (cm^3) A*B	Wettable porosity
1	402.2	0.305	163.6	49.9	0.124
2			195.1	59.5	0.148
3			167.5	51.1	0.127
4			183.3	55.9	0.139
5			139.7	42.6	0.106
6			154.4	47.1	0.117

From

, the laboratory test results showed that the wettable porosity varied from 0.1-0.15. Therefore, in the analytical solution, the magnitude of wettable porosity, μ was used 0.1 and 0.15.

5.5 RAINFALL DATA ANALYSIS

In this study, the rainfall data were collected from Precipitation Frequency Data Server of Hydrometeorological Design Studies Center, NOAA's National Weather Service. In the server, the location at Midlothian (32º29'23.6" N, 97º01'58.7" W) was fixed and corresponding precipitation data were collected. The precipitation frequency data were estimated with 90% confidence intervals for 5-min to 60-day duration and the average recurrence interval varied from 1-year to 100-years. From the interval, the average value was taken, and rainfall depth vs duration graph was prepared as shown in Figure 5.4 for 1-year to 100-years recurrence interval.

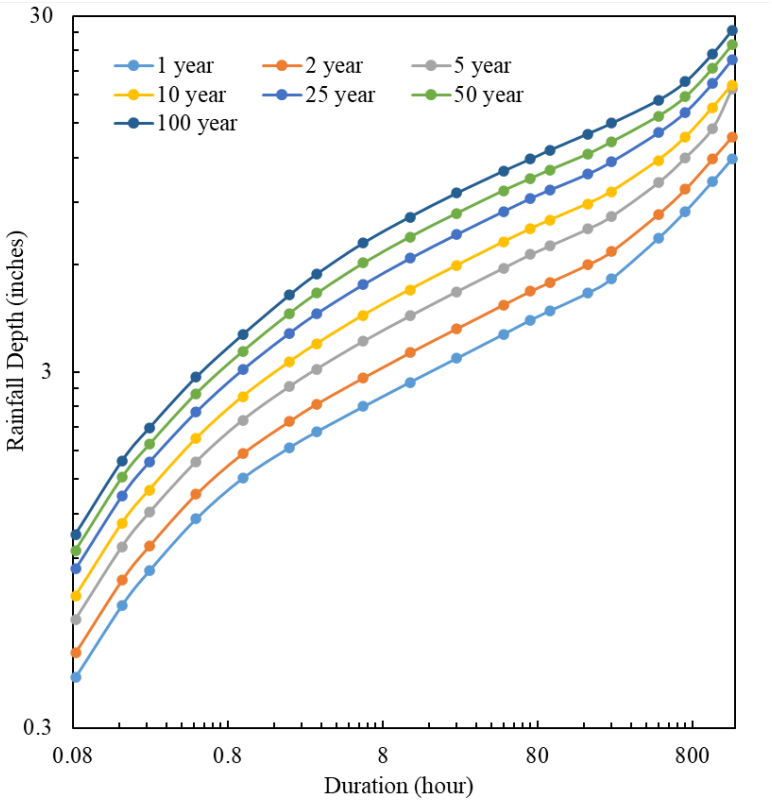

Figure 5.4 Rainfall depth vs Duration in different return period

The maximum rainfall intensity I, for a given duration T, can be calculated using the following equation:

$$I = \frac{P}{T} \dots\dots\dots\dots\dots (7)$$

Where P is the maximum precipitation.

Figure 5.5 was established utilizing the data for Midlothian TX illustrated in Figure 5.5. It was observed that as the duration of the rainfall increases, the maximum rainfall intensity decreases.

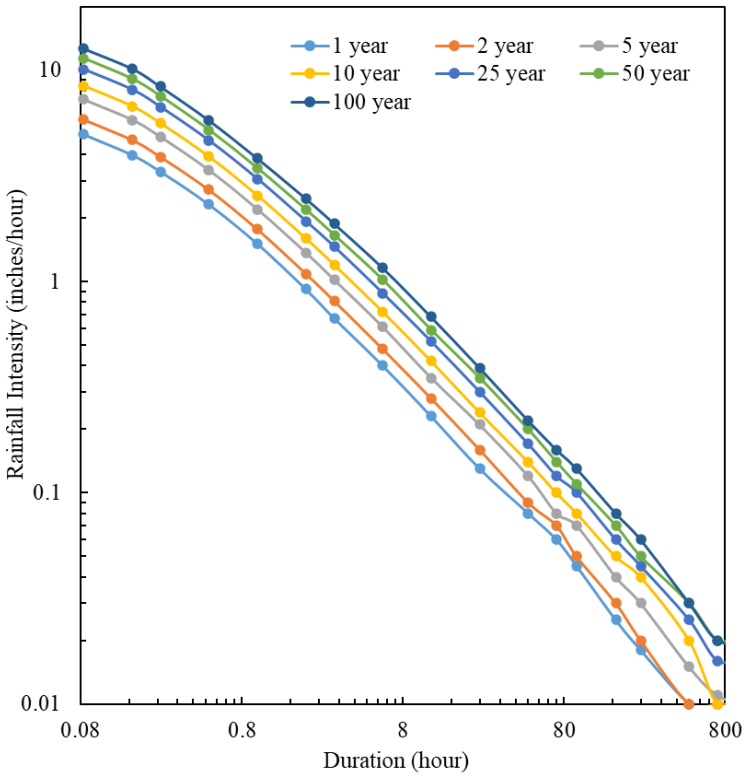

Figure 5.5: Average intensities vs duration for various period recurrence intervals.

5.6 THRESHOLD HYDRAULIC CONDUCTIVITY

The condition in (6) provides the minimum requirement for saturation at the depth z_w. This condition is compared in Figure 5.6 with the statistical data of rainfall intensity in Midlothian, Texas from Figure 5.5. The location where the line defining the maximum rainfall intensity and the line giving the minimum requirement for saturation meets, defines the minimum duration of rain capable of saturating the soil in the slope of the depth z_w.

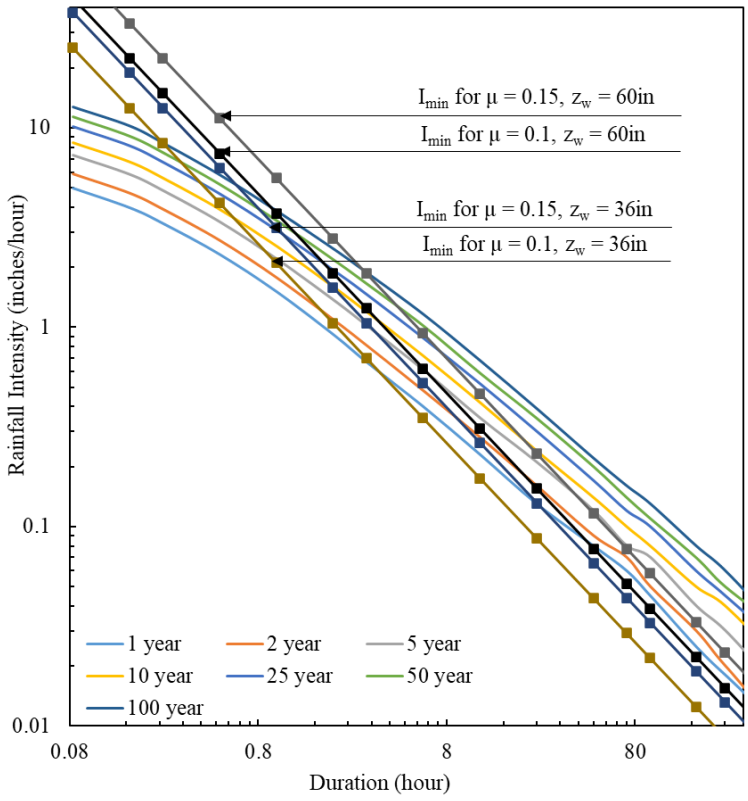

Figure 5.6 Minimum intensity and maximum rainfall for various return period in Midlothian, Texas

Figure 5.7 shows that for the in-situ soil where μ = 0.1 and z_w = 36 in, a rainfall having the return period of 1 year will have to last 6 hours and minimum intensity of 0.6 inches/hour can saturate the soil. That means the minimum rainfall intensity of 0.6 inches/hour for 6 hours can lead

the soil to saturation and according to equation (7), the defined corresponding threshold value for hydraulic conductivity is 1.8×10^{-4} cm/sec (Figure 5.8).

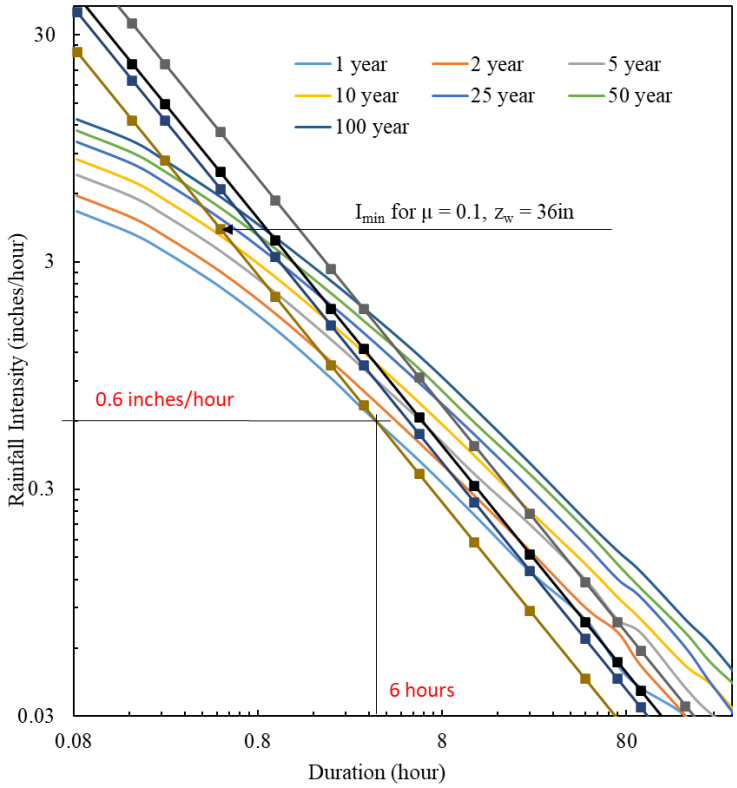

Figure 5.7 Estimation of minimum intensity and duration of rainfall to saturate soil.

Using the same procedure, the threshold hydraulic conductivity for wettable porosity of 0.1 and 0.15 and the saturation depth of 36 in and 60 in were determined and illustrated in Figure 5.8. It was observed that the greater the depth, the lower the hydraulic conductivity. For wettable porosity of 0.15 and 50 years of rainfall return period, 4.5×10^{-4} cm/sec and 8.8×10^{-4} cm/sec hydraulic conductivity is required to saturated soil at 36 in and 60 in respectively. This threshold conductivity excludes the slopes made of gravel or sandy materials.

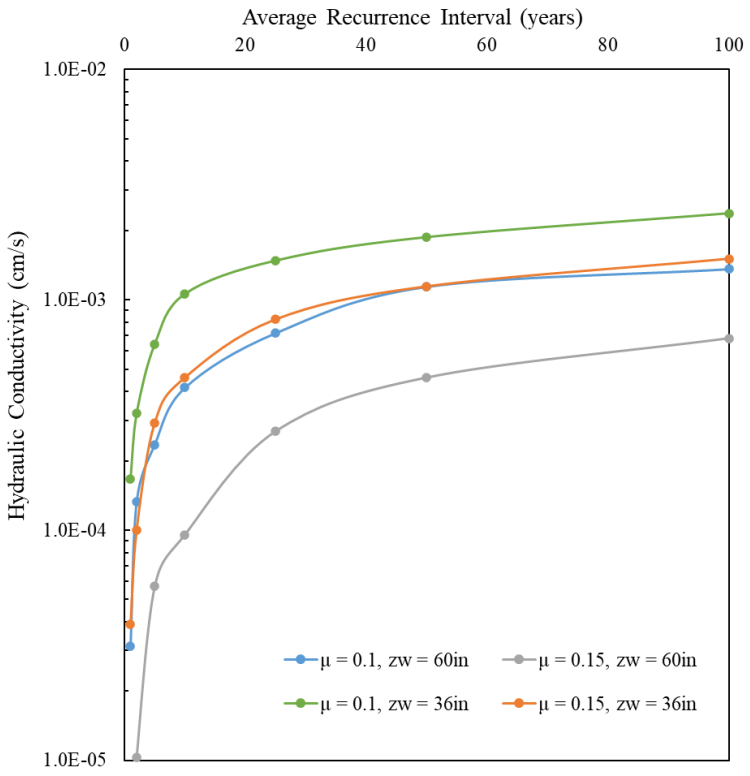

Figure 5.8 Threshold hydraulic conductivity for different soil parameters.

An intriguing observation is the inverse relationship between the decrease in permeability (k_{lim}) and the reduction in the necessary rain return period for achieving saturation, as depicted in Figure 5.8. This implies that lower permeability values correlate with a higher likelihood of saturation developing within the slope. Soils characterized as SC, ML, CL, MH, and CH tend to exhibit permeabilities consistently below 10^-4 cm/s. Consequently, clayey and silty materials could be more susceptible to creating the conditions for surface instability as elucidated by Haefeli (1948) and Skempton and DeLory (1957). It's crucial to emphasize that these equations are only applicable when the possibility of downhill flow is entirely eliminated. In natural slopes, this necessitates the presence of homogeneous material reaching depths far beyond zw, while in man-made slopes, it demands the presence of a thick uniform fill and well-structured subdrains.

Furthermore, it's important to acknowledge that the proposed equations have not been validated against actual instances of slope failures, which casts uncertainty on their accuracy.

5.7 COMPARISON WITH REGIONS WITH DIFFERENT RAINFALL INTENSITY

Texas generally experiences different patterns of rainfall from west to east due to its vast size and diverse geography (Figure 5.9). Here's a general overview of the rainfall conditions from west to east:

West Texas: West Texas is known for its semi-arid to arid climate, characterized by lower rainfall amounts. Cities like El Paso and Midland experience an average annual rainfall of around 8 to 14 inches (20 to 35 cm).

Central Texas: The central region of Texas, including cities like San Antonio and Austin, receives a moderate amount of rainfall compared to the west and east. Average annual rainfall ranges from 20 to 35 inches (50 to 90 cm).

East Texas: The eastern part of Texas, including cities like Houston and Beaumont, has a more humid climate with higher annual rainfall. Average rainfall amounts range from 40 to 60 inches (100 to 150 cm) or even higher in some areas.

Gulf Coast: The coastal areas along the Gulf of Mexico, such as Corpus Christi and Brownsville, can receive significant amounts of rainfall, often exceeding 60 inches (150 cm) annually.

In this study, the whole Texas was divided into 3 different parts (West, Central and East) according to rainfall pattern and corresponding threshold hydraulic conductivity was evaluated.

The west tends to have less rainfall whereas the east possess the record of highest rainfall in Texas, central Texas having the moderate rainfall all over the year.

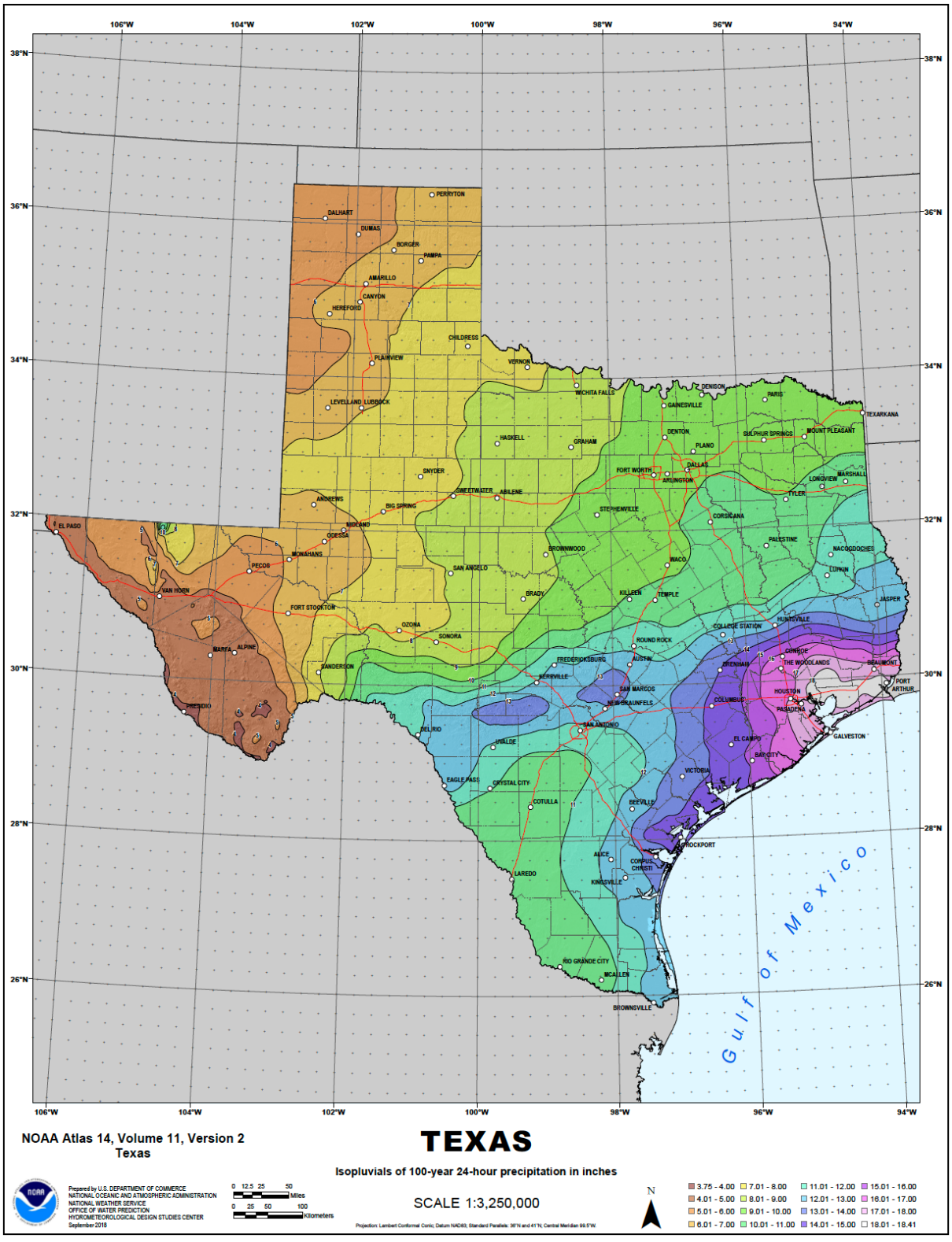

Figure 5.9 Rainfall pattern in Texas for 100 tears return period.

In this part, the soil wettable porosity was considered as 0.15 and the failure surface was estimated at 48 in depth. Using equation (6), the minimum intensity values were determined for El Paso (west), Dallas-Fortworth (central) and Houston (east). The minimum intensity vs duration plot were prepared according to different rainfall depth and return period and the minimum intensity lines defined and illustrated in Figure 5.10, Figure 5.11 and Figure 5.12.

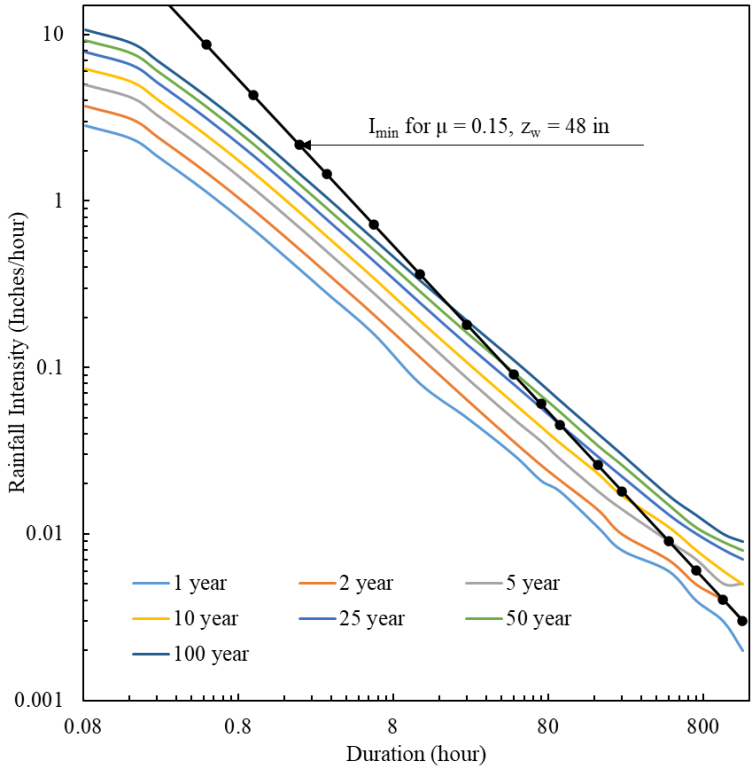

Figure 5.10: Minimum intensity vs duration chart for EL Paso

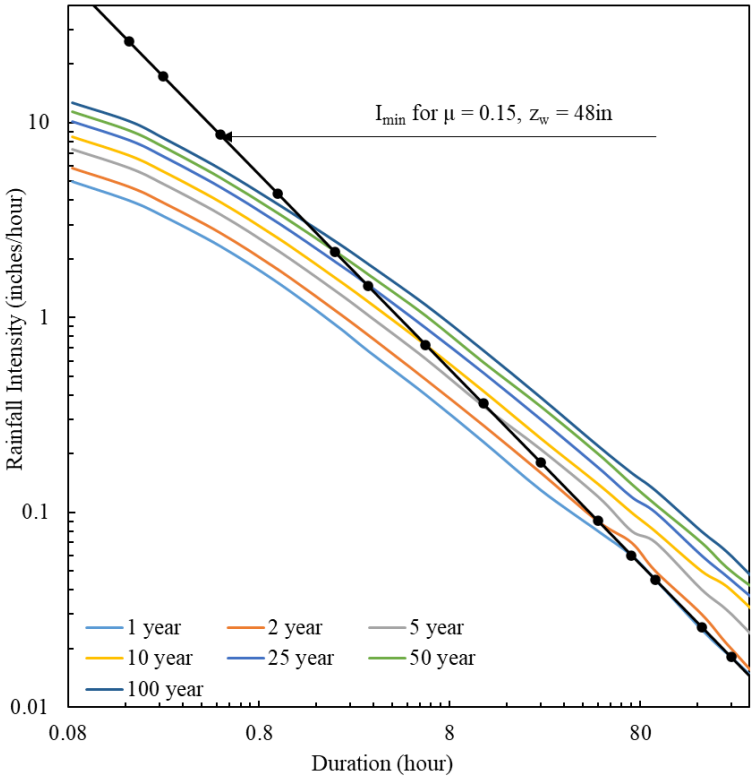

Figure 5.11: Minimum intensity vs duration chart for Midlothian

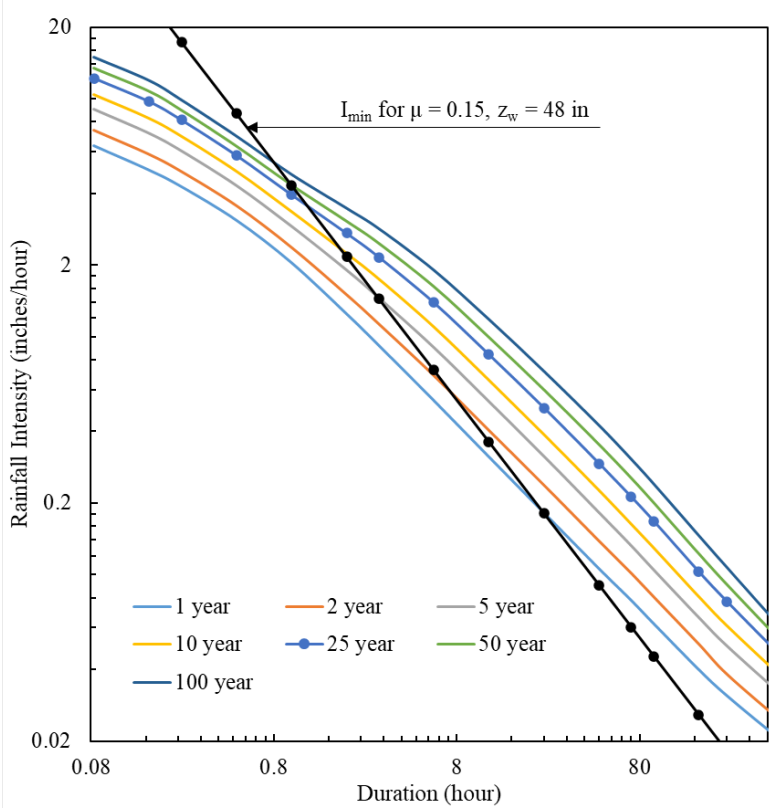

Figure 5.12: Minimum intensity vs duration chart for Houston

Table 5.2 Minimum intensity of rainfall (inches/hour) for different location for different return period

	1 year	2 years	5 years	10 years	25 years	50 years	100 years
El Paso	0.0032	0.0079	0.016	0.047	0.17	0.48	1.1
Midlothian	0.052	0.091	0.31	0.71	1.6	2.1	3.01
Houston	0.58	1.5	2.5	3.6	5.1	6.2	7.9

Table 5.2 shows that as rainfall intensity increases, the minimum amount of rainfall intensity required for the saturation of the slope also increases. Using equation (7), the threshold hydraulic conductivity was determined and presented in Figure 5.13.

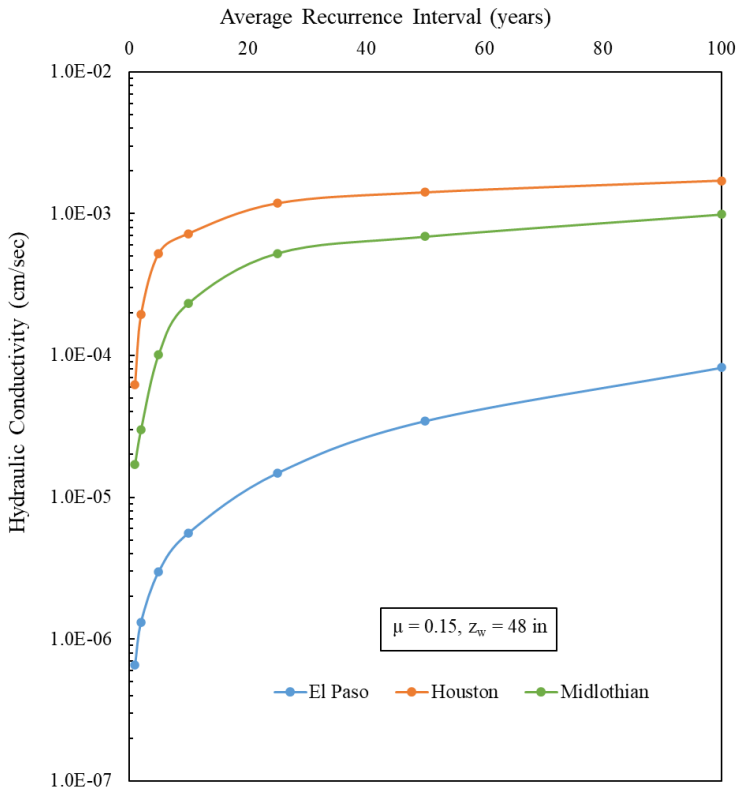

Figure 5.13 Threshold hydraulic conductivity in different regions in Texas

Figure 5.13 show that the process of saturation to a depth of 48 in is long. It requires a gradual buildup of moisture in the ground during a prolonged period of time. Hence, a short heavy rainfall after a prolonged dry period cannot create the conditions leading to saturation. However, heavy rainfall after a period of moderate rainfall may saturate the remaining upper few centimeters of unsaturated soil and trigger a slope failure. It was also observed that the more the time required for a specific return period of rainfall to saturate the soil, the less hydraulic conductivity is possessed by the soil.

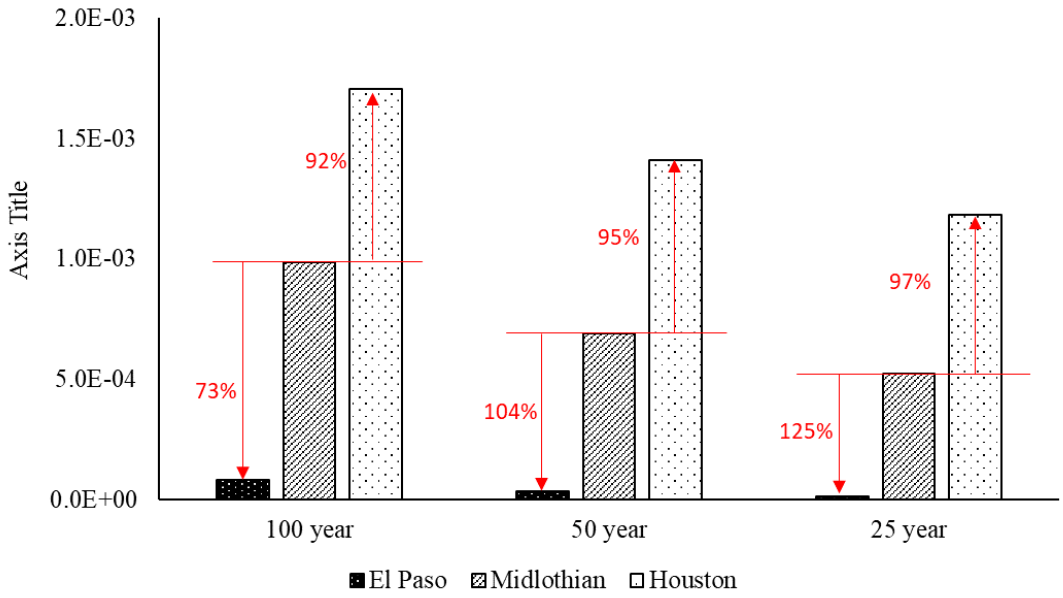

Figure 5.14 Comparison of threshold hydraulic conductivity in different regions

Figure 5.14 shows that in comparison to Central Texas, the threshold permeability increases from 92-97% in West Texas and decreases from 73-125% in East Texas. This is due to the rainfall depth over the years.

5.8 COMPARISON WITH PREVIOUS STUDIES

A similar study was performed in San Diego and Los Angeles in California depending on the rainfall pattern of the specific location for different period of rainfall and a similar trend was found as shown in Figure 5.15.

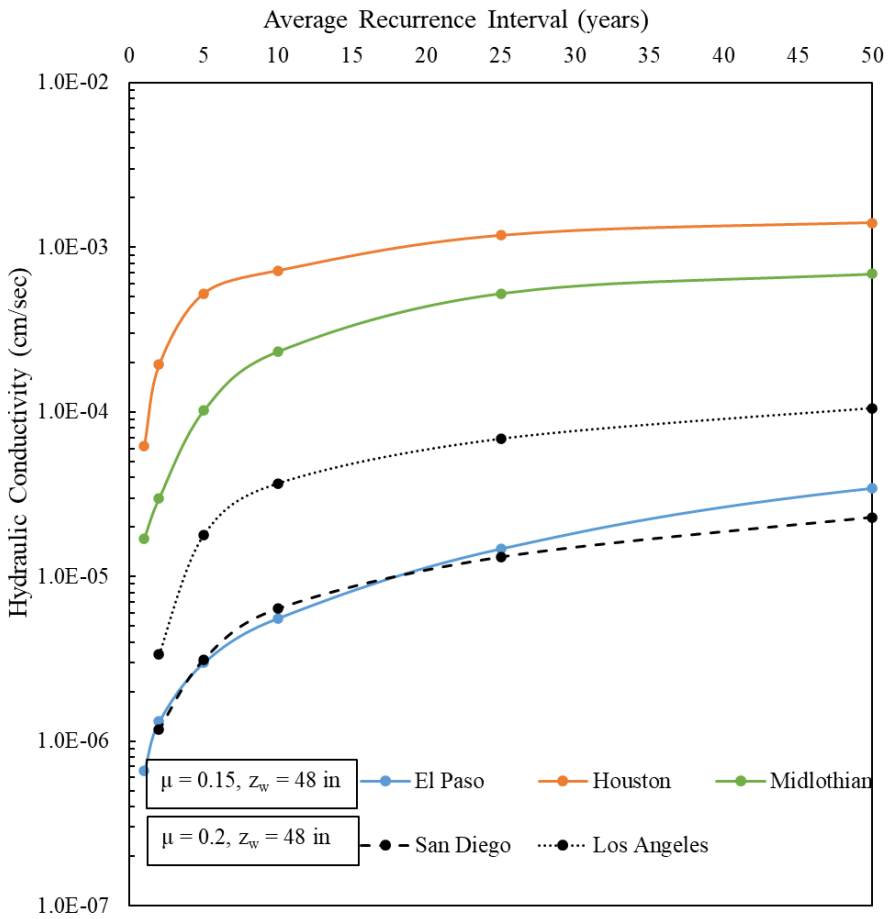

Figure 5.15 Comparison with previous study (Redrawn from Pradel 1993 and current study)

It should be noted that the values of k_{lim} in Figure 5.15 are based on a depth of z_w = 48 in (4 ft). If a different depth of saturation is considered, the values of the threshold hydraulic conductivity k_{lim} will change. The depth of saturation becomes shallower, k_{lim} increases. This would imply that surficial failures are more likely to develop along shallow planes (a few inches than along deeper planes (3-4 ft). However, this does not consider the stabilizing effects that plant roots can have (Wu et al. 1988a, 1988b). A well-developed vegetation seriously decreases the likelihood of surficial failure in the upper 3 ft. If a depth z_w = 3 ft is considered the threshold hydraulic conductivity k_{lim} becomes higher. Note that in a logarithmic scale this increase in k_{lim} is small and does not affect the aforementioned results and discussions.

5.9 CONCLUSION

From this study, it can be concluded that, surficial failures on natural slopes indicate that the potential for failure is highest for clayey and silty soils ML, MH, and CL and lowest for gravelly and sandy soils SW, GM, and SM class soils.

It also concludes that, before seepage parallel to the face of the slope can occur, the soil must reach saturation. This requires: (1) Rainfall intense enough to exceed the infiltration rate of the material; and (2) rainfall long enough to saturate the slope up to a depth, z_w. A study of the equations governing seepage in a uniform homogeneous slope and of the rainfall characteristics in three locations in Texas shows that the lower the hydraulic conductivity the higher the probability that saturation may develop in the slope. Hence, slopes made of clayey and silty soils would be more prone to develop the conditions for surficial instability than slopes made of sandy or gravelly soils. This is in agreement with actual observations (Hollingsworth and Kovacs 1981).

This study also found that soils with a hydraulic conductivity greater than a certain limiting value kli m will not become saturated. This threshold hydraulic conductivity k_{lim} is a function of the return period of the rain and the depth of saturation z_w. For the three locations included in this study it was found that rainfall pattern plays an important role in determining the threshold hydraulic conductivity.

CHAPTER 6

NUMERICAL ANALYSIS OF SLOPE STABILITY BASED ON IN-SITU HYDRAULIC CONDUCTIVITY

6.1 ABSTRACT

Rainfall-induced slope failure is one of the major problems for the highway slope constructed on highly plasticity clay Texas. During heavy and prolonged rainfall, a part of the rainwater infiltrates through the soil and seeps into the slope. The infiltrated water lowers the matric suction and increases the porewater pressure. To evaluate the effect of rainwater seepage on slope stability, it is necessary to investigate the hydraulic conductivity of the slope soil. The objective of this study is to evaluate the effect of hydraulic conductivity in slope failure mechanisms through numerical simulation. In this study, in-situ hydraulic conductivity was measured using Guelph Permeameter and volumetric water content were monitored using moisture sensors on monthly basis for three year (February 2020 to April 2023). It was observed that the hydraulic conductivity and volumetric water content are directly proportional to each other. The rainfall intensity and temperature data were analyzed to establish a relationship with hydraulic conductivity and volumetric water content. The monitoring data shows that hydraulic conductivity can vary from 2×10^{-6} to 4.5×10^{-7} cm/s. The temporal variation can depend on both infiltration of water due to heavy precipitation and evaporation due to high temperature. To determine the slope stability, these data were incorporated into numerical simulation to predict the slope failure using finite element-based software GeoStudio. In GeoStudio, the model was calibrated using the field monitoring data and coupled analysis were performed using SEEP/W and SLOPE/W to evaluate slope stability due to the continuous process of seepage. It was found that due the continuous process, the slope tends to become fully saturated, and factor of safety can decrease more than

200% (from 3 to less than 1) when both the volumetric water content and the hydraulic conductivity is high.

6.2 INTRODUCTION

Slope failures and landslides pose significant global challenges, resulting in substantial economic losses and loss of life (Wright 2005). These failures manifest in both natural landscapes and engineered slopes. The issue becomes particularly pronounced in regions where highway embankments and other man-made slopes are built on high plastic clay. While high plastic clay typically demonstrates adequate strength to uphold slopes under dry conditions, it's susceptible to cyclic swelling and shrinkage due to environmental factors such as precipitation and evapotranspiration (Abbey et al., 2020). In Texas, a considerable amount, reaching millions of dollars, is expended annually by the Texas Department of Transportation (TxDOT) to address the failures and maintain state roads and highways, adversely affecting travel times for commuters.

The failure mechanism of slopes constructed with expansive soil in response to rainfall is intricate, demanding an understanding of unsaturated soil mechanics. The relationship between soil hydraulic properties and factors like matric suction and moisture content follows a non-linear pattern. Swift shifts in pore-water pressure and moisture fluctuations significantly impact soil strength and, consequently, slope stability. Over time, the soil tends to soften, leading to a decrease in effective shear strength and the factor of safety (Mccomick and Short, 2006). In dry seasons, the expansive soil develops cracks, compromising its integrity. Additionally, the emergence of shrinkage cracks on slopes creates pathways for rainwater infiltration, facilitating potential water seepage. The combination of prolonged rainfall and cyclic swelling and shrinking renders highway slopes more susceptible to failure.

Desiccation cracks exert a profound influence on soil hydro-mechanical behavior, affecting factors such as clay volume change, slaking, permeability, residual shear, and tensile strength (Tang et al., 2005). Furthermore, high-plasticity clayey soil loses its shear strength properties, particularly the cohesion intercept (c′), after undergoing cycles of wetting and drying (Hossain 2013). During any rainfall event, rainwater quickly infiltrates through surface cracks, saturating the soil, and reducing shear strength by diminishing matric potential, while simultaneously decreasing effective stress by elevating pore water pressure. This results in a decline in resisting forces within the slope, allowing driving forces to prevail, ultimately culminating in rainfall-induced slope failures (Wang et al., 2021).

Numerous researchers have engaged in field investigations, laboratory tests, and numerical simulations to scrutinize slope failure mechanisms and identify triggering criteria (Damiano and Olivares, 2010). Standard indicators include the development of excessive strain, ground shifting, rising water levels, advancing wetting fronts, and surface cracking or loosening. Abrupt changes in any of these indicators are typically considered precursors to slope failure, with the associated rainfall event referred to as a critical rainfall. These failure indicators can be monitored using field instruments such as tilt sensors, inclinometers, extensometers for slope movement, dielectric moisture sensors, and tensiometers for soil moisture variation, and piezometers for groundwater levels. However, implementing extensive instrumentation across the entire slope of a highway embankment is impractical due to the high costs of instrumentation and long-term monitoring.

An alternative approach to establishing failure criteria involves conducting numerical studies incorporating the effects of precipitation. Researchers have conducted coupled and uncoupled analyses of seepage and slope stability to determine the time required for slope failure under different scenarios (Rahardjo et al., 2007). A fundamental distinction between saturated and

unsaturated soil shear strength lies in the additional strength induced by soil matric suction. Finite element method (FEM)-based software such as SEEP/W, PLAXIS 2D PlaxFlow, SVFLUX, Geo5, are commonly employed for seepage analyses. Slope stability analyses can be performed using methods like Limit Equilibrium (LE), FEM, and probabilistic approaches (Islam 2021). In recent years, the development of advanced modules within GeoStudio, encompassing transient seepage and deformation analysis, allows for the incorporation of soil variable parameters, enabling more rigorous analyses of rainfall-induced slope failure. Furthermore, uncoupled analyses (seepage and slope, and deformation and slope) have gained popularity for transient seepage analyses.

A potential method for monitoring slope failure involves observing the hydraulic properties of soil and their changes over time at shallow depths. Several studies have utilized numerical modeling and physical parameter analysis to establish thresholds (Islam 2021). However, a comprehensive field study, combined with numerical analysis, is necessary to assess hydraulic properties, the process of rainwater infiltration, and the behavior of rainfall-induced slope failures. Therefore, this study combines numerical analysis with field monitoring data to investigate the impact of soil hydraulic properties on slope stability. The study employed transient flow analyses using SEEP/W followed by slope stability analyses using SLOPE/W.

6.3 FINITE ELEMENT MODELLING

The Finite Element Method (FEM) is a numerical technique used to solve complex engineering problems involving structural analysis, heat transfer, fluid flow, and other physical phenomena. In the context of transportation infrastructures, FEM is employed to evaluate the performance and reliability of roads, bridges, and pavements.

One of the key advantages of FEM is its ability to represent complex geometries and material properties accurately. It breaks down the infrastructure into smaller, manageable elements or nodes, and then applies mathematical equations to these elements based on the governing physics and mechanics of the materials involved. By doing so, FEM can simulate the behavior of the structure under various loads and conditions. The FEM program uses graphical representations, such as contour plots, color maps, and displacement animations, to visualize the stress distribution, deformation patterns, and failure mechanisms within the infrastructure. This enhances engineers' comprehension of how the structure responds to different loads and how potential failures might occur. Deformation analysis is an essential aspect of FEM, as it allows engineers to understand how the infrastructure deforms under different loading scenarios. By studying these deformations, engineers can assess the structure's safety margins, identify potential weak points, and optimize the design to improve performance. Real-life monitoring of transportation infrastructures is crucial for assessing their actual in-service performance. However, real-world monitoring has limitations, such as the inability to replicate extreme or rare weather conditions, and the time required to collect meaningful data. FEM bridges this gap by allowing engineers to simulate extreme scenarios and study the structure's behavior under these conditions. By varying critical parameters like precipitation duration, intensity, road width, and pavement crack width, engineers can conduct parametric studies that explore the structure's response to a wide range of situations.

By combining real-world monitoring and FEM analysis, engineers can gain a comprehensive understanding of transportation infrastructure's performance. They can identify vulnerabilities and develop strategies to enhance the structure's resilience to adverse conditions, ultimately leading to safer and more reliable transportation systems.

Finite Element Modeling (FEM) with SEEP/W and SLOPE/W refers to the use of these specific software programs developed by GeoStudio for analyzing seepage and stability in geotechnical engineering applications. SEEP/W is primarily used for analyzing groundwater flow and seepage through porous media, while SLOPE/W focuses on stability analysis of slopes and embankments. SEEP/W is a powerful software program that employs the Finite Element Method to analyze groundwater flow and seepage problems in soils and porous materials. It allows geotechnical engineers to simulate and understand how water moves through the ground, and how it affects the stability and performance of engineering structures like dams, levees, retaining walls, and foundations. SEEP/W simulates the movement of liquid water through the layers of the soil. It can include both steady and transient groundwater flow subject to climatic boundary conditions and generate time dependent pore pressure. Using FEM, SEEP/W divides the analyzed domain into discrete elements, allowing the representation of complex geometries and material properties. The software applies governing groundwater flow equations to these elements, considering factors like hydraulic conductivity, boundary conditions, and initial water levels. Through graphical outputs and contour plots, engineers can visualize flow patterns, pore pressure distribution, and seepage paths, aiding in the identification of potential problem areas and design improvements. The water-flow governing equation used in the software for solving a transient and two dimensional seepage analysis is as follows:

$$m_w^2 \gamma_w \frac{\partial h_w}{\partial t} = \frac{\partial}{\partial x}\left(-K_x \frac{\partial h_w}{\partial x}\right) + \frac{\partial}{\partial y}\left(-K_y \frac{\partial h_w}{\partial y}\right) + Q$$

where m_w^2 =slope of soil–water characteristic curve; γ_w = unit weight of water; h_w = hydraulic head or total head; t = time; k_x = coefficient of permeability with respect to water as a function of matric suction in the x-direction; k_y = coefficient of permeability with respect to water

as a function of matric suction in the y direction; and Q = applied flux at the boundary. Soil–water characteristic curve (SWCC) and permeability functions were two primary soil properties used in the seepage analysis.

SLOPE/W, another software in the GeoStudio suite, is specifically designed for stability analysis of slopes and embankments. It utilizes the Finite Element Method to assess the stability of earth structures under different loading conditions, soil properties, and geometries. With FEM, SLOPE/W divides the slope or embankment into elements and applies relevant slope stability analysis methods, such as the limit equilibrium method or stress-based analysis. Engineers can model different slope configurations, soil profiles, and external loads to evaluate factors of safety against failure mechanisms like sliding and slope instability. The shear strength equation for unsaturated soil (Fredlund et al., 1978) which was used in the slope stability analyses that incorporated shear strength contribution from negative pore-water pressure or matric suction of unsaturated soil is as follows:

$$\tau = c' + (\sigma_n - u_w)tan\varphi' + (u_a - u_w)tan\varphi^b$$

Where, τ = shear strength of unsaturated soil; c' = effective cohesion; $(\sigma_n - u_w)$ = net normal stress; σ_n = total normal stress; u_a = pore-air pressure; ϕ' = effective angle of internal friction; $(u_a - u_w)$ = matric suction; u_w = pore-water pressure; and ϕ^b = angle indicating the rate of increase in shear strength relative to the matric suction. To compute the factor of safety, F_s, of soil slopes, Bishop's simplified method was used.

By combining FEM with SEEP/W and SLOPE/W, the impact of seepage and slope stability was conducted in this study.

6.3.1 Model Development and Soil Properties

6.3.1.1 Seepage Analysis

The modeling process commenced with the development of a 2D model, incorporating specific boundary conditions as shown in Figure 6.1 . The model comprised three layers representing the soil profile, with both sides of the domain set as no-flow boundaries. The top layer was subjected to rainfall intensity, and the relevant rainfall data were obtained from the National Oceanic and Atmospheric Administration (NOAA) website. Subsequently, the model was calibrated using field data to ensure its accuracy and reliability.

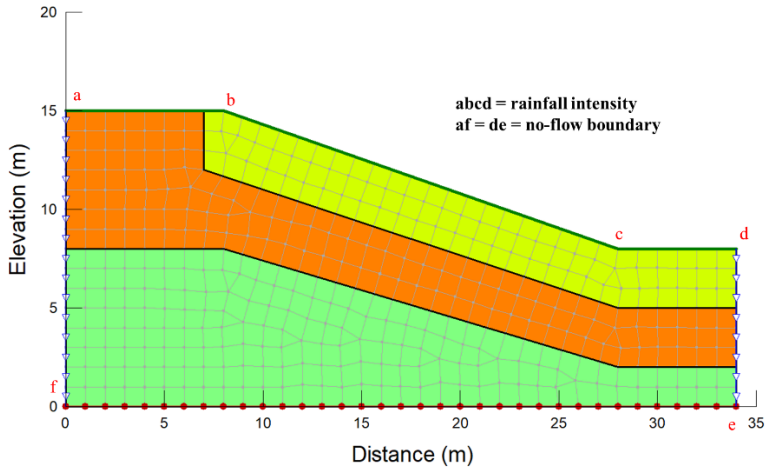

Figure 6.1 Model development in GeoStudio

The geometry was developed based on field investigation as mentioned in earlier study in Islam 2021. The highway slope angle was 19º and the slope height was 8 m. The boundary conditions used in the model was as follows:

1. The slope surface abcd was infiltration boundary where rainfall was applied as water flux.

2. The sides are no-flow boundaries af and de. Field data and laboratory performance results are used to perform this analysis.

For three different layers, the volumetric water content functions are shown in Figure 6.2. Using this volumetric water content function, the calibration was executed to compare the actual condition in the field with the current numerical analysis. The Fredlund and Xing equation for SWCC with a correction factor, C(ψ)=1 as recommended by Leong and Rahardjo (1997) was used in this study as follows:

$$\theta_w = \theta_s \, C(\varphi)[\frac{1}{[\ln (e + [\frac{u_a - u_w}{a}]^n)]^m}]$$

where: θ_w =volumetric water content; θ_a = saturated volumetric water content; a = a fitting parameter related to the air-entry value of the soil (kPa); n = a fitting parameter related to the slope of the SWCC; m = a fitting parameter related to the residual water content of the soil; e = natural number, 2.71828; $(u_a - u_w)$=matric suction (kPa); (kPa); u_a = pore-air pressure (kPa); u_w = pore-water pressure (kPa).

During the modeling phase, 30% of the total rainfall was considered, as 70% of the precipitation was assumed to result in surface runoff, based on the findings of Yunusa and Gofar in 2012 as shown in Figure 6.3.

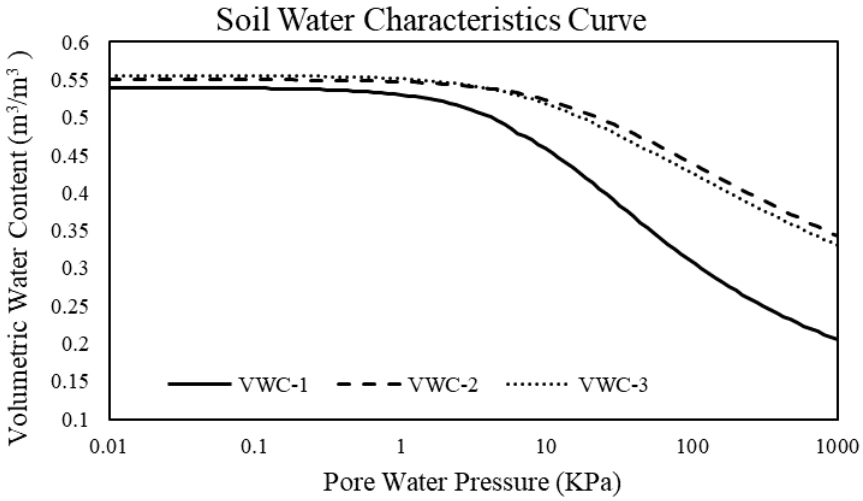

Figure 6.2 SWCC Curve used in the model

The rainfall data and the volumetric water content from the sensors of May 2020 were calibrated and compared with the current seepage analysis.

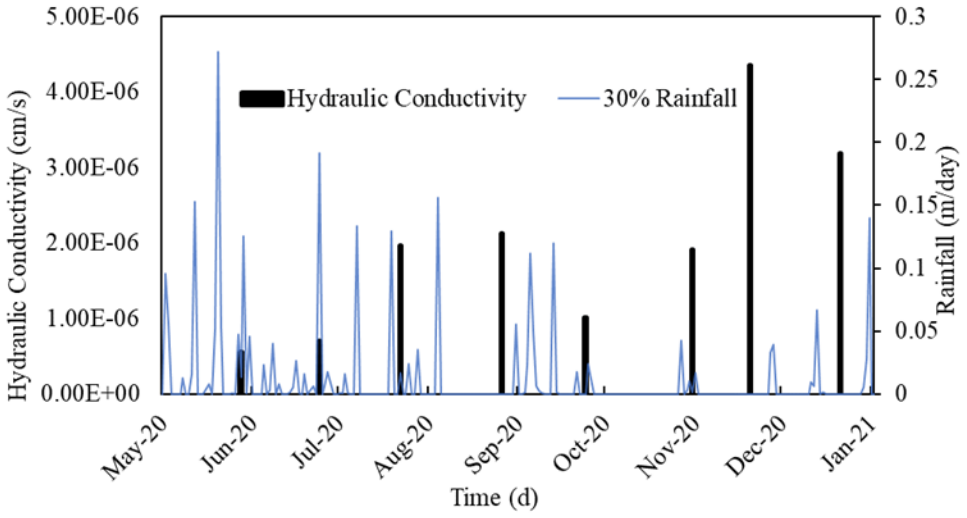

Figure 6.3 Rainfall and Corresponding hydraulic conductivity used from field study.

Figure 6.4 illustrates the initial condition of the model. To generate the seepage analysis, the steady state condition was selected first. The steady state condition develops the pore-water pressure based on the SWCC curve as defined in the model. At 2ft depth, the initial porewater

pressure was observed -140 kPa which resembles nearly the field study. From the field suction sensor, the initial reading was obtained -125 kPa which validates the modelling result.

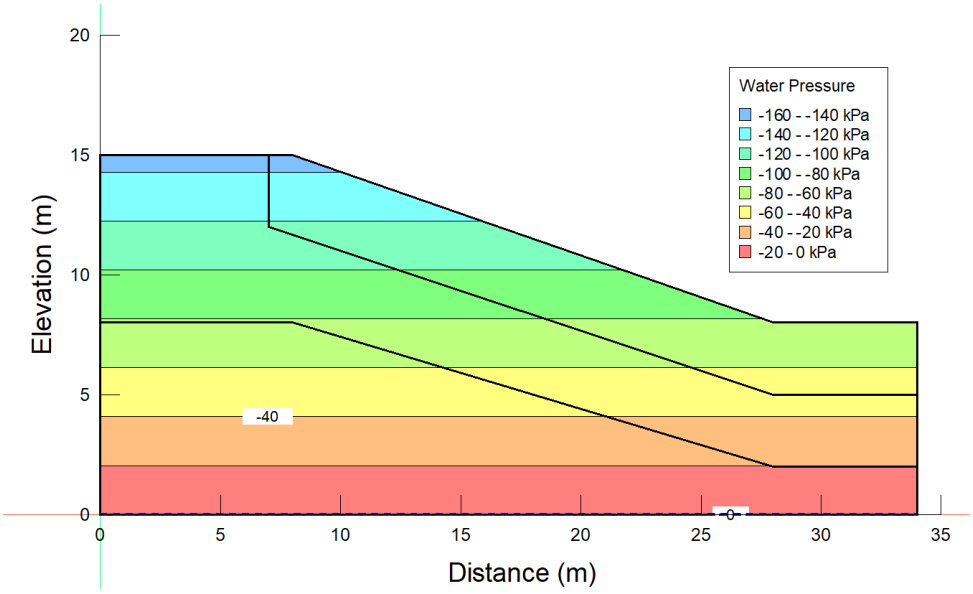

Figure 6.4 Initial condition of the model.

From Figure 6.5, it was observed that the field data and the SEEP/W analysis data show a similar pattern. However, the differences in magnitudes in the field curve and the numerical curve are evident. This is due to crack propagation and evapotranspiration occurring in the field, which was not incorporated in numerical analyses. Nevertheless, the similarity in the pattern fulfills the requirement to simulate the field conditions. It was observed that in both cases, the volumetric water contain level went up with the rainfall events. The variation changes with the change in rainfall amount.

After the steady state, the transient seepage analysis was performed for 8 months (from May 2020 to December 2020), to simulate the actual condition at site. The porewater pressure generated following the SWCC input parameter and these data were used further for slope stability analysis.

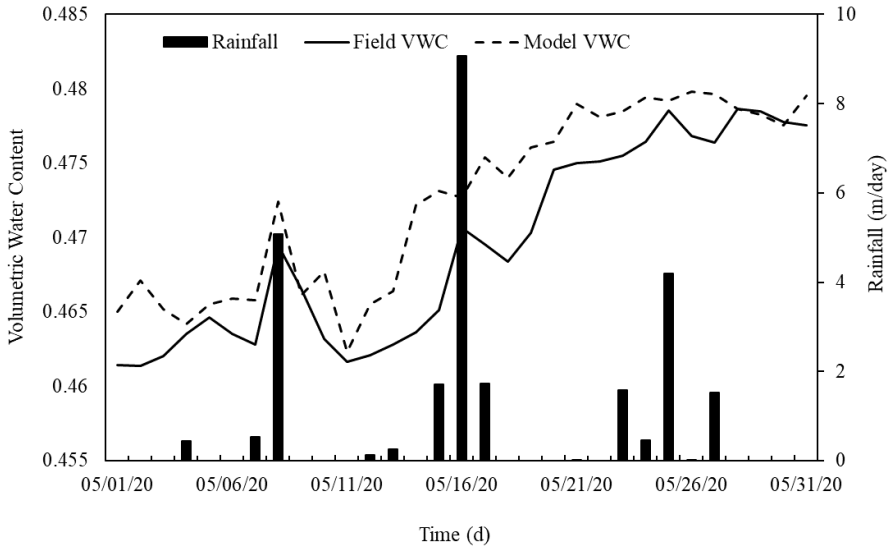

Figure 6.5 Calibration with Field and Model data

6.3.1.2 Slope Stability Analysis

To perform the slope stability analysis, the SLOPE/W module form Geostudio was used. The shear strength parameters were used from Islam 2021 for this model and the parameters are tabulated below:

Table 6.1 Shear Strength Parameters

Layer	Unit Weight (kN/m^3)	Cohesion (kPa)	Friction Angle (º)	Phi-B (º)
1	17.3	5.31	11.6	5.8
2	18.1	1.63	21.1	10.5
3	20.1	214.3	0	0

From the slope stability analysis result, it was observed that, during the initial 60 days, there was a substantial increase in the factor of safety, rising by approximately 175% from 2 to 3.5. This was primarily due to the slow seepage of water through the soil pores, caused by the low

hydraulic conductivity during May and June 2020. However, this trend changed dramatically after a period of intense rainfall, leading to a sudden drop in the factor of safety.

After the first 60 days, the hydraulic conductivity increased significantly compared to the initial conditions, allowing water to seep through the soil more easily. Consequently, the factor of safety experienced a sharp decline from day 60 to day 120, decreasing nearly threefold from 3.5 to 1.3. Between day 120 and day 150 (September 2020), the hydraulic conductivity decreased substantially, and the rainfall was not as significant as in previous months. As a result, the factor of safety showed a tendency to increase during this period. However, beyond September 2020, the hydraulic conductivity rose to 4×10^{-6} cm/s, causing water to permeate the slope easily and generating high porewater pressure. This, in turn, reduced the shear strength of the soil, resulting in a drop in the factor of safety below one. Such a situation indicates the slope's failure, as it is no longer stable under the prevailing conditions.

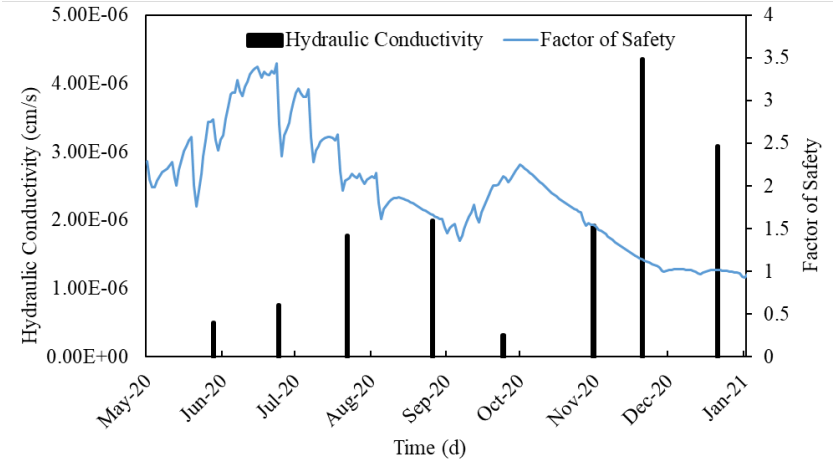

Figure 6.6 Change in Factor of safety with changing Hydraulic conductivity.

6.4 PARAMETRIC STUDY

A parametric study was conducted to investigate the controlling hydraulic properties of slope failure at US 287 site. In this study, the hydraulic properties were varied based on collected

data and previous investigations. The slope factor of safety were determined which shows to soil strength loss along with the failure plane. In this study, the focus is on the hydraulic properties and to determine the seepage and strength condition, SEEP/W and SLOPE/W modules were used. The controlling parameters used in this study are summarized in the following table.

Table 6.2 Parameter matrices for numerical analysis

Case	**Hydraulic Conductivity (m/s)**	**Rainfall Intensity (m/s)**	**Rainfall duration**	**Anisotropy of Hydraulic Conductivity (k_y/k_x)**
1	1×10^{-5}	[10^{-5} 10^{-6} 10^{-7}]	[1 hour 24 hours 7 days]	[1 5 10]
2	1×10^{-6}	[10^{-5} 10^{-6} 10^{-7}]	[1 hour 24 hours 7 days]	[1 5 10]
3	1×10^{-7}	[10^{-5} 10^{-6} 10^{-7}]	[1 hour 24 hours 7 days]	[1 5 10]
4	1×10^{-8}	[10^{-5} 10^{-6} 10^{-7}]	[1 hour 24 hours 7 days]	[1 5 10]

6.4.1 Results from parametric study

6.4.1.1 Effect of Hydraulic Conductivity

The hydraulic conductivity range was determined based on the field study and the range used in this study was 10^{-5} m/s to 10^{-8} m/s. The soil conductivity influences soil infiltration, seepage properties and slope stability. According to the findings, if the hydraulic conductivity is too low (10^{-8} m/s), the factor of safety goes high and slowly starts decreasing, however, it never reaches the lowest factor of safety. The factor of safety decreases to the lowest factor of safety if the factor of safety is higher than 10^{-6} m/s. In case of low permeable soil, the water does not penetrate the soil enough to generate high porewater pressure, causing surface runoff. Figure 6.7 shows the factor of safety-time series.

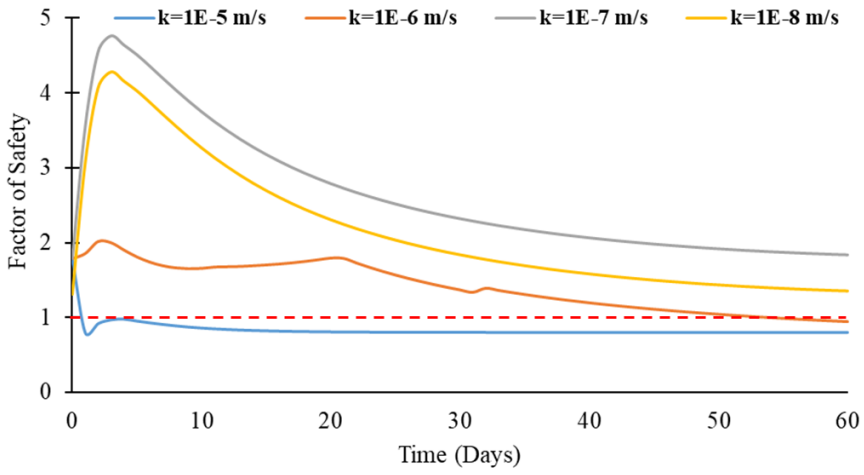

Figure 6.7 Variability in factor of safety after the beginning of rainfall in different hydraulic conductivity

6.4.1.2 Effect of Rainfall Intensity

Rainfall intensity plays a significant role in slope failure. It is one of the key factors that can trigger or contribute to slope instability and landslides. It was found in the study that, High rainfall intensity can saturate the soil, reducing its shear strength and increasing its pore water pressure. This weakening of the soil can lead to slope instability and failure. With low intensity of rainfall, the slope saturates slowly, and excess pore water cannot drain fast. Therefore, it takes more time to reach the failure condition of the slope. From Figure 6.8, it was evident that, the factor of safety gradually decreases when the rainfall intensity is 10^{-7} m/s and it reaches lower than 1 after 36 days. However, for high intensity, the risk of slope failure is very high and when the rainfall intensity is 10^{-5} m/s, it may take only take 1 day to reach the factor of safety lower than 1. The probability increases with the increasing anisotropy of hydraulic conductivity.

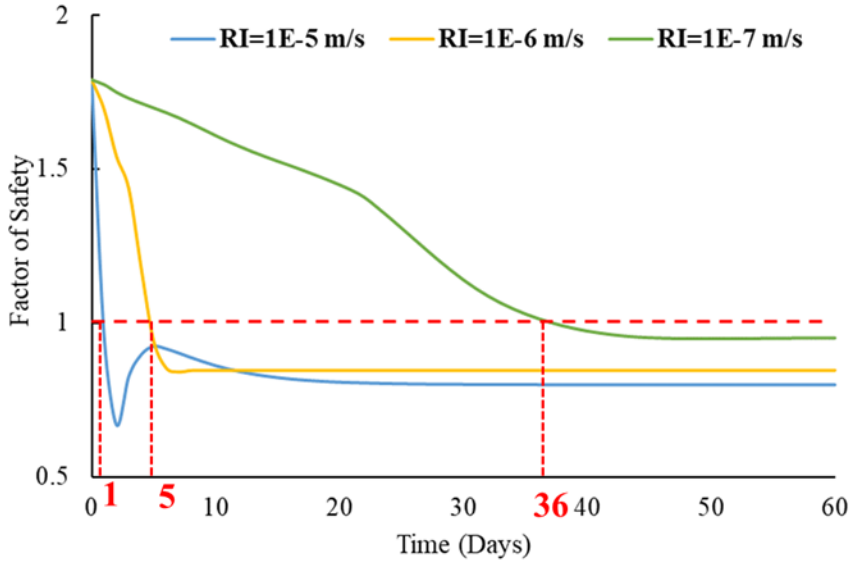

Figure 6.8 Variability in factor of safety after the beginning of rainfall in different rainfall intensity (RI)

6.4.1.3 Effect of Rainfall Duration

The duration of intense rainfall also impacts slope stability. Prolonged rainfall can lead to a prolonged increase in pore water pressure and saturation of the soil, further reducing the slope's stability. However, in this study, the effect of rainfall duration was found to be less than other parameters. The longer the rainfall, the longer it takes to saturate the slope and generate enough pore water pressure. It was found in the study that shorter rainfall with higher intensity can saturate the slope faster. However, the prolonged rainfall can affect the slope stability in long terms as the factor of safety keeps decreasing gradually.

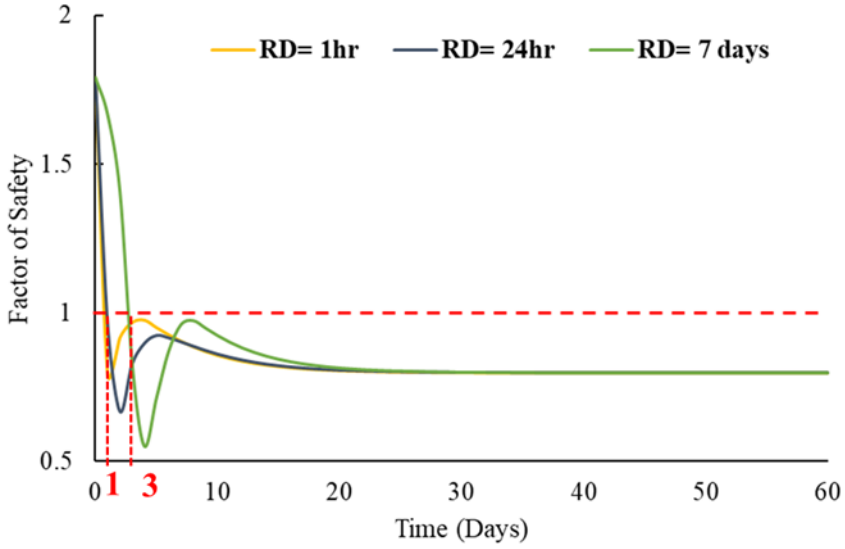

Figure 6.9 Variability in factor of safety after the beginning of rainfall in different rainfall duration (RD)

6.5 DETERMINATION OF THRESHOLD HYDRAULIC CONDUCTIVITY

The objective of this study is to determine threshold hydraulic conductivity to build an early warning system. To develop the threshold hydraulic conductivity, the results from parametric studies were used. The results were used in statistical analysis software MATLAB to develop a model that allows to determine the threshold hydraulic conductivity based on the rainfall intensity, rainfall duration, anisotropy of hydraulic conductivity and time required for factor of safety to reach a certain level.

In this Regression Learner Session in MATLAB, the data consists of 757 observations with five predictors: Rainfall intensity (RI), rainfall duration (RD), hydraulic conductivity (HC), time (T) and anisotropy of hydraulic conductivity (K_r). The goal of the prediction model is to estimate the factor of safety based on these 5 predictors.

The training process will use 5-fold cross-validation, a common technique to evaluate the model's performance. In 5-fold cross-validation, the dataset is randomly divided into five subsets (or "folds"). The model will be trained five times, each time using four of the folds for training and one-fold for validation. This helps to ensure that the model's performance is robust and not influenced by the specific data split.

By using the Regression Learner App in MATLAB, the relationships between the predictors (Rainfall intensity (RI), rainfall duration (RD), hydraulic conductivity (HC), time (T) and anisotropy of hydraulic conductivity (K_r)) and the response variable (factor of safety) can be explored to build a regression model. The app will automatically handle data preprocessing, algorithm selection, and model evaluation, making it easier to find the best model for predicting hydraulic conductivity based on the given predictors. After the training process, the model's

accuracy can be assessed using various performance metrics obtained from the 5-fold cross-validation results. For testing the data, 10% of total dataset were considered.

To train the model the following code can be used:

```
% Extract predictors and response

% This code processes the data into the right shape for training the

% model.

inputTable = trainingData;

predictorNames = {'RI', 'RD', 'Kr', 'T', 'HC'};

predictors = inputTable(:, predictorNames);

response = inputTable.FS;

isCategoricalPredictor = [false, false, false, false, false];

% Train a regression model

% This code specifies all the model options and trains the model.

regressionTree = fitrtree(...

    predictors, ...

    response, ...

    'MinLeafSize', 4, ...
```

```
    'Surrogate', 'off');

% Create the result struct with predict function

predictorExtractionFcn = @(t) t(:, predictorNames);

treePredictFcn = @(x) predict(regressionTree, x);

trainedModel.predictFcn = @(x) treePredictFcn(predictorExtractionFcn(x));

% Add additional fields to the result struct

trainedModel.RequiredVariables = {'HC', 'Kr', 'RD', 'RI', 'T'};

trainedModel.RegressionTree = regressionTree;

trainedModel.About = 'This struct is a trained model exported from Regression Learner R2023a.';

trainedModel.HowToPredict = sprintf('To make predictions on a new table, T, use: \n  yfit = c.predictFcn(T) \nreplacing "c" with the name of the variable that is this struct, e.g. "trainedModel". \n \nThe table, T, must contain the variables returned by: \n  c.RequiredVariables \nVariable formats (e.g. matrix/vector, datatype) must match the original training data. \nAdditional variables are ignored. \n \nFor more information, see <a href="matlab:helpview(fullfile(docroot, "stats", "stats.map"), "appregression_exportmodeltoworkspace")">How to predict using an exported model</a>.');

% Extract predictors and response

% This code processes the data into the right shape for training the
```

```
% model.

inputTable = trainingData;

predictorNames = {'RI', 'RD', 'Kr', 'T', 'HC'};

predictors = inputTable(:, predictorNames);

response = inputTable.FS;

isCategoricalPredictor = [false, false, false, false, false];

% Perform cross-validation

partitionedModel = crossval(trainedModel.RegressionTree, 'KFold', 5);

% Compute validation predictions

validationPredictions = kfoldPredict(partitionedModel);

% Compute validation RMSE

validationRMSE = sqrt(kfoldLoss(partitionedModel, 'LossFun', 'mse'));
```

For regression modeling, the independent variables should be independent of each other so that the variables do not have any correlation with each other. In order to ensure that, response plots were observed, and the following figure shows the independence of the variables.

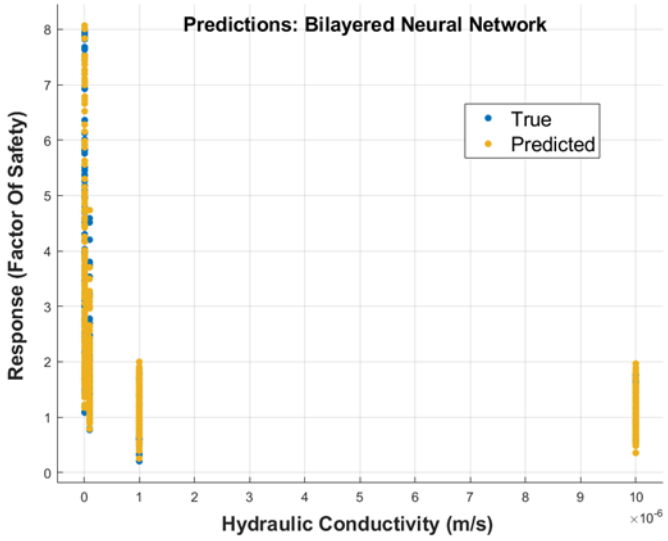
Predictions: Bilayered Neural Network
True
Predicted
Response (Factor Of Safety)
Hydraulic Conductivity (m/s)
×10^-6

(a)

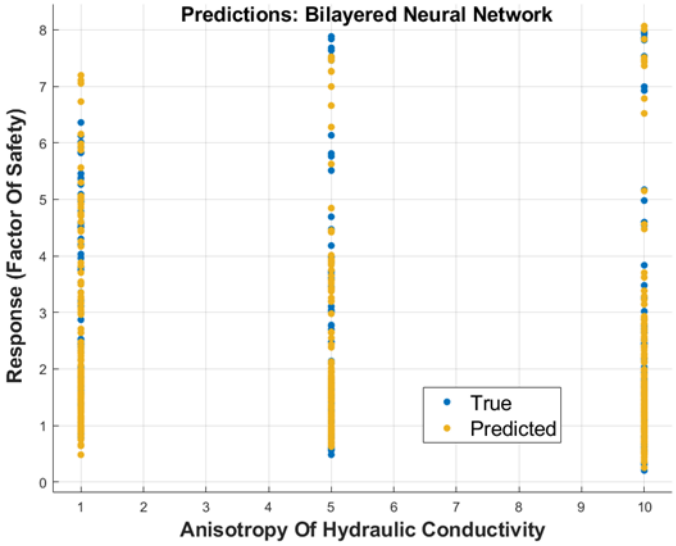
Predictions: Bilayered Neural Network
True
Predicted
Response (Factor Of Safety)
Anisotropy Of Hydraulic Conductivity

(b)

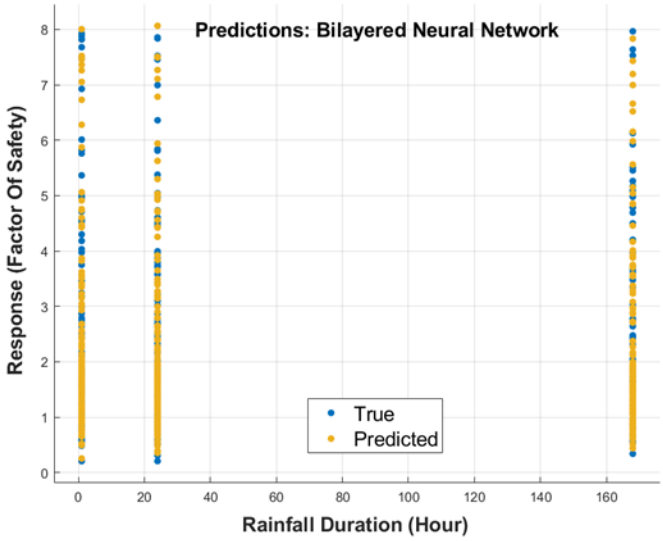
Predictions: Bilayered Neural Network
Response (Factor Of Safety)
Rainfall Duration (Hour)
True
Predicted
0
1
2
3
4
5
6
7
8
0
20
40
60
80
100
120
140
160

(c)

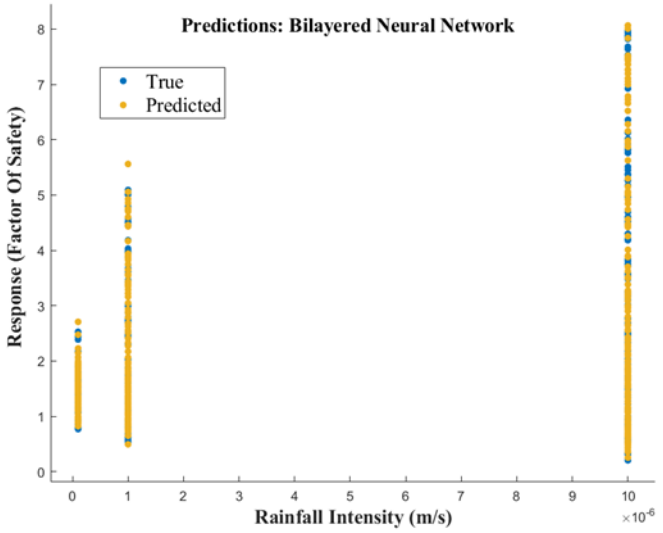
Predictions: Bilayered Neural Network
Response (Factor Of Safety)
Rainfall Intensity (m/s)
×10-6
True
Predicted
0
1
2
3
4
5
6
7
8
9
10

(d)

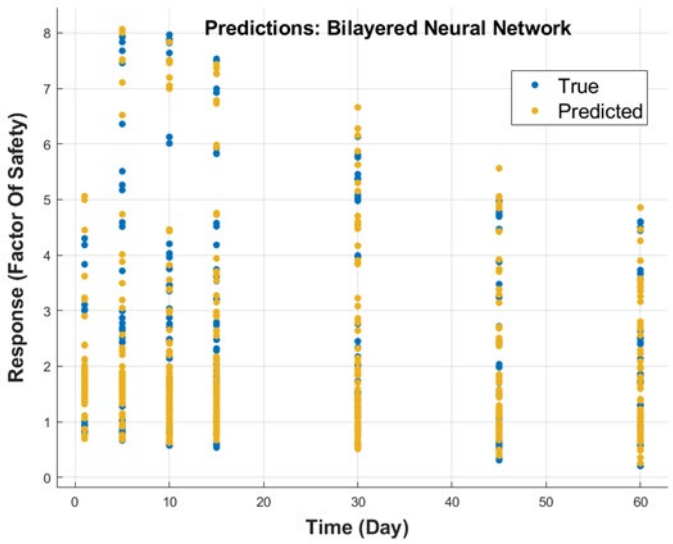

(e)

Figure 6.10 Predictor vs response plot (a) Factor of safety vs Hydraulic conductivity (b) Factor of safety vs anisotropy (c) Factor of safety vs Rainfall Duration (d) Factor of safety vs Rainfall Intensity and (e) Factor of safety vs Time

The results obtained from the training data are tabulated below:

Table 6.3 Training data results using different algorithms

Model Type	**RMSE (Validation)**	**MSE (Validation)**	**RSquared (Validation)**	**MAE (Validation)**
Tree	0.351	0.123	0.940	0.185
Linear Regression	1.251	1.566	0.230	0.889

Linear Regression	1.254	1.572	0.227	0.889
Linear Regression	1.444	2.086	-0.026	0.771
Stepwise Linear Regression	1.196	1.431	0.296	0.787
Fine Tree	0.351	0.123	0.940	0.185
Medium Tree	0.607	0.368	0.819	0.336
Coarse Tree	0.711	0.505	0.751	0.435
SVM	1.385	1.917	0.057	0.761
SVM	1.183	1.400	0.312	0.635
SVM	0.999	0.997	0.510	0.537
SVM	1.280	1.639	0.194	0.683
SVM	1.256	1.577	0.224	0.658
SVM	1.364	1.860	0.085	0.731
Ensemble	0.418	0.175	0.914	0.285

Ensemble	0.434	0.189	0.907	0.236
Gaussian Process Regression	0.976	0.954	0.531	0.653
Gaussian Process Regression	0.999	0.999	0.509	0.673
Gaussian Process Regression	1.187	1.408	0.308	0.769
Gaussian Process Regression	0.976	0.954	0.531	0.653
Narrow Neural Network	0.565	0.319	0.843	0.390
Medium Neural Network	0.463	0.214	0.895	0.305
Wide Neural Network	0.613	0.376	0.815	0.423

Bilayered Neural Network	0.325	0.146	0.951	0.255
Trilayered Neural Network	0.425	0.181	0.911	0.258
Kernel	1.507	2.270	-0.116	0.864
Kernel	1.527	2.330	-0.146	1.021

From the table, it was observed that the Bilayered Neural Network algorithms showed the best result considering R-squared value 0.95 and RMSE value of 0.325. This denoted that 95% data can be explained and predicted using these models. The true vs predicted response were shown in Figure 6.11.

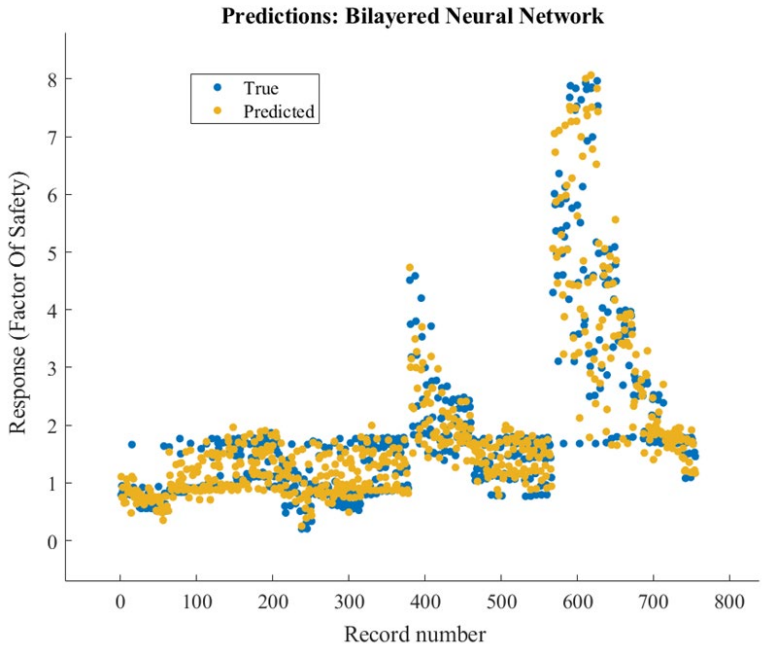

(a)

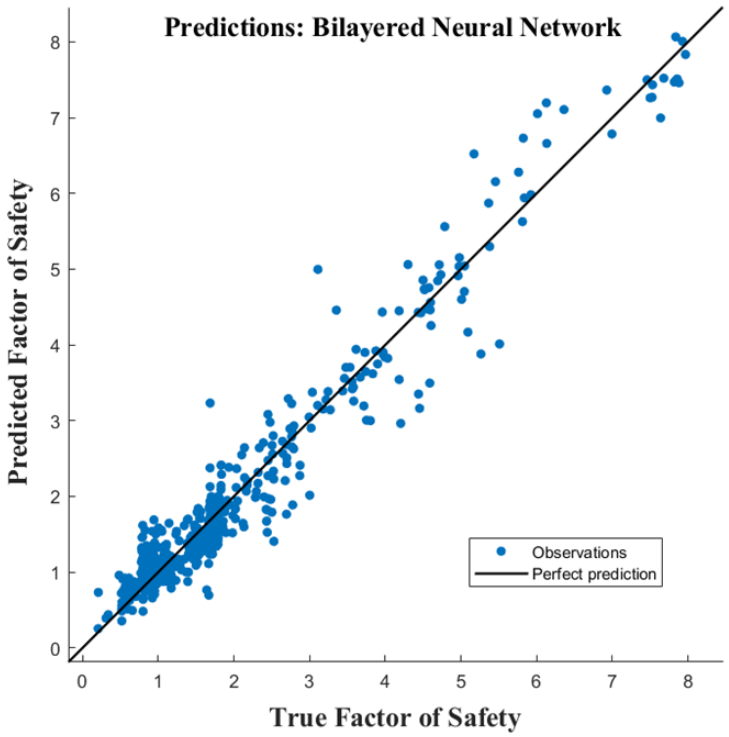

(b)

Figure 6.11 Predicted vs true response using Fine Tree algorithm for training data

To predict further using the predictor variables, the following function can be used in MATLAB, where T is the new matrix for the predictor variables:

yfit = trainedModel.predictFcn(T)

After training the data, the remaining 10% of the dataset was used to test the model. The predicted vs actual response plot in Figure 6.12. The R-squared and RMSE values for the test data were found 0.91 and 0.356 respectively. It indicates that 91% of the data can be explained using the model developed by the training data.

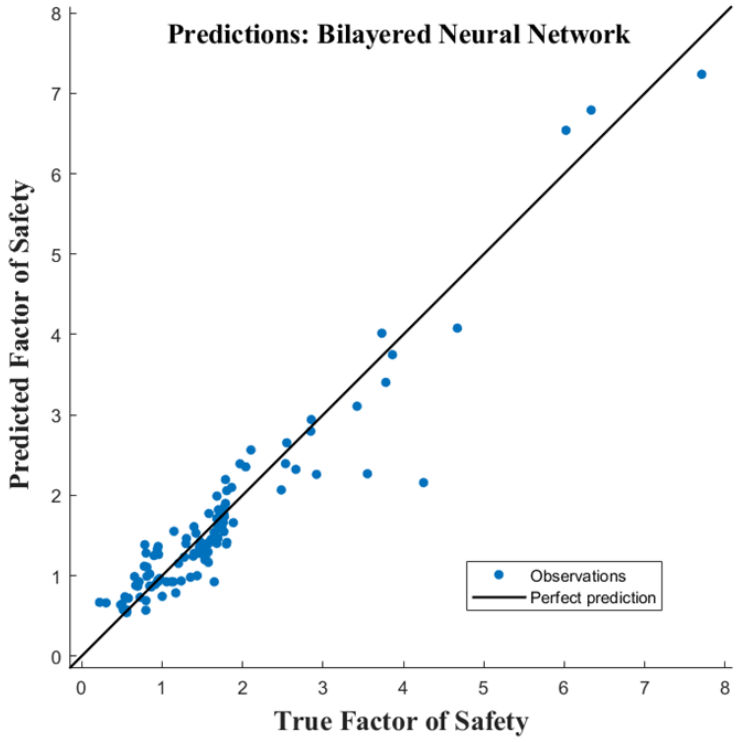

Figure 6.12 Predicted vs true response using Fine Tree algorithm for test data

From the F-test, it was found that among the predictor variables, the importance score for the predictors were found to be highest for hydraulic conductivity. That means the factor of safety was more dependent on the change of hydraulic conductivity as shown in Figure 6.13.

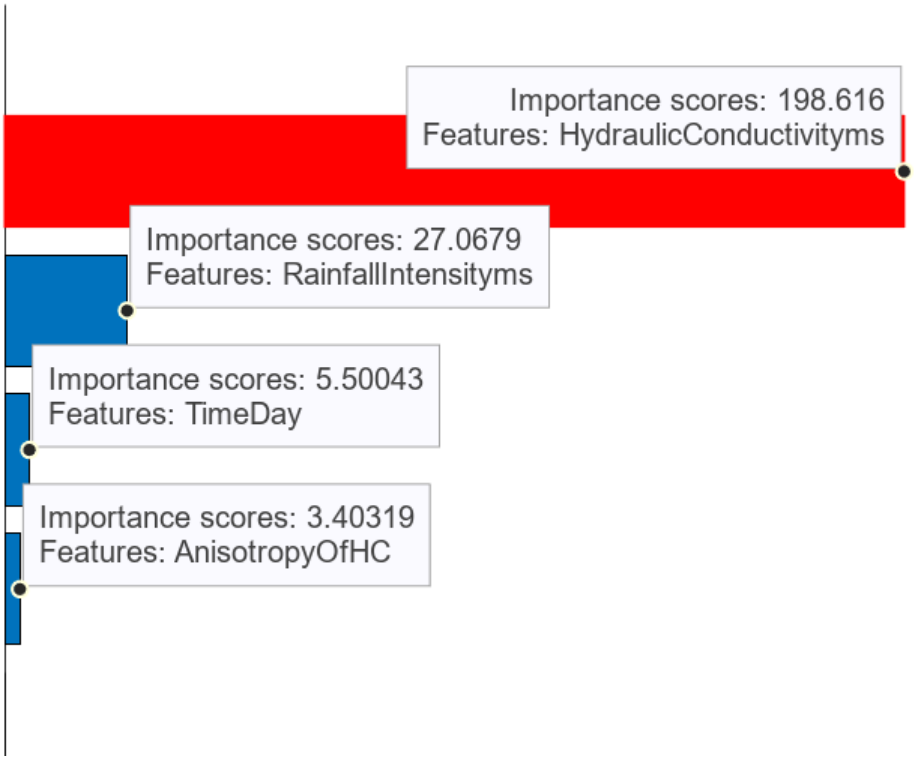

Figure 6.13 Importance scores from F-test

6.6 CONCLUSION

In this chapter, a numerical analysis was conducted using the field calibrated data. A parametric study was performed, and the results obtained from the parametric study were used to develop a model which can be used to predict the threshold hydraulic conductivity for desired factor of safety incorporating rainfall intensity, rainfall duration, anisotropy of hydraulic conductivity and required time to saturate the slope. This chapter can be concluded as below:

- For the field data, it was found that hydraulic conductivity as low as 4×10^{-6} cm/s can be responsible for water seepage through the soil and decrease the factor of safety below 1.
- The rainfall intensity plays an important role in slope failure. The higher intensity of rainfall can affect the factor of safety significantly and lead to shallow slope failure.

- Hydraulic conductivity higher than 10^{-6} cm/s can lead the water seep through the soil and be responsible for slope failure. The lower the hydraulic conductivity, less the risk of slope failure.
- From the regression modeling using the parametric study, a prediction model was developed. The best result was found using Fine Tree algorithm. The R-squared values for training and test data were found 0.95 and 0.91 respectively which denotes the accuracy of the model.
- From the importance score of F-test, it was observed that hydraulic conductivity is the primary factor which controls the factor of safety of a slope.

CHAPTER 7

DEVELOPMENT OF EARLY WARNING SYSTEM USING THE THRESHOLD HYDRAULIC CONDUCTIVITY

An early warning system for shallow slope failure based on hydraulic conductivity can help identify potential slope instability by monitoring changes in water flow through the slope. Combining the data from the early warning system with other factors such as rainfall data, slope geometry, and geological information, the level of risk can be assessed and appropriate response actions can be determined. These actions may include slope stabilization measures, evacuation plans, or temporary slope closure.

Using the framework proposed in Figure 7.1, one can determine if a slope is vulnerable to fail under different circumstances. First a location can be selected, and available data can be selected to run the model. The rainfall, moisture content data can be found in different websites such as NOAA or NASA POWER website. If site specific data cannot be found, the hydraulic conductivity prediction model can be used as mentioned in Chapter 4. A hydraulic conductivity data can be thus predicted. The best possible way is to perform in-situ testing as mentioned in Chapter 3. Once the hydraulic conductivity data is available, the program can be continued. Next step is to find out other soil parameters such as volumetric water content, anisotropy of hydraulic conductivity, slope geometry and other soil parameters. If data is not found, the hydraulic obtained conductivity data can be compared from the results obtained from analytical approach described in chapter 5. Thus threshold hydraulic conductivity can be determined. However, if data is available, one can use the parametric study results and prediction model explained in chapter 6 to determine the threshold hydraulic conductivity for desired factor of safety incorporating rainfall

intensity, rainfall duration, required time to saturate the slope etc. Based on the availability of the data, different approaches can be taken which are explained in this study.

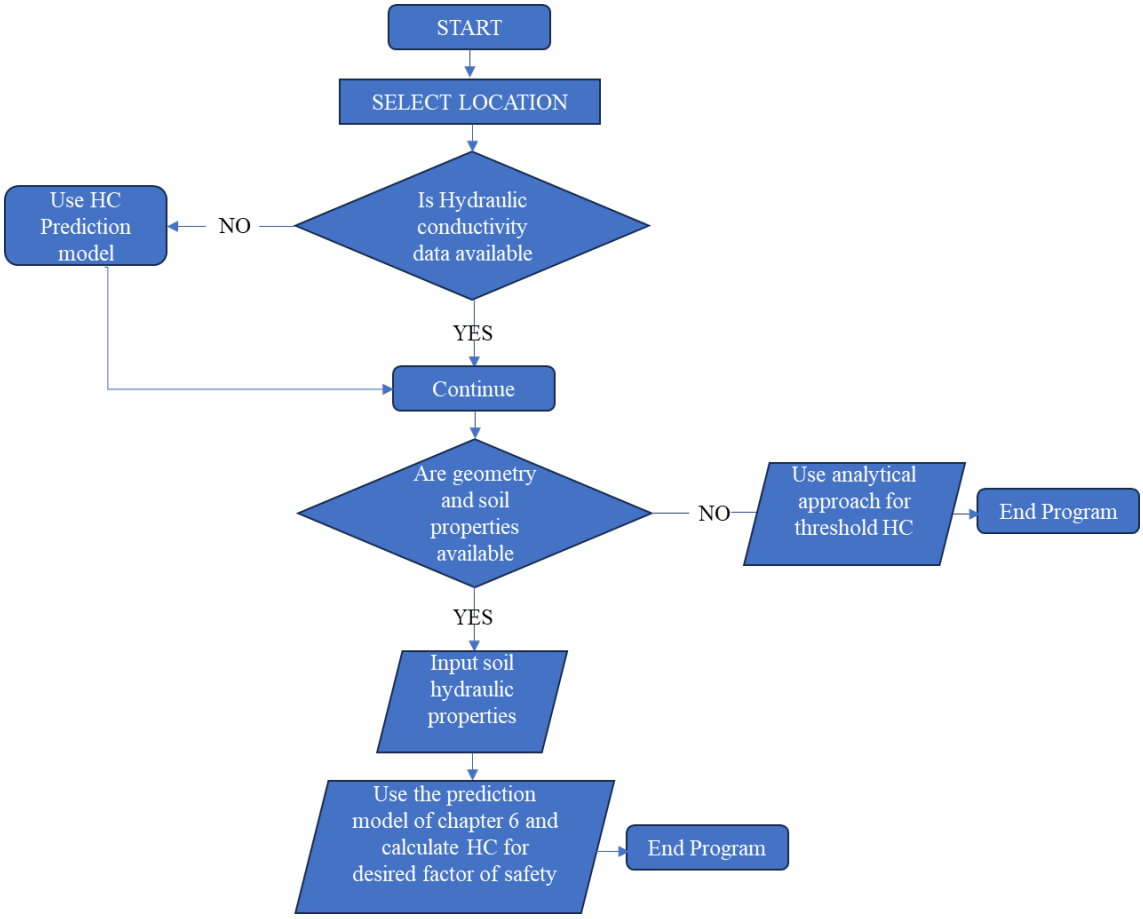

Figure 7.1 Framework for anticipating slope failure risk.

RECOMMENDATIONS FOR FUTURE STUDIES

Based on the present study, several recommendations can be mentioned to be considered in future studies. Such as:

- Crack propagation is a common problem in high plastic clay. To reduce the complexity of the present study, the nature of cracks, the depth of cracks and cyclic crack propagation was not considered. In future studies, crack propagation due to cyclic shrinking and swelling can be incorporated.
- In this study, the focus was on the soil hydraulic conductivity. Therefore, the hydraulic conductivity tests were done at field level. In-situ shear strength parameters can be monitored monthly and shear strength parameters can be modified considering the climate loading. Due to excess pore water pressure, the soil can lose the shear strength and during dry season, the same soil can obtain high shear strength. This case can be incorporated in future studies.
- In this study, the in-situ hydraulic conductivity was determined without considering the evaporation of vegetation effects. While very humid subtropical areas, such as Dallas-Fort Worth have high temperature and densely vegetated slopes, evaporation and vegetation can be important factors in fluctuation of soil moisture.
- Based on field observation on the study area, the slopes had uneven circular or semicircular plane, undulating in the center and bulging at the bottom. It is therefore recommended to assess 3D seepages and stability analysis while performing the slope stability analysis using different softwares.

REFERENCES

Abu-Hassanein, Z. S., Benson, C. H., & Blotz, L. R. (1996). Electrical resistivity of compacted clays. *Journal of geotechnical engineering*, *122*(5), 397-406.

Ahmed, A., & Hossain, S. (2022). Field determination of unsaturated permeability and flow properties through subgrade instrumentation. *Geosciences*, *12*(2), 95.

Ahmed, A., Hossain, M. S., Pandey, P., Sapkota, A., & Thian, B. (2019). Deformation modeling of flexible pavement in expansive subgrade in texas. *Geosciences*, *9*(10), 446.

Ahmed, Z. (2022). *Evaluation of Relationship Between Sulfate Content and Electrical Resistivity* (Doctoral dissertation, The University of Texas at Arlington).

Akhtar, M. A., Mahjabin, S., Hossain, M. S., Mina, Z., & Hossain, M. I. (2022). Characterization of Eagle Ford Shale by Using Laboratory Electrical Resistivity Imaging. In *Geo-Congress 2022* (pp. 159-168).

Aleotti, P. (2004). A warning system for rainfall-induced shallow failures. *Engineering geology*, *73*(3-4), 247-265.

Angulo-Jaramillo, R., Thony, J. L., Vachaud, G., Moreno, F., Fernandez-Boy, E., Cayuela, J. A., & Clothier, B. E. (1997). Seasonal variation of hydraulic properties of soils measured using a tension disk infiltrometer. *Soil Science Society of America Journal*, *61*(1), 27-32.

Asare, S. N., Rudra, R. P., Dickinson, W. T., & Wall, G. J. (1993). Seasonal variability of hydraulic conductivity. *Transactions of the ASAE*, *36*(2), 451-457.

Aurpa, S. S., Hossain, S., & Islam, M. A. (2022). Effect of Plastic Waste on Volume Consumption of Landfill during the COVID-19 Pandemic.

Bachmaier, J. (2010). *Correlation between volumetric water content and water movement in a soil column experiment*. na.

Badhon, F. F., Islam, M. A., Bhandari, P., & Hossain, M. S. (2023). Performance of Recycled Plastic Pins for Improving Unsuitable Foundation Soil. *Transportation Research Record*, *2677*(6), 852-865.

Bagarello, V., Iovino, M., & Reynolds, W. D. (1999). Measuring hydraulic conductivity in a cracking clay soil using the Guelph permeameter. *Transactions of the ASAE*, *42*(4), 957-964.

Barry, D. A., Parlange, J. Y., Li, L., Jeng, D. S., & Crapper, M. (2005). Green–ampt approximations. *Advances in Water Resources*, *28*(10), 1003-1009.

Bhandari, P., Hossain, M. S., Islam, M. A., & Badhon, F. F. (2022). Controlling base movement of MSE walls using recycled plastic pins. *Transportation Geotechnics*, *32*, 100707.

Bormann, H., & Klaassen, K. (2008). Seasonal and land use dependent variability of soil hydraulic and soil hydrological properties of two Northern German soils. *Geoderma*, *145*(3-4), 295-302.

Brakensiek, D. L., & Onstad, C. A. (1977). Parameter estimation of the Green and Ampt infiltration equation. *Water Resources Research*, *13*(6), 1009-1012.

Campbell, G. S. (1974). A simple method for determining unsaturated conductivity from moisture retention data. *Soil science*, *117*(6), 311-314.

Carman, P. C. (1939). Permeability of saturated sands, soils and clays. *The Journal of Agricultural Science*, *29*(2), 262-273.

Carsel, R. F., & Parrish, R. S. (1988). Developing joint probability distributions of soil water retention characteristics. *Water resources research*, *24*(5), 755-769.

Chae, B. G., & Kim, M. I. (2012). Suggestion of a method for landslide early warning using the change in the volumetric water content gradient due to rainfall infiltration. *Environmental Earth Sciences*, *66*, 1973-1986.

Chen, M., & Jiang, Q. (2020). An early warning system integrating time-of-failure analysis and alert procedure for slope failures. *Engineering Geology*, *272*, 105629.

Cho, W. J., Lee, J. O., & Chun, K. S. (1997). Influence of temperature on hydraulic conductivity in compacted bentonite. *MRS Online Proceedings Library (OPL)*, *506*, 305.

Constantz, J. (1982). Temperature dependence of unsaturated hydraulic conductivity of two soils. *Soil Science Society of America Journal*, *46*(3), 466-470.

Das Gupta, S., Mohanty, B. P., & Köhne, J. M. (2006). Soil hydraulic conductivities and their spatial and temporal variations in a vertisol. *Soil Science Society of America Journal*, *70*(6), 1872-1881.

Deb, S. K., & Shukla, M. K. (2012). Variability of hydraulic conductivity due to multiple factors. *American Journal of Environmental Sciences*, *8*(5), 489.

Dohnal, M., Dusek, J., & Vogel, T. (2010). Improving hydraulic conductivity estimates from minidisk infiltrometer measurements for soils with wide pore-size distributions. *Soil Science Society of America Journal*, *74*(3), 804-811.

Dong, J. J., Tu, C. H., Lee, W. R., & Jheng, Y. J. (2012). Effects of hydraulic conductivity/strength anisotropy on the stability of stratified, poorly cemented rock slopes. *Computers and geotechnics*, *40*, 147-159.

Fredlund, D. G. (2006). Unsaturated soil mechanics in engineering practice. *Journal of geotechnical and geoenvironmental engineering*, *132*(3), 286-321.

Fredlund, D. G., & Rahardjo, H. (1993). An overview of unsaturated soil behaviour. *Geotechnical special publication*, 1-1.

Flerchinger, G. N., Watts, F. J., & Bloomsburg, G. L. (1988). Explicit solution to Green-Ampt equation for nonuniform soils. *Journal of irrigation and drainage engineering*, *114*(3), 561-565.

Gao, H., & Shao, M. (2015). Effects of temperature changes on soil hydraulic properties. *Soil and Tillage Research*, *153*, 145-154.

Giraldo, E. V. A., Upegui, J. I. V., & Carvajal, H. E. M. (2016). Influences of antecedent rainfall and hydraulic conductivity on landslides triggered by rainfall occurrence using the model SHIA_LANDSLIDE. *Revista EIA/English version*, *13*(26).

Glade, T., Crozier, M., & Smith, P. (2000). Applying probability determination to refine landslide-triggering rainfall thresholds using an empirical "Antecedent Daily Rainfall Model". *Pure and Applied Geophysics*, *157*, 1059-1079.

Glade, T. (2000). Modelling landslide-triggering rainfalls in different regions of New Zealand-the soil water status model. *Zeitschrift für Geomorphologie. Supplementband*, (122), 63-84.

Green, W. H., & Ampt, G. A. (1911). Studies on Soil Phyics. *The Journal of Agricultural Science*, *4*(1), 1-24.

Gupta, R. K., Rudra, R. P., Dickinson, W. T., & Wall, G. J. (1994). Spatial and seasonal variations in hydraulic conductivity in relation to four determination techniques. *Canadian Water Resources Journal*, *19*(2), 103-113.

Haofang, Y., Chuan, Z., Oue, H., Guangjie, P., & Darko, R. O. (2017). Determination of crop and soil evaporation coefficients for estimating evapotranspiration in a paddy field. *International Journal of Agricultural and Biological Engineering*, *10*(4), 130-139.

Harris, S., Orense, R. P., & Itoh, K. (2016). Site-specific warning system for rainfall-induced slope failure. *Japanese Geotechnical Society Special Publication*, *2*(32), 1171-1176.

Hayden, A. H. (2010). Correlation Between Falling Head and Double Ring Testing for a Full-Scale Infiltration Study.

Heddadj, D., & Gascuel-Odoux, C. (1999). Topographic and seasonal variations of unsaturated hydraulic conductivity as measured by tension disc infiltrometers at the field scale. *European Journal of Soil Science*, *50*(2), 275-283.

Hoyos, L., Alam, M. J. B., Hossain, M. S., & Haney, B. (2019, March). Monitoring Seasonal Variation of Soil Hydraulic Conductivity of Evapotranspiration (ET) Cover. In *Eighth*

International Conference on Case Histories in Geotechnical Engineering (pp. 72-81). Reston, VA: American Society of Civil Engineers.

Hu, W., Shao, M. A., & Si, B. C. (2012). Seasonal changes in surface bulk density and saturated hydraulic conductivity of natural landscapes. *European Journal of Soil Science*, *63*(6), 820-830.

Islam, M. A., Gupta, A., Gupta, N., & Islam, T. (2021). Laboratory Investigation of Soil Plugs in Open Ended Model Piles Driven into Sand. In *IFCEE 2021* (pp. 108-118).

Islam, M. A., Gupta, A., Gupta, N., Jeet, A. A., & Islam, T. (2022). Soil Plug Response and Load-Settlement Behavior of Open-Ended Model Piles in Sandy Soil. In *Geo-Congress 2022* (pp. 207-217).

Islam, M. A., Hossain, M. S., Badhon, F. F., & Bhandari, P. (2021). Performance Evaluation of Recycled-Plastic-Pin-Supported Embankment over Soft Soil. *Journal of Geotechnical and Geoenvironmental Engineering*, *147*(6), 04021032.

Islam, M. A., Jeet, A. A., Gupta, N., Gupta, A., & Islam, T. (2022). Factors Affecting the Stability and Behavior of an MSE Wall: A Numerical Approach. In *Geo-Congress 2022* (pp. 375-385).

Islam, M. A., Sara Aurpa, S., Masiyat, M., & Hossain, M. S. Case History of Recycled Plastic Pins Supported Embankment on a Soft Clay Overlying Shale in Texas. In *Geo-Congress 2023* (pp. 20-30)

Jarvis, N., Koestel, J., Messing, I., Moeys, J., & Lindahl, A. (2013). Influence of soil, land use and climatic factors on the hydraulic conductivity of soil. *Hydrology and Earth System Sciences*, *17*(12), 5185-5195.

Khan, M. S., Hossain, S., Ahmed, A., & Faysal, M. (2017). Investigation of a shallow slope failure on expansive clay in Texas. *Engineering geology*, *219*, 118-129.

Keery, J., Binley, A., Crook, N., & Smith, J. W. (2007). Temporal and spatial variability of groundwater–surface water fluxes: Development and application of an analytical method using temperature time series. *Journal of Hydrology*, *336*(1-2), 1-16.

Latif, M. B., Islam, M. A., Hossain, M. S., & Aurpa, S. S. (2023). Effect of Sludge Content on the Decomposition of Different Types of Food Waste. *Sustainability*, *15*(3), 2782.

Leung, A. K., Feng, S., Vitali, D., Ma, L., & Karimzadeh, A. A. (2020). Temperature effects on the hydraulic properties of unsaturated sand and their influences on water-vapor heat transport. *Journal of Geotechnical and Geoenvironmental Engineering*, *146*(4), 06020003.

Levy, GJ*, Smith, HJC* and Agassi, M. (1988). Water temperature effect on hydraulic conductivity and infiltration rate of soils. *South African Journal of Plant and Soil*, *6*(4), 240-244.

Louati, F., Houcem, T., & Jamei, M. (2018, August). Unsaturated permeability prediction using natural evaporation method in cracked clay. In *Proceedings of the 7th international conference on unsaturated soils (2018), Hong Kong, China*.

Louati, F., Trabelsi, H., Jamei, M., & Taibi, S. (2021). Impact of wetting-drying cycles and cracks on the permeability of compacted clayey soil. *European Journal of Environmental and Civil Engineering*, *25*(4), 696-721.

Lu, H., Liu, J., Li, Y., & Dong, Y. (2015). Heat transport and water permeability during cracking of the landfill compacted clay cover. *Journal of Chemistry*, *2015*.

Malaya, C., & Sreedeep, S. (2012). Critical review on the parameters influencing soil-water characteristic curve. *Journal of Irrigation and Drainage Engineering*, *138*(1), 55-62.

McCartney, J. S., Villar, L., & Zornberg, J. G. (2007, November). Estimation of the hydraulic conductivity function of unsaturated clays using an infiltration column test. In *Proc., 6th Brazilian Conference on Unsaturated Soils (NSAT)*.

Messing, I., & Jarvis, N. J. (1990). Seasonal variation in field-saturated hydraulic conductivity in two swelling clay soils in Sweden. *Journal of soil science*, *41*(2), 229-237.

Mualem, Y. (1986). Hydraulic conductivity of unsaturated soils: prediction and formulas. *Methods of Soil Analysis: Part 1 Physical and Mineralogical Methods*, *5*, 799-823.

Naik, A. P., Ghosh, B., & Pekkat, S. (2019). Estimating soil hydraulic properties using mini disk infiltrometer. *ISH Journal of Hydraulic Engineering*, *25*(1), 62-70.

Ng, C. W., & Pang, Y. W. (2000). Experimental investigations of the soil-water characteristics of a volcanic soil. *Canadian Geotechnical Journal*, *37*(6), 1252-1264.

Ng, C. W., & Pang, Y. W. (2000). Influence of stress state on soil-water characteristics and slope stability. *Journal of geotechnical and geoenvironmental engineering*, *126*(2), 157-166.

Ng, C. W. W., Zhan, L. T., Bao, C. G., Fredlund, D. G., & Gong, B. W. (2003). Performance of an unsaturated expansive soil slope subjected to artificial rainfall infiltration. *Geotechnique*, *53*(2), 143-157.

Oosterbaan, R. J., & Nijland, H. J. (1994). 12 Determining the Saturated Hydraulic Conductivity.

Pisano, M., & Cardile, G. (2023). Probabilistic Analyses of Root-Reinforced Slopes Using Monte Carlo Simulation. *Geosciences*, *13*(3), 75.

Pradel, D., & Raad, G. (1993). Effect of permeability on surficial stability of homogeneous slopes. *Journal of geotechnical engineering*, *119*(2), 315-332.

Qiu, G. Y., & Ben-Asher, J. (2010). Experimental determination of soil evaporation stages with soil surface temperature. *Soil Science Society of America Journal*, *74*(1), 13-22.

Rawls, W. J., & Brakensiek, D. L. (1989). Estimation of soil water retention and hydraulic properties. In *Unsaturated flow in hydrologic modeling: Theory and practice* (pp. 275-300). Dordrecht: Springer Netherlands.

Rienzner, M., & Gandolfi, C. (2014). Investigation of spatial and temporal variability of saturated soil hydraulic conductivity at the field-scale. *Soil and Tillage Research*, *135*, 28-40.

Rose, C. W., Stern, W. R., & Drummond, J. E. (1965). Determination of hydraulic conductivity as a function of depth and water content for soil in situ. *Soil Research*, *3*(1), 1-9.

Sadek, M. S. (1993). *A comparative study of the electrical and hydraulic conductivities of compacted clay*. University of California, Berkeley.

Santoso, A. M., Phoon, K. K., & Quek, S. T. (2011). Effects of soil spatial variability on rainfall-induced landslides. *Computers & Structures*, *89*(11-12), 893-900.

Sättele, M., Krautblatter, M., Bründl, M., & Straub, D. (2016). Forecasting rock slope failure: how reliable and effective are warning systems?. *Landslides*, *13*, 737-750.

Schuhmann, R., Königer, F., Emmerich, K., Stefanescu, E., & Stacheder, M. (2011). Determination of hydraulic conductivity based on (soil)-moisture content of fine-grained soils. *Hydraulic conductivity-issues, determination and applications*.

Shopnil, M. S. R., Imtiaz, T., Mahjabin, S., & Hossain, M. S. (2023). Hydraulic Conductivity Prediction of Cement Stabilized Pavement Base Incorporating Recycled Plastics and Recycled Aggregates. *International Journal of Structural and Construction Engineering*, *17*(6), 260-264.

SILVA, G. S. D., SILVA, J. S. D., PEREIRA, F. A. D. C., SANTANA, R. A., FIRMO, R. S., & LOPES SOBRINHO, O. P. (2019). Spatial variability of the saturated hydraulic conductivity of soil in cocoa farming in recôncavo baiano. *Revista Caatinga*, *32*, 786-794.

Singh, D., Patra, S., Mishra, A. K., Mariappan, S., & Singh, N. (2022). Temporal variation of saturated and near-saturated soil hydraulic conductivity and water-conducting macroporosity in a maize-wheat rotation under conventional and conservation tillage practices. *Land Degradation & Development*, *33*(13), 2208-2219.

Su, G. W., Jasperse, J., Seymour, D., & Constantz, J. (2004). Estimation of hydraulic conductivity in an alluvial system using temperatures. *Ground Water*, *42*(6/7), 890.

Tasnim, J. (2022). *Reuse of Recycled Plastic for Subgrade Treatment* (Doctoral dissertation, The University of Texas at Arlington).

Tuller, M., Or, D., & Hillel, D. (2004). Retention of water in soil and the soil water characteristic curve. *Encyclopedia of Soils in the Environment*, *4*, 278-289.

Van Genuchten, M. T. (1980). A closed-form equation for predicting the hydraulic conductivity of unsaturated soils. *Soil science society of America journal*, *44*(5), 892-898.

Vauclin, M., Elrick, D. E., Thony, J. L., Vachaud, G., Revol, P., & Ruelle, P. (1994). Hydraulic conductivity measurements of the spatial variability of a loamy soil. *Soil Technology*, *7*(3), 181-195.

Wallace, K. B. (1977). Moisture transients at the pavement edge: analytical studies of the influence of materials and cross-section design. *Géotechnique*, *27*(4), 497-516.

Wang, C. C., Chang, W. J., Huang, A. B., Chou, S. H., & Chien, Y. C. (2018). Simplified monitoring and warning system against rainfall-induced shallow slope failures. *Canadian Geotechnical Journal*, *55*(10), 1421-1432.

Wan, Y., Xue, Q., Liu, L., & Wang, S. (2018). Crack characteristic and permeability change of compacted clay liners with different liquid limits under dry-wet cycles. *Advances in Civil Engineering*, *2018*, 1-9.

Yang, G., Xu, Y., Huo, L., Wang, H., & Guo, D. (2022). Analysis of Temperature Effect on Saturated Hydraulic Conductivity of the Chinese Loess. *Water*, *14*(9), 1327.

Zhu, Y., Ishikawa, T., Subramanian, S. S., & Luo, B. (2021). Early warning system for rainfall- and snowmelt-induced slope failure in seasonally cold regions. Soils and Foundations, 61(1), 198-217.